



# WISC SPACE RACE

**— PHASE ONE —**  
**PRELIMINARY DESIGN REPORT**

# **WI Space Race**

## **Preliminary Design Report**

**Prepared For The Base 11 Space Challenge**

**Submitted on March 22nd, 2019**



NOTICE: The Contents of this report are privileged and confidential. Please do not circulate outside of the appropriate Base 11 Space Challenge judges, representatives, and other authorized Base 11 Space Challenge personnel without prior permission from the WI Space Race team.

# Table of Contents

<b>1.0 Introduction</b>	<b>12</b>
1.1 Description of Overall System Architecture	12
1.2 Mission Concept of Operations Overview	14
1.2.1 Flight Controllers	14
1.2.1.1 Flight Director (FLIGHT)	14
1.2.1.2 Safety Officer (SO)	14
1.2.1.3 Flight Dynamics Officer (FIDO)	15
1.2.1.4 Instrumentation and communications officer (INCO)	15
1.2.1.5 Electrical and Consumables Manager (ECOM)	15
1.2.1.6 Propulsion Engineer (PROP)	15
1.2.1.7 Ground Controller (GC)	15
1.2.2 Mission Phases	15
1.2.2.1 Loaded to Rail	15
1.2.2.2 Avionics Powered	15
1.2.2.3 Helium loading	16
1.2.2.4 Pad validation	16
1.2.2.5 Fueling	16
1.2.2.6 Fueled	16
1.2.2.7 Pressurized (armed)	16
1.2.2.8 Firing	16
1.2.2.9 Coasting	16
1.2.2.10 Recovery	17
<b>2.0 Mission Analysis</b>	<b>18</b>
2.1 Requirements	18
2.2 Altitude Prediction	19
2.3 Mass Budget	22
2.3.1 Mass Budget Analysis	23
2.3.2 Component Size and Mass Tracking	23
2.4 Overview of Rocket Parameters	24
2.5 Predicted Performance	25
<b>3.0 Propulsion System Design</b>	<b>27</b>
3.1 Overview of Design	27

3.2 Propellant Selection	32
3.3 Combustion Chamber & Nozzle	33
3.3.1 Combustion Chamber & Nozzle Design Parameters	33
	38
3.4 Injector	41
3.5 Catalyst Bed Design	41
3.5.1 Dimensions	42
3.5.2 Thermal analysis	42
3.5.3 Chemical analysis:	44
3.5.4 Catalyst Bed Testing and Development	44
3.5.4.1 Silver Plating Monel Mesh	44
3.5.4.2 Experimental Goals	44
3.5.4.3 Catalyst Test Reactor Design	45
3.5.4.4 Full-Scale Catalyst Bed Test Design	45
3.6 Valves & Plumbing	47
<b>4.0 Engine test stand design and test plan</b>	<b>48</b>
4.1 Test Engine	48
4.2 Test Stand	49
4.3 Test Plan	51
<b>5.0 Range Safety Systems</b>	<b>53</b>
5.1 Trajectory Control	53
5.2 Drift Predictions	53
5.2 Propulsion Aborts	54
<b>6.0 Airframe Structure</b>	<b>55</b>
6.1 Main Body	56
6.1.1 Frame	56
6.1.1.1 Engine to Oxidizer Tank Interconnect	65
6.1.1.2 Oxidizer Tank Encasement	65
6.1.1.3 Oxidizer Tank to Fuel Tank Interconnect	66
6.1.1.3 Fuel and Pressurant Tank Encasements and Interconnect	68
6.1.1.4 Pressurant Tank and Nose Cone Interconnect	70
6.1.2 Fuel, Oxidizer, and Pressurant Tanks	71
6.1.2.1 Tank Style	72
6.1.2.2 Tank Material Selection	73
6.1.2.3 Tank Design	76
6.1.3 Skin	80
6.2 Nose Cone	82
6.3 Fins	87
6.4 Fastening	92

<b>7.0 Flight dynamics</b>	<b>94</b>
7.1 Proposed Flight Dynamics Design	94
7.2 Equations of Motion	94
7.3 Roll Stabilization Technique	96
7.4 Aerodynamic Fin Control Approach	96
7.5 Static Stability Analysis	97
7.6 Dynamic Stability Analysis	99
7.7 Selection of Aerodynamic Shapes	100
7.7.1 Nose Cone	100
7.7.2 Nose Cone	101
<b>8.0 Electronics and Altitude Monitoring</b>	<b>103</b>
8.1 Flight Computer	103
8.1.1 Engine control and monitoring	104
8.3.1.1 Pressure Transducers	105
8.3.1.2 Temperature Measurement and Thermocouples	106
8.3.1.3 Valve Control	106
8.1.2 Backup Systems Controller	106
8.2 Power Supply	106
8.3 Electrical Ruggedization	108
8.3.1 Harnessing	109
8.4 Position and Altitude monitoring	110
8.4.1 Telemetry	110
8.4.1.1 Flight and Ground Antennas	111
8.4.1.2 Telemetry Downlink	112
8.4.1.3 Command Uplink	113
8.4.1.4 Telemetry Protocol	113
8.4.1.5 APRS Data Downlink	113
8.4.1.6 Doppler Analysis	114
8.4.2 In-Flight Altitude Prediction	114
<b>9.0 Software</b>	<b>114</b>
9.1 Rocket Embedded Software	116
9.1.1 Flight Controller (FCU)	116
9.1.2 Engine Controller (ECU)	117
9.2 Ground Dashboard Software	118
9.2.1 Technology Stack	118
9.2.2 Graphical User Interface (GUI)	119
<b>10.0 Recovery System</b>	<b>120</b>
10.1 Parachute Sizing and Deployment Altitude	121

10.2 Recovery system electronics	123
10.2.1 Lightweight Recovery Module (LRM)	123
<b>11 Ground Support Equipment</b>	<b>123</b>
11.1 Launch Rail	124
11.1.1 Launch Lugs	124
11.1.2 Mounting the Rocket	125
11.1.3 Electrical Umbilicals	125
11.2 Antenna Tracking Station	126
11.3 Fueling Operations	128
11.4 Contingency De-Fueling	129
<b>12.0 Safety</b>	<b>130</b>
12.1 Hazard Analysis	130
12.1.1 Transport	131
12.1.3 Launch Rail Operations	131
12.1.4 Fueling	132
12.1.5 Fueled on Pad	132
12.1.6 Pad Abort	132
12.1.7 Powered Flight	132
12.1.8 Un-Powered Flight	133
12.1.9 Recovery	133
12.2 Risk Assessment	134
12.2.1 Transport	134
12.2.2 Assembly	134
12.2.3 Powered Flight	135
12.2.8 Un-Powered Flight	135
12.3 Safety Training	136
12.4 Quality Management System	136
12.4.1 External Documents	137
12.4.2 Internal Requirements Documents	137
12.4.3 Design Documents	137
12.4.4 Step by Step Procedures	138
12.4.5 Certification Documents	138
12.4.6 Material Handling Documents	139
12.4.7 Gates	139
12.4.8 Actions	139
<b>13.0 Team Development</b>	<b>140</b>
13.1 Succession Planning	140
13.2 Knowledge Retention	140
13.3 Outreach	141

<b>14.0 Business and Marketing</b>	<b>141</b>
14.1 Budget Estimate & Management	142
14.1.1 Budget Estimates	142
14.1.2 Budget Management	142
14.2 Fundraising	142
14.3.1 Our Brand	144
14.3.3 Our Marketing	144
<b>Appendices</b>	<b>145</b>
Appendix A - References	146
Appendix B - Sponsorship Packet	150
Appendix C - Propulsion Calculations	157
Nozzle sizing calculation	157
Injector Sizing Calculations	159
Procedure for Silver Plating Monel Mesh for Catalyst Bed	161
Materials	161
Procedure	162
Appendix D - MATLAB code for altitude prediction and rocket param	164

# 1.0 Introduction

Wisconsin has a rich history of making massive contributions to American spaceflight. We plan to propel Wisconsin onto the mainstream of today's new-space industry by winning the competition and deploying the winnings to strategically invigorate a space-startup ecosystem in Madison, WI.

We aim to take this legacy into the new-space era, by winning the Base 11 Space challenge, and cementing Badger Engineers as the first students to build and launch a liquid rocket to the Karman line, within the next 14 months, by launch window number one in May 2020. This report gives detailed insight into our research, design, and development work done to date to achieve this goal.

Beyond the technical challenge of launch a liquid rocket to space, we acknowledge the complexity of operating with a team that is, for the most part, under 22 years in age. To accomplish this challenging feat., we recognize that empowering strong leaders and cultivating self-starting team members is critical to accomplishing the task at hand. Therefore, we prioritized engineering our team culture and organization structure over the past few months. Likewise, we understand that we must cultivate a culture of entrepreneurship and a startup mentality for each of our team members.

The work in this document reflects the efforts and inputs of ten team leads and nearly 25 general team members. Their efforts reflect our team's core values include: Ownership, courageous persistence, and gratitude for the opportunity to compete in this competition.

With our cultural foundation in place, we moved into rocket design. Here, we provide a high-level description the WI Space Race Rocket propulsion, structural, electrical, software, and recovery subsystems. Likewise, we detail the launch operations, safety, and testing plans for each of these systems. We conclude with a high-level description of our business plan for fundraising, marketing, and managing the 250,000 dollars plus needed to procure the hardware and services to build the rocket.

## 1.1 Description of Overall System Architecture

The WI Space Race rocket, is designed to achieve an apogee of 100 km and be recovered via parachutes. The engine outputs approximately 3700 lb thrust for 46 seconds (172,000 lb-s impulse). The rocket will accelerate off the launch pad at 2.5 g's and leave the 60 ft long launch rail at 16 m/s (36 mph), ensuring aerodynamic stability as it leaves the launch pad. An onboard flight computer autonomously nulls any roll by actuating control surfaces at the bottom of the fins. The control system also corrects any lateral perturbations to ensure the rocket remains vertical. The rocket will achieve a maximum acceleration of 4.5 g' and go Mach 4.25. A roll rate is introduced after engine burnout to spin stabilize the rocket as it leaves the atmosphere. Once the rocket reaches apogee, the nose cone opens

via a spring/latch mechanism. A drogue parachute (with reefing) deploys prior to re-entry to slow the rocket down as it enters the atmosphere. The drogue parachute will fully open at approximately 3.5 km. A main parachute is deployed at 1.5 km to slow the rocket down to final velocity of approximately 7 m/s (15 mph).

To achieve these performance values our team has designed a 400 lb, 27 ft tall rocket, using 90% hydrogen peroxide (HTP) as an oxidizer, and kerosene as a fuel. 660 lb of propellant will be pressure fed to the engine at a mass flow rate of 14.21 lb/s. To prevent the engine from melting, a portion of the HTP is fed to the bottom of the nozzle and flows through cooling channels around the nozzle and combustion chamber. It is then fed into the catalyst bed, where it is decomposed to high temperature oxygen and steam. The HTP is injected into the combustion chamber at high velocity, which impinges the kerosene in an unlike-triplet stream. The mixing of oxygen and kerosene at a temperature of 1250 K (1800 °F) auto-ignites to a temperature of approximately 2700 K (4400 °F), which eliminates the need for an igniter.

The structure is that of a semi-monocoque—both the riveted 0.0124 in thick Ti-6Al-4V skin and the 0.5 in tube stock of 6061-T6 welded into a frame, acting as the skeleton, bare the load. Additionally, as much of the length of the body consists of pressure vessels, they are also designed to share the load. There are three integral pressure vessels: one for the oxidizer, fuel, and pressurant. They are designed as composite overwrap pressure vessels, are to be manufactured in house, consist of 6061-T6 liners to ensure compatibility with hydrogen peroxide, and wrapped with Torayca T-1000 to significantly reduce the weight of the vessels. The general rocket dimensions are governed by a 25.75 ft long, 13.214 in outer diameter main body tube, 36 in long Von Karman nose cone, and four NACA 0006 based fins with 30 in root chords, 14 in tip chords, 16 in sweeps, 2 in major thicknesses, and 12 in widths. This leaves the entire rocket 29.1 ft long. Currently, it is designed, in general, with high factors of safety such that when hot fire testing is done, more exact loading conditions can be determined allowing for design optimization. Access doors with standard screws are located in several places along the rocket to provide access to critical components.

Four fins (NACA 0006 profile) are symmetrically attached to the bottom of the rocket to provide aerodynamic stability. Control surfaces make up the aft 4 in of each fin, are hinged to each fin and controlled by an onboard computer, which sends a signal to turn direct drive stepper motors independently. The motor chosen has a 1.8° basic step angle, an 18:1 gearbox, and 416 oz-in of holding torque, allowing for the control surfaces to actuate 12.5° under maximum loading. The flight computer records and transmits pertinent flight data to the ground station, including flight dynamics data from IMUs as well as performance and monitoring data from the engine.



Figure 1.1.1: Rendering of Preliminary Design

## 1.2 Mission Concept of Operations Overview

### 1.2.1 Flight Controllers

The flight controller positions are loosely based on NASA's Apollo- and Space Shuttle-era control centers. These positions include the Flight Director, Safety Officer, Flight Dynamics Officer, Instrumentation and Communications Officer, Electrical and Consumables Manager, Propulsion Engineer, and Ground Controller.

#### 1.2.1.1 Flight Director (FLIGHT)

Overall head of operations. Responsible for overseeing all other controller posts.

#### 1.2.1.2 Safety Officer (SO)

The safety officer will manage the other flight controllers under the supervision of FLIGHT for all operations before the Go/No go for launch and

after touchdown. In particular they will instruct the flight controllers through the pre and post launch procedures.

#### **1.2.1.3 Flight Dynamics Officer (FIDO)**

The flight dynamics officer is responsible for the rocket subsystems that control direction (eg, fins).

#### **1.2.1.4 Instrumentation and communications officer (INCO)**

The instrumentation and communications officer will manage the radio and umbilical data links between the flight computer and ground control. This includes pre-flight checks, antenna placement/adjustment, as well as the detection and mitigation of radio interference. They will also monitor the functionality of the flight computer before launch as well as in flight.

#### **1.2.1.5 Electrical and Consumables Manager (ECOM)**

The electrical and consumables manager will monitor the temperature of the battery and tanks, as well as the battery's charge state and the tank's pressure levels.

#### **1.2.1.6 Propulsion Engineer (PROP)**

The propulsion engineer will command all valves open and closed as well as monitor the pressure and temperature of the combustion chamber in flight.

#### **1.2.1.7 Ground Controller (GC)**

The ground controller will oversee the assembly, fueling and recovery teams.

### **1.2.2 Mission Phases**

#### **1.2.2.1 Loaded to Rail**

The mission enters the Loaded To Rail phase following the Assembly and Integration team's successful hoisting of the rocket and mounting to the launch rails. In this phase, the system is static; nothing is powered on, pressurized, or fueled. The team has an umbilical for power and data has been connected to the rocket.

#### **1.2.2.2 Avionics Powered**

Following an order from the INCO, remote umbilical power is applied and a physical switch on the rocket body is engaged, turning on power to avionics. Since umbilical power is present, it is defaulted to; the batteries aren't discharging.

The INCO then verifies that avionics are running nominally, FIDO will perform a functionality test of all mechanical stability aids such as fins. Once the operation of these systems has been established, the SO will hold a go / no go for consumable loading.

### **1.2.2.3 Helium loading**

The fueling team begins pressurizing the helium tanks by order of the GC. Tank pressure is monitored via umbilical telemetry. When nominal pressure is reached, helium loading is complete and the GC orders progression to pad validation. Before clearing the pad the fueling team will arm the run valves to allow for pad validation to commence.

### **1.2.2.4 Pad validation**

After He loading, the fueling team will clear the pad before ECOM and PROP follow a procedure to perform a final leak check of all tanks and lines. During this procedure, all valves will be cycled to confirm nominal functionality.

### **1.2.2.5 Fueling**

After pad validation is complete, the fueling team will return to the pad, re-inhibit the run valves and replace the expending He. Next they will follow nominal fueling procedures to fill the HTP and RP-1 tanks, respectively.

### **1.2.2.6 Fueled**

After the fuel loading has been completed, the fueling team will arm the run valves and clear the pad. ECOM will monitor tank temperature and pressure for a brief hold to insure no chemical reactions are taking place. Once tank stability has been established SO will hold a go / no go for pressurization of the propellant tanks.

### **1.2.2.7 Pressurized (armed)**

Once go for pressurisation has been given, PROP remotely opens the valves to pressurize the propellant tanks. A final brief hold will allow for all instrumentation to be reviewed for nominality. SO will hand control to FLIGHT, and FLIGHT will hold a go / no go for launch.

### **1.2.2.8 Firing**

On a successful go call, PROP will command the run valves open to launch the rocket; the engine will self-ignite from the heat generated from HTP decomposition and RP-1 injection.

### **1.2.2.9 Coasting**

Engine shutdown is registered by the flight compute. A roll rate will be induced by deflecting the control surfaces to spin stabilize the rocket prior to exiting earth's atmosphere. Then the vehicle then simply coasts to the target altitude of 100 km. Any additional propellant is vented at this point.

### **1.2.2.10 Recovery**

Drogue parachute ejection is initiated by the flight computer based on inertial and altitude sensor data post apogee. The drogue parachute will be reefed to prevent a sudden impulse that destroys the parachute or rocket structure. At 3.5 km the drogue chute will fully open to reduce the descent rate. At 1.5 km, the main parachute will deploy to reduce the descent velocity to < 7m/s. GPS coordinates from wireless telemetry data in combination with radio tracking will be used to locate the rocket.

## 2.0 Mission Analysis

The WI Space rocket was defined by creating a parametric model in MATLAB. This model determined the optimal parameters, such as vehicle radius, propellant mass fraction, and nozzle expansion ratio. The model also predicts the performance parameters of the rocket, such as altitude, velocity, acceleration, Mach #, drag force, etc.

Section 2.1 outlines the requirements set out by the WI Space Race team in combination with the Base 11 Space Challenge system requirements. Section 2.2 describes the methods used to calculate the rocket parameters. Section 2.3 discusses the team's mass budget and our current estimates of component masses. Section 2.4 presents an overview of WI Space Race's rocket parameters. Finally, Section 2.5 outlines the predicted performance of the rocket, such as acceleration, altitude, etc.

### 2.1 Requirements

Although the complete set of system requirements is defined in the Base11 System Requirements document, the only constraints that need to be considered in terms of rocket performance are:

- 3.1.5. The rocket shall be designed to achieve an apogee of not less than 100 km, but not more than 150 km per Requirement 3.1.16.1
- 3.1.16.2. The total impulse shall not exceed 889,600 Newton-seconds (200,000 pounds-seconds) in accordance with the FAA upper limit for a class 3 amateur rocket.

All other system requirements defined by Base11 provide design constraints on the vehicle components. These additional requirements primarily affect size and mass constraints (outlined in Section 2.3 Mass Budget). Other design constraints outlined in the Systems Requirements document are considered in their respective sections.

With these performance constraints defined, initial parameterization of the rocket can be achieved by creating an altitude prediction model for a sounding rocket that reaches a maximum altitude of 100 km. Then, the key rocket parameters (such as vehicle radius, mass, thrust, etc.) are varied using guess and check methods in combination with knowledge of physical constraints to parameterize the overall vehicle. The model is written in MATLAB in a modular fashion so it can be iterated on as our team further defines the rocket design.

## 2.2 Altitude Prediction

A mathematical model was constructed to predict the maximum altitude, as well as other important flight characteristics of a sounding rocket during vertical ascent. The governing equations minimized idealized assumptions to provide an accurate representation of the flight characteristics of the rocket and are valid for compressible flow up to altitudes greater than 100 km. The equations of motion were numerically integrated and compared to experimental data from small scale rocket tests, which resulted in a maximum error of 2.03% of the maximum altitudes. More data is needed to further validate this model in supersonic flow regimes (not tested) however, the results from this experiment provide an acceptable model for Mach number regimes below Mach 0.75. Further testing with a supersonic solid propelled rocket is planned for summer 2019, which will further provide insight in the validity of the model. Additional use of CFD methods will further refine the model to ensure the WI Space Race team passes the Karman line (100 km).

The equation of motion (EOM) of a rocket during vertical ascent, assuming purely vertical flight can be written as:

$$m(t) \frac{d^2y(t)}{dt^2} + \frac{dm(t)}{dt} \frac{dy(t)}{dt} + F_D - F_T(t) - mg = 0 \quad EOM\ 1$$

The rocket mass is a function of time when the propellant is being expelled:

$$\text{if } t < \text{burnTime}: m(t) = m_0 - \dot{m}t$$

$$\text{else: } m(t) = m_{empty}$$

The force due to thrust is derived from conservation of momentum and calculated by the following equation:

$$F_T = \dot{m}u_e + A_e(P_e - P_{atm})$$

Ultimately, a thrust of 15 kN at sea level was chosen to optimize the maximum altitude by running several simulations at different thrust levels.

The final piece of EOM 1 is the force due to drag, which is a function of the air density, the coefficient of drag, the cross-sectional area of the vehicle, and the velocity of the vehicle:

$$F_D = \frac{1}{2}\rho C_D A_{proj} \left( \frac{dy(t)}{dt} \right)^2$$

Density ( $\rho$ ) is dependent on the atmospheric pressure and temperature. The altitude prediction model uses NASA's Earth Atmospheric Model to calculate density,

temperature, and pressure at each data point for a given altitude (Shown in Figure 2.1).



## **Earth Atmosphere Model**

**Metric Units**

**Glenn Research Center**

---

**For  $h > 25000$  (Upper Stratosphere)**

$$T = -131.21 + .00299 h$$

$$p = 2.488 * \left[ \frac{T + 273.1}{216.6} \right]^{-11.388}$$

**For  $11000 < h < 25000$  (Lower Stratosphere)**

$$T = -56.46$$

$$p = 22.65 * e^{(1.73 - .000157 h)}$$



**For  $h < 11000$  (Troposphere)**

$$T = 15.04 - .00649 h$$

$$p = 101.29 * \left[ \frac{T + 273.1}{288.08} \right]^{5.256}$$

$\rho$  = density (kg/cu m)
 $p$  = pressure (K-Pa)
 $T$  = temperature ( $^{\circ}$ C)

$\rho$  =  $p / (.2869 * (T + 273.1))$ 
 $h$  = altitude (m)

Figure 2.2.1: NASA Atmospheric model used in WI Space Race's altitude prediction/rocket parameterization model.

The drag coefficient ( $C_d$ ) is a function of the Mach, Reynolds, Froude, and Prandtl numbers. A simple model proposed in "Rocket and Spacecraft Propulsion", by Martin was used [2.2]:

$$\begin{aligned} \text{If } M < 1: C_d &= a + bM^6 \\ \text{else: } C_d &= a + \frac{b}{M^2} \end{aligned}$$

Experimental plots of  $C_d$  vs  $M$  show a minimum value of  $\sim 0.15$  during the non-compressible regimes, then peak at a value of  $\sim 0.45$  at Mach 1. Using this information, the coefficients "a", and "b" can be solved for, which generates the following drag coefficient vs Mach # correlation:

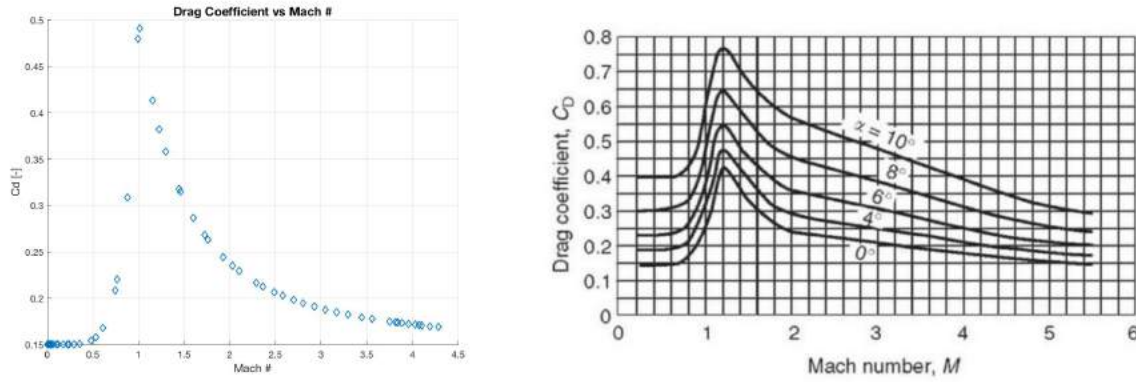


Figure 2.2.2: Left: Drag coefficient vs Mach # from WI Space Race MATLAB code. Right: Drag coefficient vs Mach #. Results show that drag coefficients obtained from our calculations match predictions from Sutton [2.1].

With all equations for EOM 1 known, the second-order nonlinear differential equation can be written in matrix form using separation of variables:

$$\begin{bmatrix} \dot{y} \\ \ddot{y} \end{bmatrix} = \begin{bmatrix} F_T - \frac{F_D}{m} - \frac{my_2}{m} - g \\ y_2 \end{bmatrix} \quad \text{Final EOM}$$

The final EOM can then be solved using MATLAB's ODE45 differential equation (from the MathWorks Optimization Toolbox). Comparisons of experimental results vs actual data is shown in Figure 2.3. The results of this experiment show that our model accurately predicts the rocket's altitude.

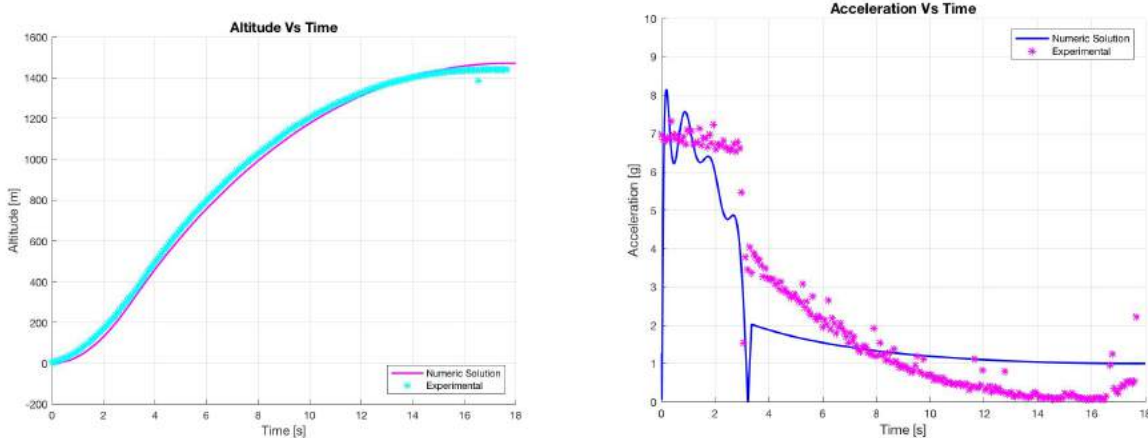


Figure 2.2.3: Predicted model vs actual data from small scale rocket tests.

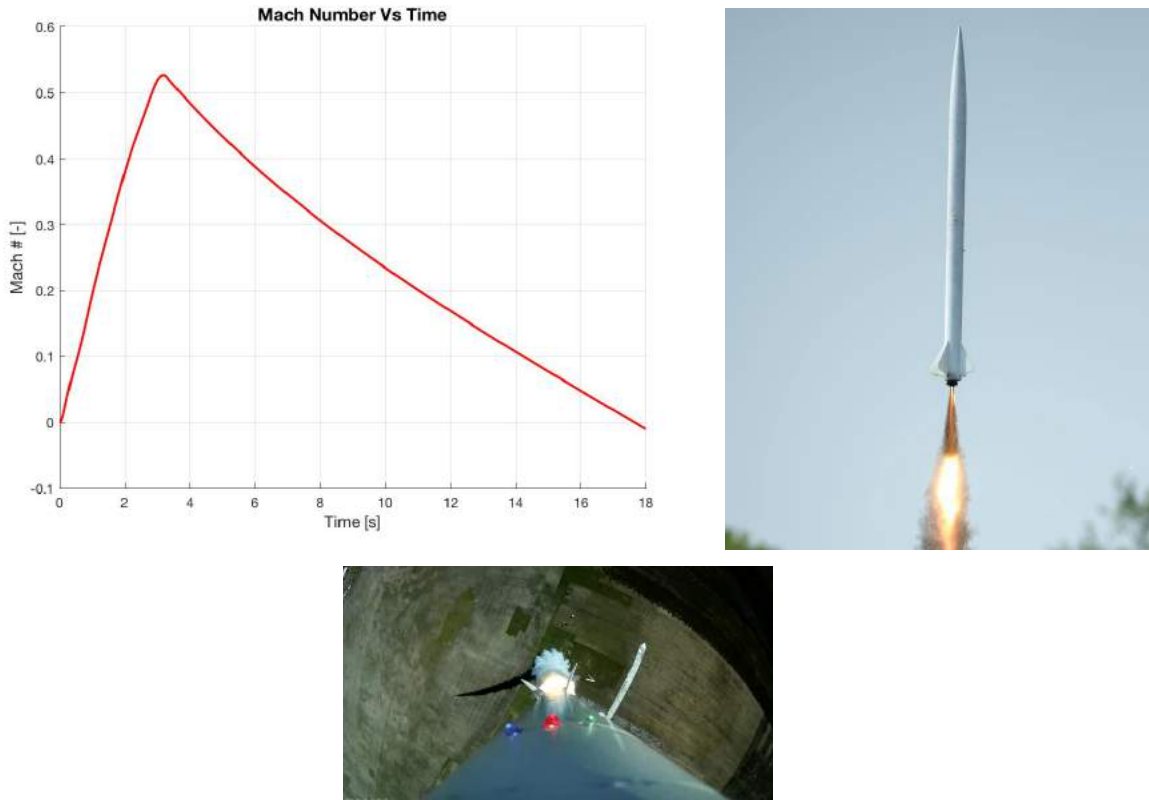


Figure 2.2.4: Top Left: Mach # vs time. Results show this model is accurate in subsonic regime. Top Right & Bottom: Test rocket flown with flight computer onboard. Experimental maximum altitude matched prediction model within 2%.

## 2.3 Mass Budget

### 2.3.1 Mass Budget Analysis

The mass budget of a rocket is dictated by Tsiolkovsky Equation:

$$\Delta V = Isp * g * \ln\left(\frac{m_0}{m_f}\right)$$

Where  $m_0$  and  $m_f$  is the initial and final mass of the rocket, respectively. From this equation it is clear to see that as the mass ratio decreases, the available  $\Delta V$  (total change in velocity) exponentially increases. Therefore, a rocket with a light-weight structure and large propellant mass are highly desired.

The rocket parameterization model shows that the maximum dry mass of the WI Space Race Rocket is approximately 400 lbs. This assumes a total impulse of

172,000 lb-s, which leaves a margin of error to allow for longer burn times if the rocket's actual mass is greater than 400 lbs upon completion.

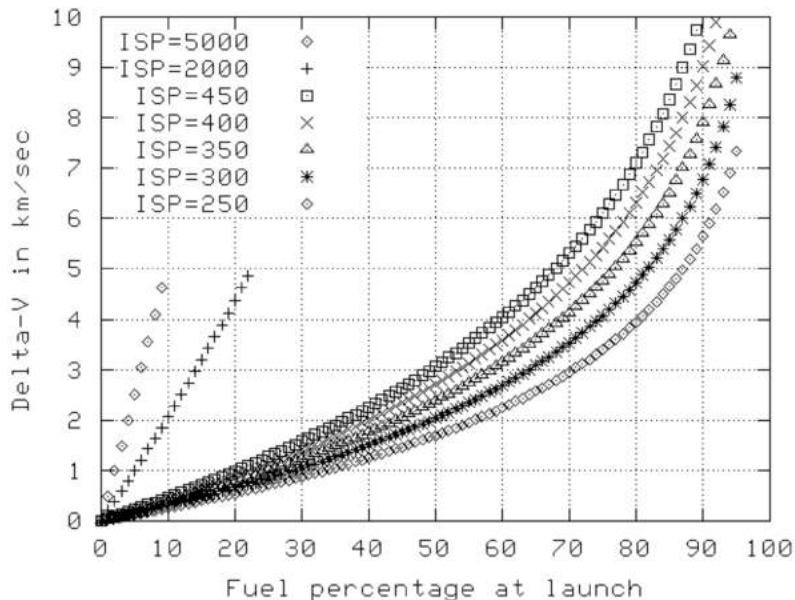
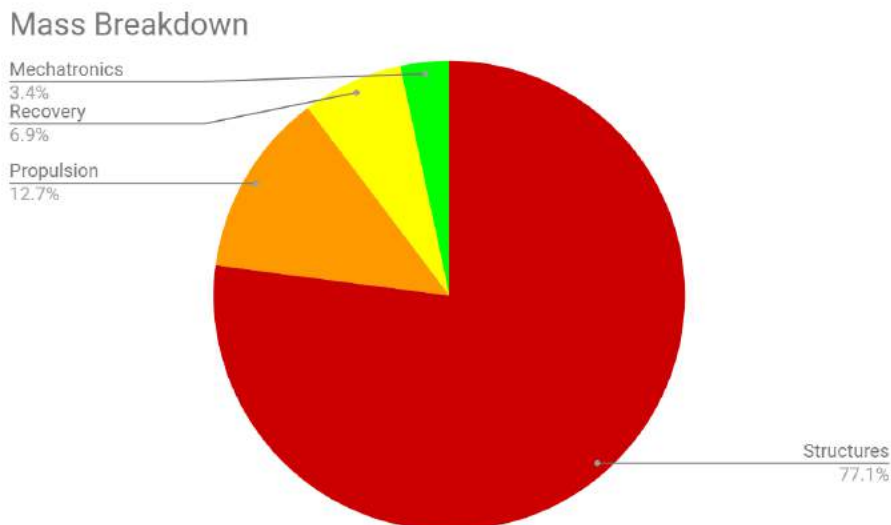


Figure 2.3.1.1:  $\Delta V$  vs fuel percentage at launch ( $\frac{m_f}{m_0} * 100\%$ ). Plot shows lower specific impulse requires a larger percentage of fuel. Plot also shows that a large fuel percentage at launch (light structure, with a large amount of propellant), results in an exponential increase in  $\Delta V$ . [2.3]

## 2.3.2 Component Size and Mass Tracking

The mass of the launch vehicle is tracked in excel spreadsheets, broken down by subsystem and then by parts. This enables us to read in all of the mass and location data from a MATLAB file, which can be used for flight dynamics calculations.



**Figure 2.3.2.1:** Mass break down by subsystem.

The dry mass distribution of the WI Space Race Rocket is constrained by the maximum limit set to us by the Tsiolkovsky Equation, i.e. 400 lbs. The majority of the budget is allocated to the tank structure. Preliminary analysis shows we would need 0.25 cubic meters of combined propellant to maintain thrust for approximately 47 seconds. This combined with a maximum operating pressure of around 1210 psi leads to set design constraints and when modeled and analyzed we get combined tank and skeleton structure weights of approximately 196 lbs. The current total estimated structural mass, including fins, the nose cone and other structural support, is 413 lbs.

The propulsion system includes the engine, catalyst bed, plumbing and valves. The catalyst bed, injector, a combustion chamber and the nozzle account for another 8 lbs. The ball valves for the feed system will be approximately 10 lbs each (20 lbs total). Relief valves, solenoid valves, burst discs, instrumentation and feed lines will be approximately 40 lbs. This results in a total propulsion system weight of approximately 68 lbs.

The mechatronics system accounts for 18 lb in the mass budget. These components include sensors, antennae, circuit boards, batteries, and solenoids to control our helium lines. This estimate also accounts for wiring and wire management.

The parachutes and the recovery system take another 37 lbs from the budget. These components include parachute cord, parachutes, and harness.

The total dry mass of the rocket is predicted to be 536 lbs, which is overweight. However, we are confident that we can trim weight from the structure and recovery system, especially given the large factors of safety on certain heavy components of the rocket (room for optimization).

## 2.4 Overview of Rocket Parameters

An overview of the WI Space Race Rocket's key parameters is shown below. These ultimately set the constraints used to design our rocket.

### ----- Rocket Parameters -----

- Vehicle dry weight:** 398.64 [lb]
- Vehicle wet weight:** 1060.02 [lb]
- Vehicle diameter:** 1.17 [ft]
- Propellant mass (total):** 300.00 [kg], 661.39 [lb]
- Peroxide mass:** 262.50 [kg], 578.71 [lb]
- Kerosene mass:** 37.50 [kg], 82.67 [lb]
- Propellant mass fraction:** 0.62 [-]
- Propellant tank Weight:** 134.08 [lb]
- Peroxide tank Wall thickness:** 0.24 [in]
- Kerosene tank Wall thickness:** 0.24 [in]
- Peroxide tank length (inner dim):** 10.02 [ft]

**Kerosene tank length (inner dim):** 2.69 [ft]  
**Peroxide tank volume:** 0.20 [ $m^3$ ]  
**Kerosene tank volume:** 0.05 [ $m^3$ ]  
**Peroxide tank max operating pressure:** 1209.14 [psi]  
**Kerosene tank max operating pressure:** 1210.61 [psi]  
**Peroxide tank mean operating pressure:** 604.57 [psi]  
**Kerosene tank mean operating pressure:** 605.31 [psi]

----- Propulsion Parameters -----

**Sea level thrust:** 14.99 [kN], 3370.85 [lbf]  
**Expansion ratio:** 8.00 [-]  
**Chamber Pressure:** 2.76 [MPa], 400.30 [psia]  
**Exit Pressure:** 0.05 [MPa], 7.88 [psia]  
**Chamber temperature:** 2734.00 [K]  
**Molar mass of propellant:** 21.90 [kg/kmol]  
**Specific heat ratio of propellant (frozen-flow):** 1.14 [-]  
**Pressure at catalyst bed:** 600.38 [psia]  
**Pressure at injector:** 500.31 [psia]  
**Mass flow rate (total):** 6.45 [kg/s]  
**Mass flow rate (oxidizer):** 5.64 [kg/s], 12.44 [lb/s]  
**Mass flow rate (fuel):** 0.81 [kg/s], 1.78 [lb/s]  
**Nozzle exit diameter:** 7.42 [in]  
**Throat Diameter:** 2.72 [in]  
**Peroxide feed line diameter:** 1.33 [in]  
**Kerosene feed line diameter:** 0.30 [in]

## 2.5 Predicted Performance

With the rocket fully defined, the performance of the rocket is calculated and the results are shown below. These results show that our design meets Base11's primary system requirement of reaching an apogee between 100-150 km. Furthermore, the rocket is predicted to liftoff the launch pad at approximately 2.25 g's. This results in a velocity of roughly 65 ft/s at the point where the rocket leaves the 60 ft tall launch rail. The rocket will be aerodynamically stable at this point, which ensures the rocket will be safe leaving the launch pad.

----- Performance Results -----

**Max Altitude:** 106697.32 [m], 349967.21 [ft]  
**Max Velocity:** 1263.46 [m/s]  
**Max Mach #:** 4.25 [-]  
**Max Thrust:** 17.95 [kN], 4034.65 [lbf]  
**Specific Impulse:** 259.36 [s]  
**Max Drag Force:** 2.53 [kN], 568.07 [lbf]  
**Max dynamic pressure:** 95.59 [kPa]  
**Total impulse:** 172,000 lb-s  
**Burn time:** 46.51 [s]

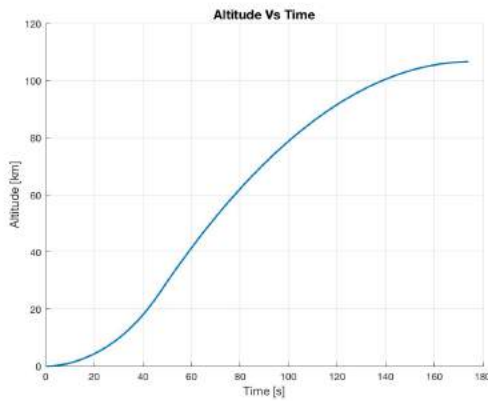


Figure 2.5.1: Altitude vs Time. Max altitude: 106 km.

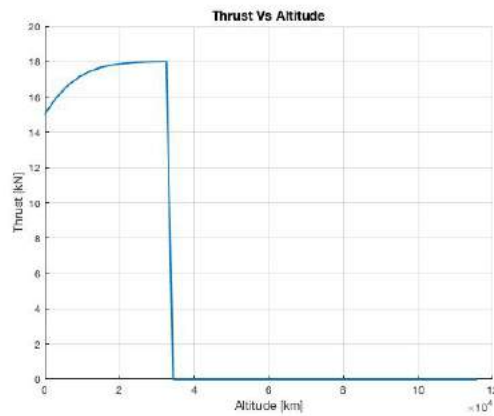


Figure 2.5.3: Thrust vs Altitude. Thrust at sea level: 15 kN, Maximum thrust: 17.95 kN at 24 km.

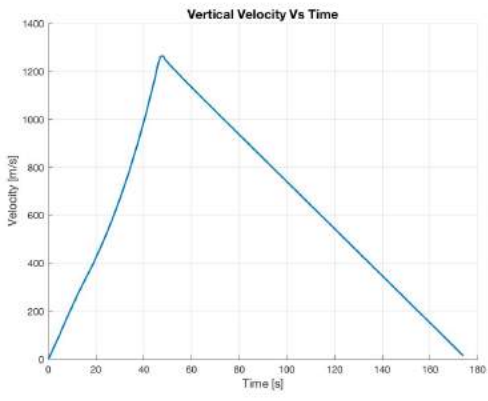


Figure 2.5.2: Vertical velocity vs time. Maximum velocity: 1264 m/s (Mach 4.25)

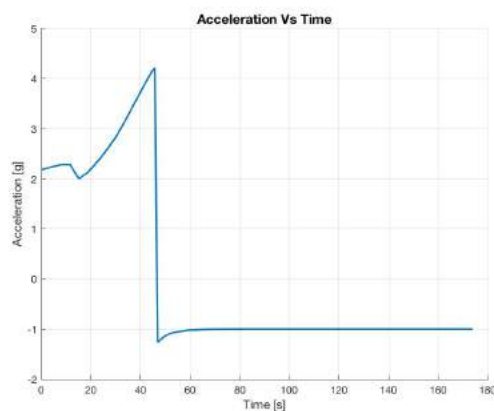


Figure 2.5.4: Acceleration vs time (in g's). Maximum acceleration: 4.25 g's. Max change in acceleration: 5.5 g's

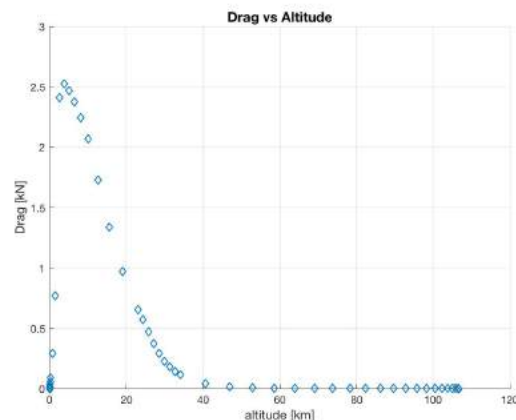


Figure 2.5.5: Drag Force vs Altitude

# 3.0 Propulsion System Design

## 3.1 Overview of Design

The engine is designed to provide 15 kN of thrust (3400 lbf at sea level) for ~46 seconds, resulting in a total impulse of < 200,000 lb-s, per competition requirements. An expansion ratio of 8 was chosen because it optimized the thrust vs altitude curve, resulting in an overall increase in altitude (as shown in Figure 3.1.1). This results in a maximum thrust of 18 kN (4050 lbf) at 25 km in altitude, producing a total impulse of 172,000 lb-s (obtained by integrating thrust vs time curve).

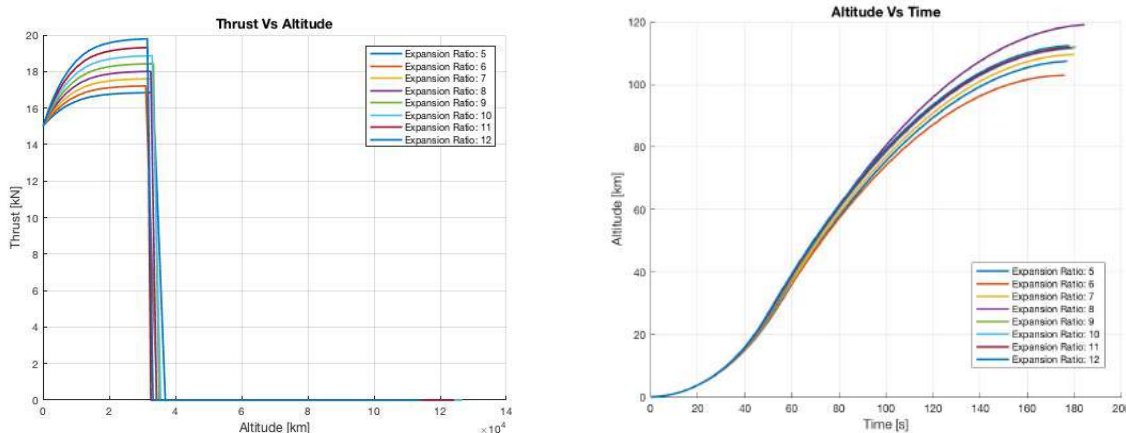


Figure 3.1.1: Left: Thrust vs Altitude (Expansion Ratio as a parameter). Right: Altitude vs Time. Maximum altitude occurs with an expansion ratio of 8, resulting in a maximum thrust of 18 kN (4050 lbf).

The engine is pressure fed and utilizes 90% hydrogen peroxide (HTP) and RP-1 at a 7:1 oxidizer/fuel ratio at a rate of 5.7 kg/s (12.5 lb/s). The HTP flows through a catalyst bed, which decomposes the peroxide into gaseous O<sub>2</sub> and H<sub>2</sub>O vapor. The mixture is injected into the combustion chamber through the injector plate, which impinges the HTP and RP-1 streams at high velocity and temperature (~1200 K, 925 °C), enough to auto-ignite the O<sub>2</sub> / RP-1 mixture to an adiabatic flame temperature of ~2700 K (2426 °C) and a chamber pressure of 400 psia.

Due to the high combustion temperature, a portion of HTP is used for cooling. It enters a set of cooling channels within the nozzle walls (not shown in model), which acts as a heat exchanger to cool the nozzle and combustion chamber walls. The HTP is then plumbed into the top of the catalyst bed for decomposition. Decomposition temperatures in the catalyst bed will be ~1200 K, which is near the melting point of the silver catalyst. To assist in cooling the catalyst bed, the RP-1 flows through a cooling jacket around the catalyst bed wall, which acts as a

counterflow heat exchanger. Aside from lowering temperatures, preheating the RP-1 also assists with combustion performance. The following Figure 3.1.2 depicts the overall process.



Figure 3.1.2: Cross section of engine design #3

Multiple configurations of the engine have been considered. The first design involves a vortex injection system, where the fuel passes through a radial fuel injector entirely separate from the oxidizer injection system. The decomposed HTP flows through a spacer plate and into a strainer-shaped injector, which injects the fluid into the path of the fuel. Both the fuel and oxidizer are injected at an angle such that the flow would follow a vortex trajectory throughout the combustion chamber, as is shown in the following images.

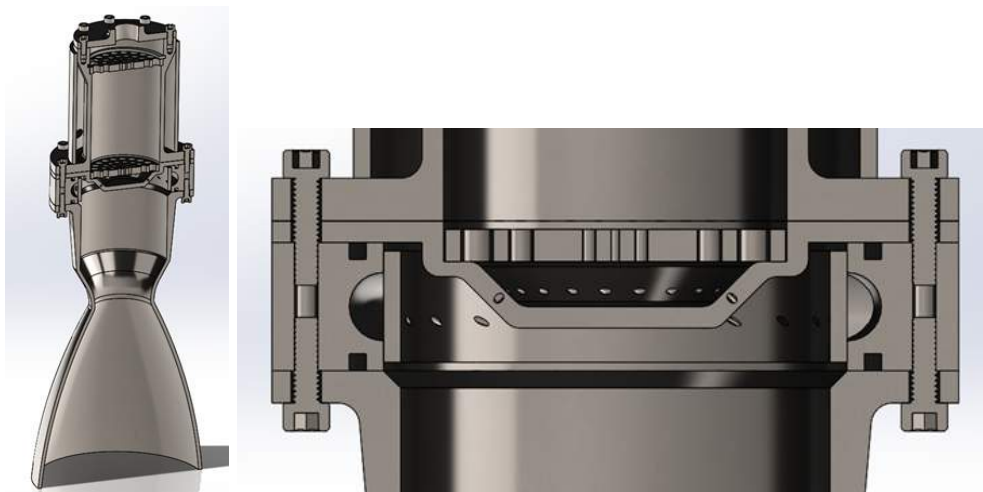


Figure 3.1.3: Cross section of engine design #1.



Figure 3.1.4: Oxidizer injection strainer for engine design #1.



Figure 3.1.5: Different angles and cutaway renderings of the fuel injection ring for engine design #1.

A cooling jacket around the catalyst bed, which RP-1 flows through prior to injection, maintains reduced catalyst bed temperatures. Note that the design of the injection ring involves a fillet weld around the perimeter of the inner diameter to secure the two pieces to one another, creating a toroidal chamber. Despite being designed as two pieces, the ring injector still imposes some manufacturing difficulties, and therefore will likely need to be redesigned if this idea is further pursued.

The second configuration involves a single injector plate for both the oxidizer and peroxide. Rather than supplying the fuel radially, it is instead passed through the catalyst bed itself and into an injector plate, as shown in the images below.

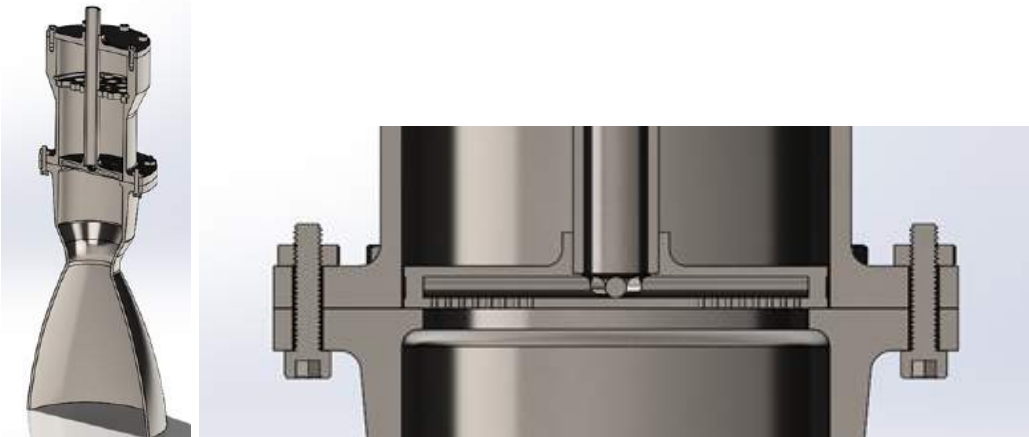


Figure 3.1.6: Cross section of engine design #2.



**Figure 3.1.7:** Fuel/oxidizer injector plate for engine design #2

This design allows for a greater simplicity as compared to design #1, since the fuel and oxidizer are passed through a single plate. This allows for less components involved and less weight, and it also provides more options for ways to configure the holes such that the fuel and oxidizer impinge upon each other in an effective manner. This design also allows for the possibility of cooling the catalyst bed from the inside as the RP-1 travels through. However, this does pose some concern, since a small leak in the fittings for the tube carrying the RP-1 would allow it to mix with the peroxide in the catalyst bed, potentially leading to dangerous consequences. Therefore, a third design option has been proposed to combine the best traits from designs #1 and #2.

Engine design #3 maintains separate injection of the fuel and oxidizer; however, it mitigates the risk of fuel and oxidizer contacting one another until they enter the combustion chamber. Both fluids are passed through the same injector plate, which has separate flow paths into the combustion chamber.



**Figure 3.1.8:** Engine #3 cutaway



Figure 3.1.9: Engine #3 fuel/oxidizer injector plate.

This third design incorporated the simplicity from design #2, while avoiding safety concerns. It also is shaped in such a way that the cooling jacket from design #1 can still be implemented. Due to the preferred design characteristics of engine design #3, it is the preliminary design chosen to continue with design optimization.



**Figure 3.1.10:** Full assembly of engine design #3.

## 3.2 Propellant Selection

The primary limiting factor of oxidizer and fuel selection was the team's inability to store cryogenic fluids. Many fluids commonly used in propulsion, including liquid oxygen, liquid hydrogen, and liquid methane, require safe and reliable storing capabilities at incredibly low temperatures. Since the University of Wisconsin - Madison has not had a liquid-propelled rocket team in the past, there is no equipment available to students for cryogenic storage. Therefore, the team has decided to use 90% hydrogen peroxide as the oxidizer and kerosene (RP-1) as the fuel.

HTP decomposes into steam and oxygen gas, which is non-toxic, making it relatively safe to handle and environmentally friendly. It is decomposed by a catalyst, such as silver, nickel, or platinum, which creates high temperature steam that is used to ignite the RP-1, O<sub>2</sub> mixture, eliminating the need for an igniter.

While peroxide does have many benefits, it does pose some concerns. First, peroxide is highly reactive with organic materials (including skin), which raises safety concerns during handling. To avoid incidents, the team has implemented a series of standard operating procedures for HTP handling. Another hazard with HTP is its reactivity with many commonly-used materials. This includes carbon steel, copper, and a wide variety of plastics. This imposes a material constraint to all components in contact with HTP. This applies not only to major components, but also to all hardware, including seals, fasteners, tubing, etc. Specifically, these components should abide to the tables below, which lists materials that are known to be compatible with HTP [3.1].

Table 3.1.2: Metals compatible with HTP (A - Excellent, B - Good, C - Fair)

Aluminum	Zirconium	316 Stainless Steel	303/304 Stainless Steel
A	B	C+	C-

Table 3.1.3: Plastics compatible with HTP (A - Excellent, B - Good, C - Fair)

Teflon	Viton	HDPE
A	B	C

It should be noted that, in addition to corroding the material surface, contact between HTP and an incompatible material causes it to decompose and therefore lose its potency. Therefore, it is strongly preferred to use aluminum for components in contact with peroxide for long periods of time, such as the oxidizer tank.

The fuel selected for this propulsion design is RP-1, which is a high-grade kerosene typically used in rocket propulsion. It is also the most common fuel of choice when used in conjunction with decomposed HTP, due to its high energy

density. RP-1 is compatible with most common materials, including all steels, aluminums, and plastics, and therefore does not pose a design constraint. RP-1 is toxic if ingested and is flammable, so safety measures will need to be taken to prevent accidents.

## 3.3 Combustion Chamber & Nozzle

### 3.3.1 Combustion Chamber & Nozzle Design Parameters

Combustion composition was modeled using NASA's Chemical Equilibrium Analysis (CEA) software with a 7:1 oxidizer/fuel ratio of 90% liquid H<sub>2</sub>O<sub>2</sub>, 10% liquid H<sub>2</sub>O, and RP-1 at a chamber pressure of 400 psi (Figure 3.3.1.1). This produced a stagnation temperature T<sub>0</sub> = 2736 K, and a sea level specific impulse (Isp) of 260 s (283 s at vacuum).

COMPOSITION DURING EXPANSION FROM INFINITE AREA COMBUSTOR					
	REACTANT	WT FRACTION (SEE NOTE)	ENERGY KJ/KG-MOL	TEMP K	
FUEL	RP-1	1.000000	-24717.700	298.150	
OXIDANT	H <sub>2</sub> O(L)	0.1000000	-285830.088	298.150	
OXIDANT	H <sub>2</sub> O <sub>2</sub> (L)	0.9000000	-187780.000	272.740	
O/F=	7.00000	%FUEL= 12.500000	R,EQ.RATIO= 1.067552	PHI,EQ.RATIO= 1.149276	
	CHAMBER	THROAT	EXIT		
P <sub>inf</sub> /P	1.0000	1.7396	57.031		
P, BAR	27.579	15.853	0.48358		
T, K	2736.46	2568.67	1516.78		
RHO, KG/CU M	2.6208 0	1.6139 0	8.3955-2		
H, KJ/KG	-5956.78	-6519.97	-9208.66		
U, KJ/KG	-7009.08	-7502.28	-9784.66		
G, KJ/KG	-39328.0	-37845.0	-27705.9		
S, KJ/(KG)(K)	12.1950	12.1950	12.1950		
M, (1/n)	21.622	21.742	21.895		
(dLV/dLP)t	-1.00712	-1.00413	-1.00000		
(dLV/dLT)p	1.1697	1.1052	1.0001		
Cp, KJ/(KG)(K)	4.0968	3.5377	2.2400		
GAMMAS	1.1381	1.1467	1.2042		
SON VEL, M/SEC	1094.3	1061.3	832.8		
MACH NUMBER	0.000	1.000	3.062		
PERFORMANCE PARAMETERS					
Ae/At	1.0000	8.0000			
CSTAR, M/SEC	1610.1	1610.1			
CF	0.6592	1.5839			
Ivac, M/SEC	1986.9	2776.1			
Isp, M/SEC	1061.3	2550.2			

Figure 3.3.1.1: Chemical Equilibrium Analysis results (obtained by NASA CEARUN).

The thrust was chosen to be 15 kN at sea-level for mission optimization. Using thrust, the expansion ratio, and the results from CEA, the nozzle was sized

using isentropic relations (See Appendix D for calculation), resulting in the following parameters:

----- **Combustion and Nozzle Parameters** -----

- Sea level thrust:** 14.99 [kN], 3370.85 [lbf]
- Expansion ratio:** 8.00 [-]
- Chamber Pressure:** 2.76 [MPa], 400.30 [psia]
- Exit Pressure:** 0.05 [MPa], 7.88 [psia]
- Chamber temperature:** 2734.00 [K]
- Molar mass of propellant:** 21.90 [kg/kmol]
- Specific heat ratio of propellant (frozen-flow):** 1.14 [-]
- Mass flow rate (total):** 6.45 [kg/s]
- Nozzle exit diameter:** 7.69 [in]
- Throat Diameter:** 2.72 [in]

The nozzle geometry was sized using the Rao parabolic method, developed by G.V.R. Rao, as outlined in Design of Liquid Propellant Rocket Engines, by Huzel and Huang [3.2]. Beginning with a throat radius, obtained from Section 3.3, the nozzle geometry is obtained by the following method:

Near-optimum nozzle: Rao parabolic approximation

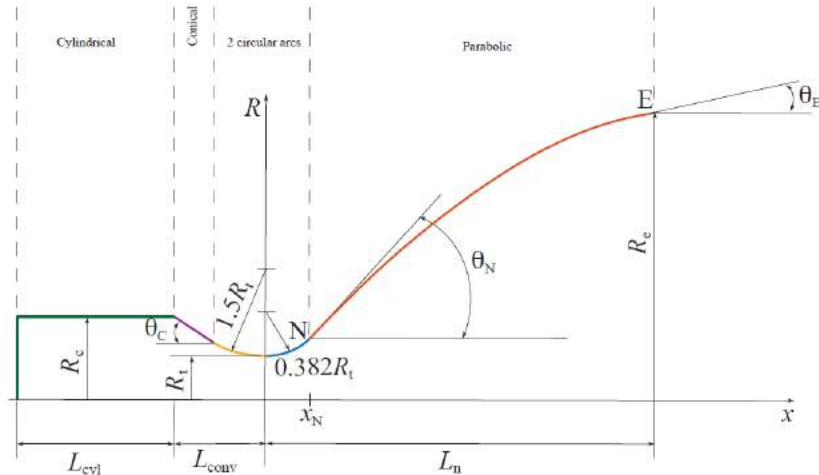


Figure 3.3.1.2: Rao nozzle geometry approximation

With a throat radius ( $R_t$ ) determined, the following parameters must still be defined:  $\theta_c$ ,  $\theta_N$ ,  $\theta_E$ ,  $R_e$ ,  $R_c$ ,  $L_{cyl}$ ,  $L_{conv}$ , and  $L_n$ .  $R_e$  is determined from the expansion ratio:

$$\varepsilon = \frac{A_e}{A_t}$$

$$R_e = R_t \sqrt{\varepsilon}$$

The next step is to select a value for  $L_f$ , which is the fraction of nozzle length compared to a  $15^\circ$  half-angle conical nozzle. This can be determined by following Figure 3.3.1.3, provided by the Huzel and Huang text.

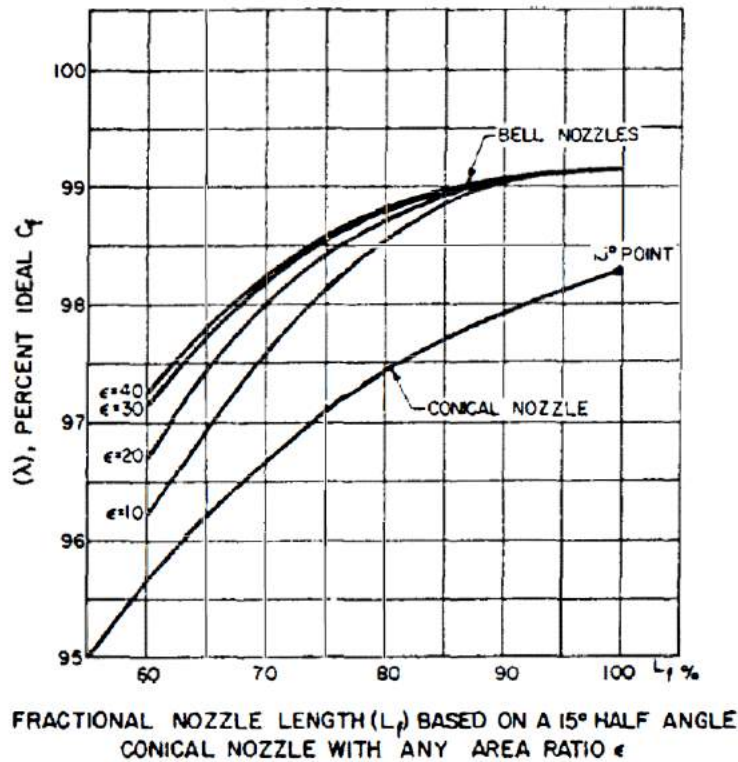


Figure 3.3.1.3: Thrust efficiency v. bell nozzle fractional length  $L_f$

From this figure, it is apparent that for an expansion ratio of 8, the thrust efficiency is significantly influenced by nozzle length. Therefore, for the first iteration of design, the  $L_f$  is selected to be equal to 90%, such that only minimal performance is sacrificed while minimizing nozzle length, which would add unwanted weight to the engine.

After selecting a fractional length, Figure 3.3.1.4 can be used to determine values of  $\theta_N$  and  $\theta_E$ .

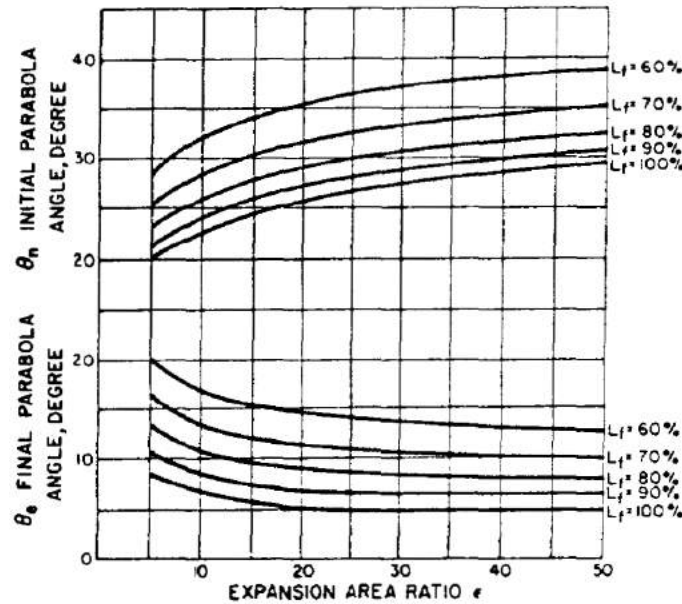


Figure 3.3.1.5: Nozzle geometry guidelines for Rao design, as a function of  $\epsilon$

From this figure, assuming that  $\epsilon = 8$  and  $L_f = 90\%$ , it can be estimated that  $\theta_N = 23^\circ$  and  $\theta_E = 8^\circ$ . With that, the entire geometry of the nozzle downstream of the throat is fully defined.

With the above information, the Rao parabolic method can be used to produce the nozzle geometry shown in Figure 3.3.1.6:

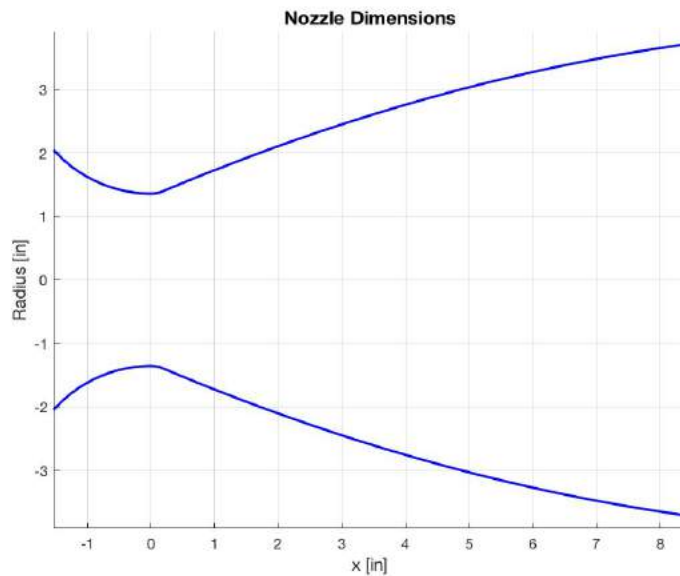


Figure 3.3.1.6: Nozzle geometry solved in MATLAB

The final step is to define the geometry of the combustion chamber. Huzel and Huang's text suggests using a combustion chamber contraction ratio,  $\epsilon_c$ , of 1.6. Therefore, the combustion chamber radius is defined by the following equation.

$$R_c = R_t \sqrt{\varepsilon_c}$$

Using this equation with values  $R_t = 1.3$  in and  $\varepsilon_c = 1.6$  yields the solution  $R_c = 1.64$  in.

The combustion chamber volume can be calculated by introducing the variable  $L^*$ , which is the characteristic length of the nozzle, and defined as the combustion chamber volume divided by the throat area:  $L^* = \frac{V_c}{A_t}$ . The characteristic length is also dependent on the combustion residence time, which affects combustion efficiency. Huzel and Huang recommend using  $L^*$  values of 60-70 in for HTP/RP-1 propellant. With this information, the diameter of the combustion chamber can be solved by the following calculation:

$$V_c = \pi R_c^2 L_{cyl} + \frac{\pi}{3} L_{conv} (R_c^2 + R_c R_t + R_t^2)$$

$$L_{conv} = \frac{R_c - R_t - 1.5R_t(1 - \cos(\theta_c))}{\tan(\theta_c)} + 1.5R_t + \sin(\theta_c) = 2.66 \text{ in}$$

$$L^* = \frac{V_c}{A_t} \Rightarrow \text{Solve for } L_{cyl} = 9.8 \text{ in (including catalyst bed)}$$

The combustion chamber length calculated using the contraction ratio of 1.6 defined by Huzel and Huang was excessively long due to the added catalyst bed. Our team decided to increase the contraction ratio to 3.25 resulting in the final geometry:

**Nozzle exit diameter:** 7.42 [in]  
**Throat diameter:** 2.72 [in]  
**Combust chamber diameter:** 5.01 [in]  
**Combustion Chamber Length (including cat bed):** 18 [in]

Further testing on combustion chamber length vs engine performance will be required to minimize the final length of the combustion chamber to minimize mass.

While there is still much to be done in properly designing the nozzle cooling system, a very simple model can be used to explain the basis behind the team's design goals. A 1-dimensional heat transfer model, from the inside of the combustion chamber to the outside, can be modeled as three resistors in series.

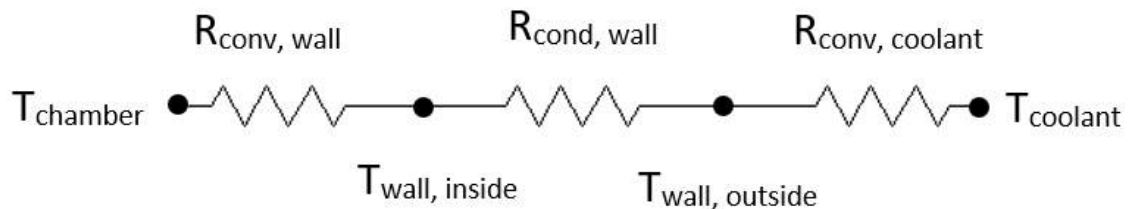


Figure 3.3.1.7: 1-D nozzle heat transfer model for combustion chamber and nozzle

$R_{\text{conv, wall}}$  indicates the resistance of convection from the combustion gases to the nozzle wall,  $R_{\text{cond, wall}}$  indicates the resistance of conduction through the nozzle wall, prior to contacting the cooling channels, and  $R_{\text{conv, coolant}}$  indicates the resistance of convection from the nozzle wall to the coolant in the cooling channels. The stagnation temperature, or  $T_{\text{chamber}}$ , has been designed for 2734 K; however, the melting temperature of potential nozzle materials, such as Inconel or Hastelloy, are in the range of 1300 K - 1400 K. Therefore, to avoid melting the combustion chamber walls, the temperature drop across  $R_{\text{conv, wall}}$  will have to be significant, such that  $T_{\text{wall, inside}}$  remains a factor of safety below the material's melting temperature. To achieve this temperature drop, this resistance circuit can be compared to a voltage divider. The equation to solve for the wall temperature then becomes:

$$T_{\text{wall}} = T_{\text{chamber}} - \left( \frac{R_{\text{conv, wall}}}{R_{\text{conv, wall}} + R_{\text{cond, wall}} + R_{\text{conv, coolant}}} \right) (T_{\text{chamber}} - T_{\text{coolant}})$$

To minimize  $T_{\text{wall}}$ , the second term must be maximized. Hence, the resistance to convection must be proportionally much larger than the other two resistances. Since the resistance to conduction will be relatively small and likely will not change much, due to geometric constraints and structural reasons, the main goal becomes lowering  $R_{\text{conv, coolant}}$  as much as possible. The image below gives an idea of how the cooling channels in this nozzle may look.

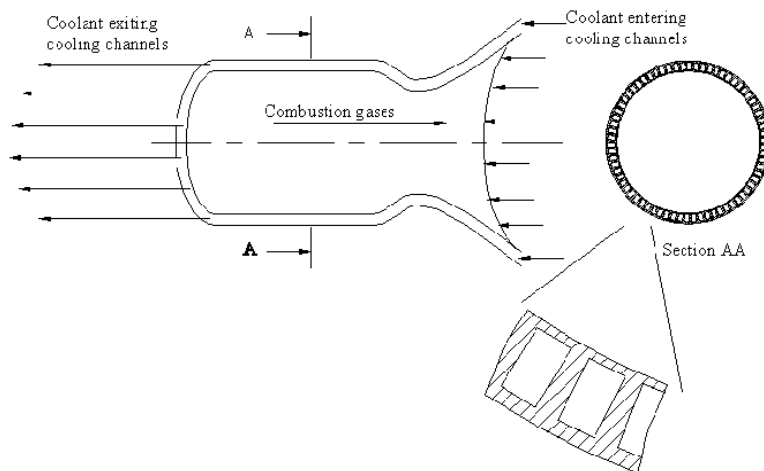


Figure 3.3.1.8: Design idea for nozzle cooling channels [3.8]

To accomplish a geometry like this, the most cost-effective way will most likely be to 3D print the nozzle. With this geometry, the material in contact with the coolant can be approximated as multiple fins in parallel with one another. To minimize  $R_{\text{conv, coolant}}$ , the surface area of material in contact with the coolant must be maximized, and the heat transfer coefficient  $h$  will have to be maximized as well. Therefore, a higher flow velocity through the cooling channels is desirable, as this will increase  $h$ .

Another way to minimize  $T_{\text{wall}}$  is to keep  $T_{\text{coolant}}$  as low as possible. To achieve this, the mass flow rate of the coolant will become critical, as a greater mass flow rate will allow for a lower coolant temperature throughout the nozzle and combustion chamber walls. Lastly, another way to decrease  $T_{\text{wall}}$  is to increase  $R_{\text{conv, wall}}$ , or in other words, add a contact resistance in series between  $T_{\text{chamber}}$  and  $R_{\text{conv, wall}}$ . This can be accomplished using an ablative material or coating on the surface of the chamber walls, which will require more research as the propulsion design progresses.

It is understood that a more detailed heat transfer model will need to be developed, as well as complete calculations. This more robust model is still in development.

### 3.4 Injector

The injector is designed to be easily manufacturable to allow for testing of different hole patterns. One of the goals of the injector is that it can maintain adequate separation of the kerosene and peroxide until they are injected into the combustion chamber. There should be about a 25% pressure drop across the injector to avoid the flame propagating backwards. The flow streams when injected will impinge upon each other to create a mist. This will maximize the mixing between the reactants to have the most complete combustion.

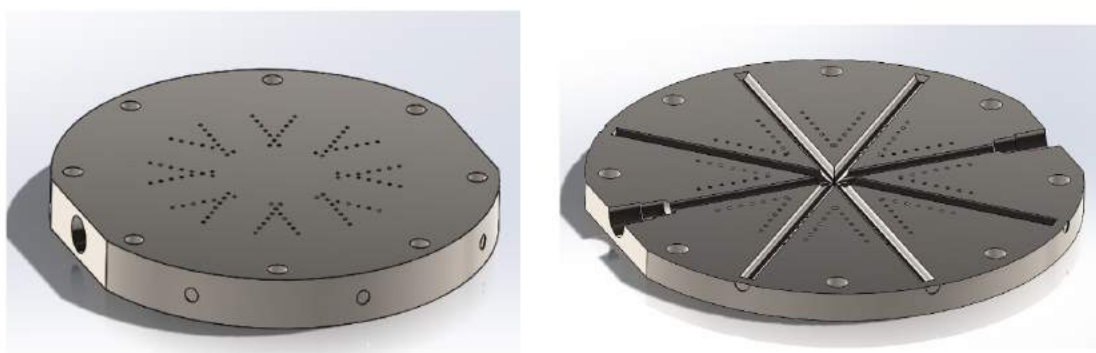


Figure 3.4.1: Injector plate preliminary design.

The injector orifices are sized such that the streams impinge on each other with similar momentum, maintain a pressure drop of 25% of the combustion chamber,

and are sized such that the mass flow is choked (See Appendix D for calculations). The results are shown below:

Table 3.4.1 Injector orifice parameters

Symbol (units)	HTP	RP-1
Mass Flow (kg/s)	5.64	.81
Number of Holes (-)	32	16
Pressure Drop (psi)	100	100
Density (kg/m <sup>3</sup> )	8.86	810
Orifice Diameter (mm)	3.16	1.44

As seen above, the hole diameters have been determined for the oxidizer and fuel to achieve the desired mass flow rate and pressure drop given the predetermined design parameters. This calculation, however, does not address the hole pattern and how the streams will impinge upon one another.

Along each line of RP-1 holes, the holes will be divided into pairs, each of which will impinge on one another at an angle yet to be determined. Note that this is a design feature that was recently added, and therefore is not present in the CAD model of engine design #3. The oxidizer holes, which will straddle the line of RP-1 holes, will be angled as well, such that they impinge at the same point as, or possibly slightly downstream of, the RP-1 impingement point. The figures below depict the fuel (red) and oxidizer (blue) trajectories.

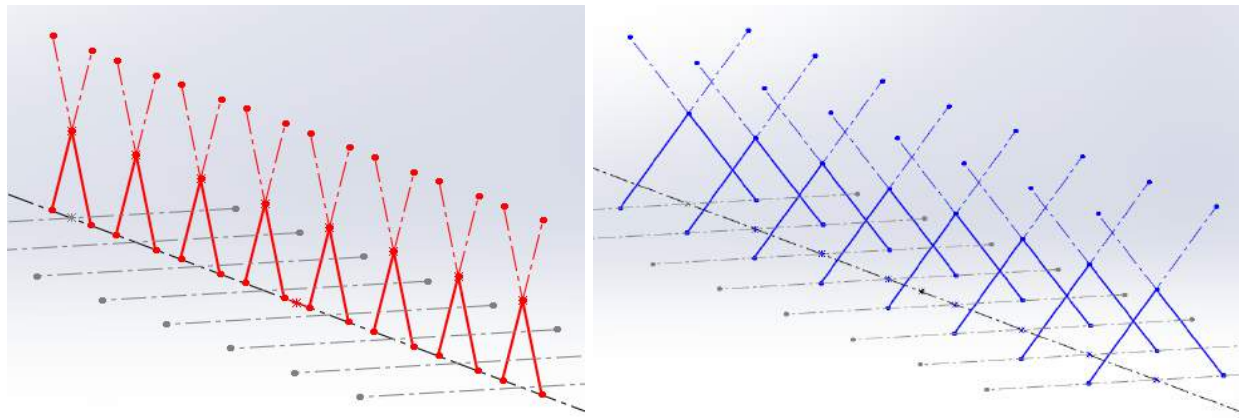


Figure 3.4.2: Fuel (left) and oxidizer(right) injection path for one line of holes.

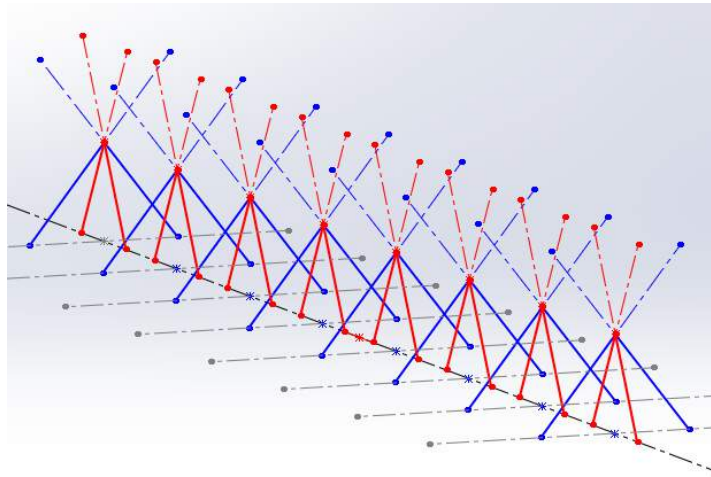


Figure 3.4.3: Fuel (red) and oxidizer (blue) combined injection impingement.

Note that these figures only resemble the fluid trajectories for one individual line of RP-1 holes, which is radially patterned in the complete design. More analysis will need to take place involving what impingement angles are ideal, as well as how far from the injector plate the fluids should impinge, as this has a direct influence on heat flux applied at the surface of the injector plate. Once a final design has been decided on, various hole patterns will be tested to measure which performs the best,

### 3.5 Catalyst Bed Design

Silver-plated monel mesh (40 x 40, 0.015" opening) packed into a  $\mu$  catalyst bed will be used to decompose 5.64 kg/s HTP to gaseous oxygen and superheated steam before combustion chamber injection.

Silver-plated monel mesh was chosen over pellets because mesh can be more meticulously manufactured to meet the catalyst performance specifications. Additionally, with a large HTP flow rate, a maximum surface area of silver will be necessary. To use pellets, a fine "almost dust" of silver would be needed to

theoretically have the same catalyst performance for the mass of catalyst in the bed. Additionally, the high temperatures of the catalyst bed would melt the silver pellets.

The effluent mixture will have a temperature greater than the auto-ignition temperature of the kerosene, oxygen mixture; a key component in engine startup.

### 3.5.1 Dimensions

A thermodynamic and chemical analysis of the catalyst bed over its length was done to determine a design length of 4 inches. Theoretical optimization of the radius to minimize the pressure drop was done and a radius of 3 inches was found. A minimum pressure drop of  $42.2 + 0.3t$  psi [t is in seconds] was found.

It should be noted that the kinetic data used in these calculations have been pieced together from multiple sources that do not accurately represent the temperature range in which the catalyst bed will be operating. Changes in mesh size, packing strategy, and catalyst preparation will affect these dimensions. Catalyst optimization and preparation procedures will be done experimentally, and an optimal radius and length will be found during full-scale catalyst bed testing.

### 3.5.2 Thermal analysis

The catalyst bed was modeled as an ideal plug-flow reactor. Cooling was assumed to be due only to ambient air. Thermodynamic properties were gathered from the NIST chemical properties database. Kinetic data was gathered from [3.3].

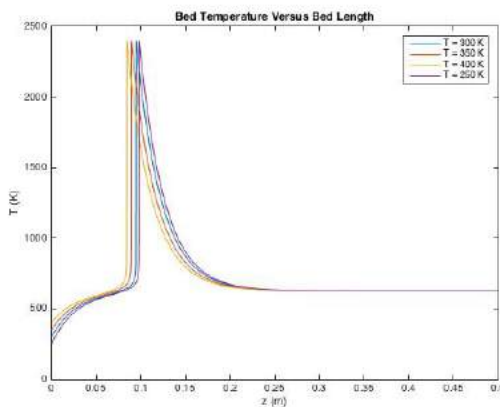


Figure 3.5.2.1: Temperature vs. Length from inlet at various HTP feed temperatures.

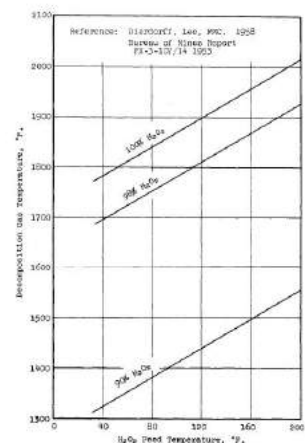


Figure 3.5.2.2: Decomposition temperature vs. inlet temperature. [3.4]

Although, the temperature profile exhibits a maximum of 2,400 K, this will not be observed in practice. Figure 3.5.2.2 shows that at an inlet temperature of 70°C (160 °F), the decomposition temperature should be approximately 1100 K.

Therefore, this model is only being used to determine the length of the catalyst bed and the amount of catalyst needed for decomposition.

The kinetic data used for this model was determined ranging from -20 °C to 112 °C [3.5]. The experimental decomposition kinetics displayed a distinct transition in reaction mechanism at 20°C. Kinetic data at the catalyst bed operating conditions was extrapolated and it was assumed that no further reaction mechanism change occurred. Due to the excessive temperature maximum found in the catalyst bed model, this assumption is not valid. High-temperature kinetic data will be experimentally obtained to increase the validity of the catalyst bed model. Full-scale catalyst bed testing will provide an experimental temperature model. Team members are enrolled in independent research study to solely focus on catalyst bed testing.

### 3.5.3 Chemical analysis:

The remaining fraction of HTP is defined as the molar fraction of HTP remaining in the oxidizer stream after passing through the catalyst bed. Explicitly it can be written as follows:

$$\frac{N_{\text{feed}} - N}{N_{\text{feed}}}$$

Where  $N_{\text{feed}}$  is the molar concentration of the catalyst bed feed and  $N$  is the molar concentration of the catalyst bed effluent stream. The remaining fraction of HTP approaches zero four inches down from the catalyst bed inlet. This determined the design length of the catalyst bed. A higher HTP feed temperature was correlated with a lower design length.

This model assumes ideal mixing in the radial direction. Development of an efficient HTP injector plate will be necessary to validate this assumption. Similar concerns about the validity of the kinetic data at high temperatures is present in this chemical model. High-temperature kinetic data will be experimentally obtained to increase the validity of the chemical model. It will be difficult to obtain a HTP fraction profile doing full-scale catalyst bed testing, but such data will not be necessary unless it is evident that the reaction mechanism will transition down the length of the catalyst bed. Optimization of the catalyst mesh will allow the length of the catalyst bed to be the sole factor in determining the conversion of HTP.

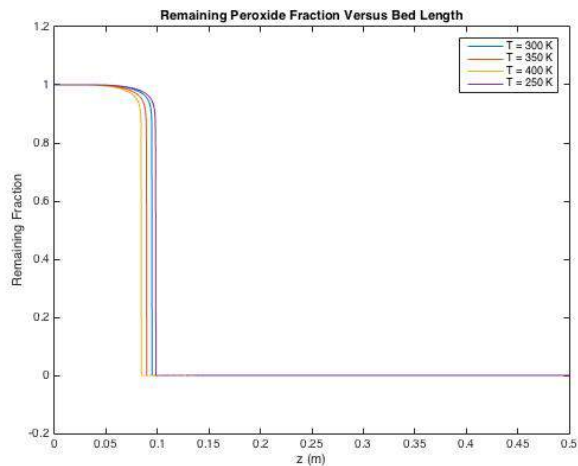


Figure 3.5.3.1: Remaining HTP Fraction vs. length from inlet for various HTP feed temperatures.

## 3.5.4 Catalyst Bed Testing and Development

### 3.5.4.1 Silver Plating Monel Mesh

Silver plated monel mesh screens will be used as the catalyst for the WI Space Race engine. Using these, we will be able to experiment with different configurations of screens (including the total number of screens), and different mesh sizes. Our team plans on plating these screens ourselves, rather than outsourcing them so we can develop an optimal procedure that is accurately reproducible in our lab. (See Appendix C for Silver Plating Procedure).

### 3.5.4.2 Experimental Goals

Optimization of the silver-mesh catalyst is defined as the maximization of HTP decomposition to catalyst mass ratio. Small-scale catalyst testing will be done to determine the effect of current density,  $\text{Ag}^+$  ion concentration, and plate thickness on catalyst optimization. Full-scale catalyst bed testing will be done to test the effects of mesh size, catalyst bed packing strategy, catalyst bed radius, and length on the minimization of pressure drop and catalyst performance. Additionally, full-duration burns will be performed to verify catalyst bed thermal integrity.

Pressure drop was theoretically found to be:  $42.2 + 0.3t \text{ psi}$  [ $t$  is in seconds]. Variables affecting the pressure drop are tortuous flow problems as well as screen clogging of pores due to silver loss. This gives a linear pressure drop increase with time. The pressure drop was calculated using this silver-loss kinetic data, Equation

4-49 from "Design of Liquid-Propellant Rocket Engines" from NASA, and the Ergun Equation.[3.6]

Full-scale catalyst bed testing will allow for experimental parameters to be fit to Equation 4-49 from "Design of Liquid-Propellant Rocket Engines" to model the pressure drop over time.[3.6]

### 3.5.4.3 Catalyst Test Reactor Design

The small-scale catalyst test reactor will employ a  $\frac{3}{8}$  inch tubular reactor and will operate adiabatically. HTP will be fed to the reactor at 0.1 g/s. Temperature data will be taken to determine the chemical efficiency of the catalyst. Reactor effluent will be collected, condensed, and analyzed using gas chromatography to determine the catalyst yield.

### 3.5.4.4 Full-Scale Catalyst Bed Test Design

The catalyst bed test design will employ a set of pressure taps to measure pressure drop over time. Thermocouples will be spaced throughout the radius of the bed to determine a temperature profile. Effluent will be collected, condensed, and analyzed using gas chromatography to determine the reaction yield.

## 3.6 Valves & Plumbing

The feed system of the rocket was designed to minimize size and mass, while maximizing safety. It is composed of the following components:

- Helium pressurant tank: Provides pressure for the propellant tanks (regulated to tank pressure)
- RP-1 tank: Stores pressurized RP-1 fuel
- Hydrogen peroxide tank: Stores pressurized HTP oxidizer
- Pneumatically actuated ball valves: 2-way valves, main run valves for engine
- Solenoid valves: Allows for remote depressurization, filling and emptying of propellant tanks and helium tanks, and provide low pressure helium to ball valves for actuation
- Pressure regulators: Regulates high pressure Helium to feed system pressure
- Relief valves: Relieves excess feed system pressure
- Burst discs: Emergency mechanism to relieve system pressure in overpressurization event
- Check valves: Restricts fluid flow to one direction; prevents unwanted mixing of fuel and oxidizer
- Pressure transducers: Measures pressure differences
- Thermocouples: Measures temperature

The helium tank is pressurized to 2000 psia and is regulated down to approximately 600 psia for the propellant tanks, which ensure constant feed

pressure as the propellant is fed through the engine. A bust disc, relief valve and electrically actuated vent valve is connected to both propellant tanks to relieve excess system pressure. The propellant is isolated from the engine with pneumatically actuated ball valves. Lines of 316-stainless steel were chosen for the feed system because it is compatible with HTP and readily available.

The feed system pressure was calculated by summing the combustion chamber pressure, pressure drops at the injector, catalysts bed, and pressure losses in the feed lines. The injector is designed to have a 20% pressure drop (relative to combustion chamber pressure), resulting a pressure drop of 80 psid. This is a typical design parameter used in industry, and is suggested as a starting point in "Modern engineering for design of liquid-propellant rocket engines" to ensure perturbations in chamber pressure cannot propagate back into the catalyst bed and/or feed system [3.7]. Furthermore, the injector is sized such that the flow is choked. This ensures there is a constant mass flow through the injector without adding a device for metering the propellant flow, thus reducing system complexity, weight and pressure losses.

The flow through the catalyst bed is a two-phase flow through a tortuous path, thus estimating the pressure drop through this region is not possible. To estimate this, our team spoke with an employee of Sierra Nevada Corporation that had experience with designing and testing catalyst beds for rocket propulsion. The employee stated that the pressure drop will likely be in the range of 50-100 psid, and that 50 psid should be achievable with moderate development and testing. Our calculations used the upper end of this estimate as a worst case scenario.

Frictional losses in the feed lines were calculated using the Darcy-Weisbach and Colebrook equations:

$$\Delta P = \rho \frac{fL}{2D} V^2$$

$$if Re > 2200 \Rightarrow \frac{1}{\sqrt{f}} = -2 \log \left( \frac{\epsilon}{3.7d} + \frac{2.51}{Re\sqrt{f}} \right)$$

$$if Re \leq 2200 \Rightarrow f = \frac{Re}{64}$$

The feed lines were then sized based on guess and check methods using MATLAB (See Appendix D). This resulted in 1.5 in OD feed lines for the peroxide system and 0.5 in lines for the kerosene system, resulting in a total feed pressure of 605 psia. An overview of the P&ID is shown below in Figure 3.6.1:

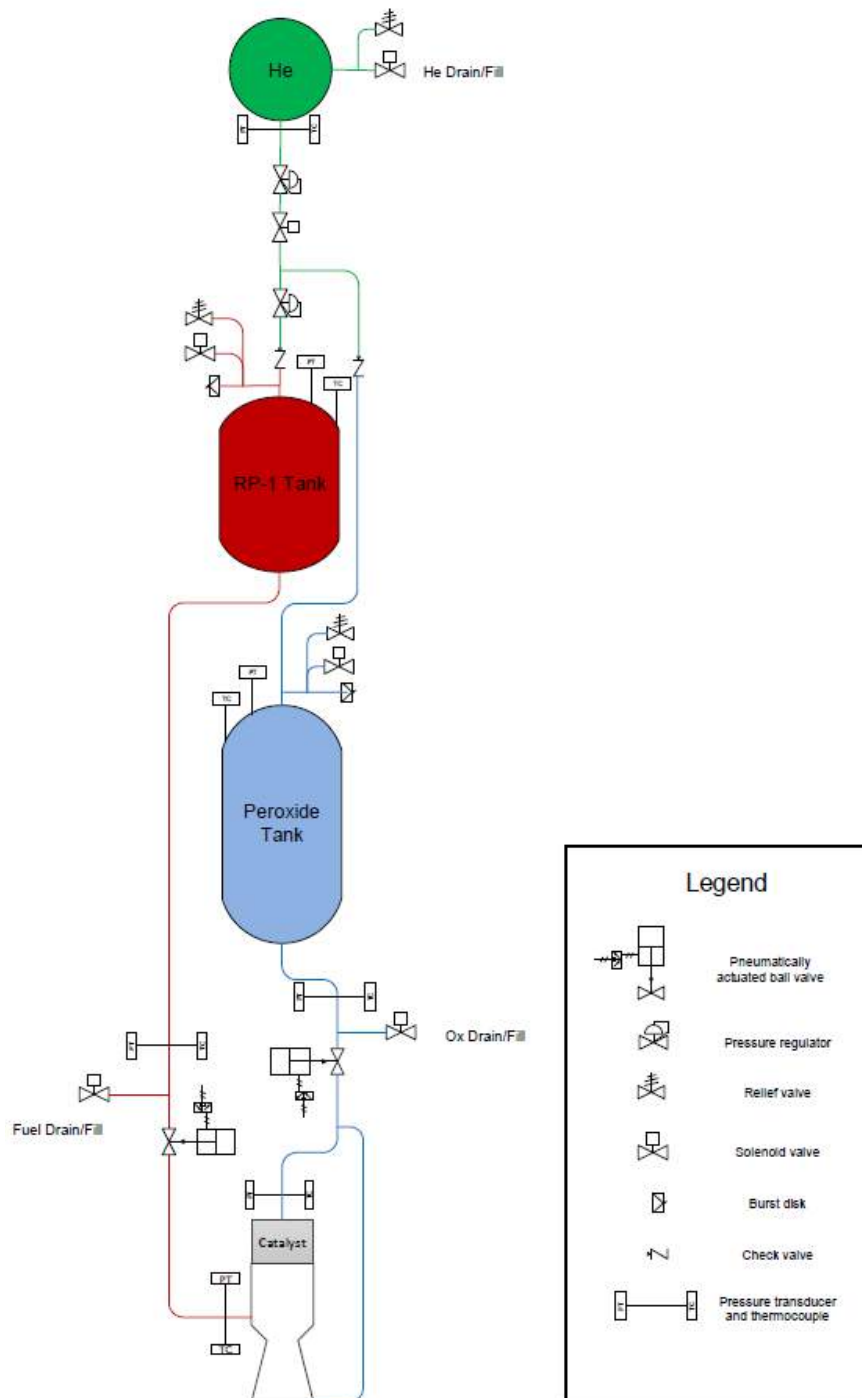


Figure 3.6.1: P&ID for the feed system of the WI Space Race Rocket.

# 4.0 Engine test stand design and test plan

## 4.1 Test Engine

The test engine will have all the main features of the rocket engine; however, it will do so in a minimalistic fashion. The internal nozzle geometry will be machined out of round copper stock, leaving the rest of the material. This will create a highly thermally conductive, high thermal capacitance heat sink surrounding the combustion chamber and nozzle. The geometry of this piece will be designed such that, in the short duration that the hot fire test is run, the temperature rise within the part will be negligible. Creating the test engine in this fashion will also allow for ease of placing thermocouples and pressure transducers, which will be used to measure the following locations along the engine.

Table 4.1.1: Test engine sensor locations

<b>Location</b>	<b>Pressure</b>	<b>Temperature</b>
Before catalyst bed	X	X
After catalyst bed, before injector plate	X	X
Immediately after injector plate, inside combustion chamber	X	X
Inside combustion chamber, immediately before converging section	X	X
Nozzle throat	-	X
Nozzle exit	-	X

The thermocouples will be inserted into blind holes drilled radially into the copper piece, leaving a small gap between the bottom of the hole and the internal geometry of interest. By placing the thermocouples against the bottom of these holes, the estimated wall temperatures can be measured. The pressure transducers will be installed by incorporating radially-drilled thru holes at each location of interest, along with NPT tapped holes. Since the pressure transducers require the internal geometry to be modified, the pressure cannot be read at the throat or exit of the nozzle, since it may cause flow separation or otherwise affect the propulsion characteristics.

From this data, the chamber stagnation pressure, as well as the pressure drop across the catalyst bed, and injector plate, and combustion chamber can be determined. The wall temperatures of the nozzle and combustion chamber can also be determined, which, with analytical tools, can be used to approximate the chamber temperature immediately after the injector plate and after the combustion has fully developed.

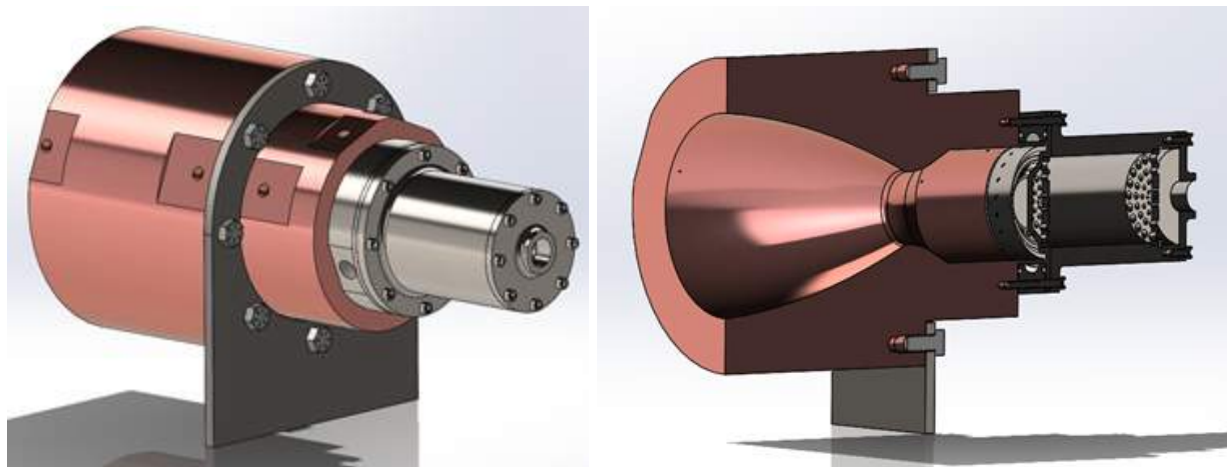


Figure 4.1.1: Test engine rendering and geometry.

## 4.2 Test Stand

The WI Space Race team is fortunate to have Sierra Nevada Corporation (formerly Orbitec) in the city of Madison, WI. The company has decades of experience developing propulsion systems, and will be an invaluable resource for the development of our engine. Our team is currently in contact with them, and we are extremely optimistic that we will be able to use their test facility for the development of our engine. Their facility currently has a vertical test stand that was used for the development of an engine with similar thrust, which we hope to use.

As a backup plan, UW-Madison has a plot of land outside of the city that is currently used for shock tube testing and other dangerous experiments. The major drawback of using this facility is the fact that we would have to build our own data acquisition system and propellant storage facility.

Based on these assumptions, our team has focused on designing the feed system for the test engine. The test stand feed system is minimalistic, and is very similar to the feed system of the launch vehicle. Additional isolation valves were added for safety purposes, more instrumentation is added for data analysis, and a cavitating venturi is used upstream of the engine to ensure a constant mass flow rate. The following P&ID outlines the test stand feed system (Figures 4.2.1 and 4.2.2).

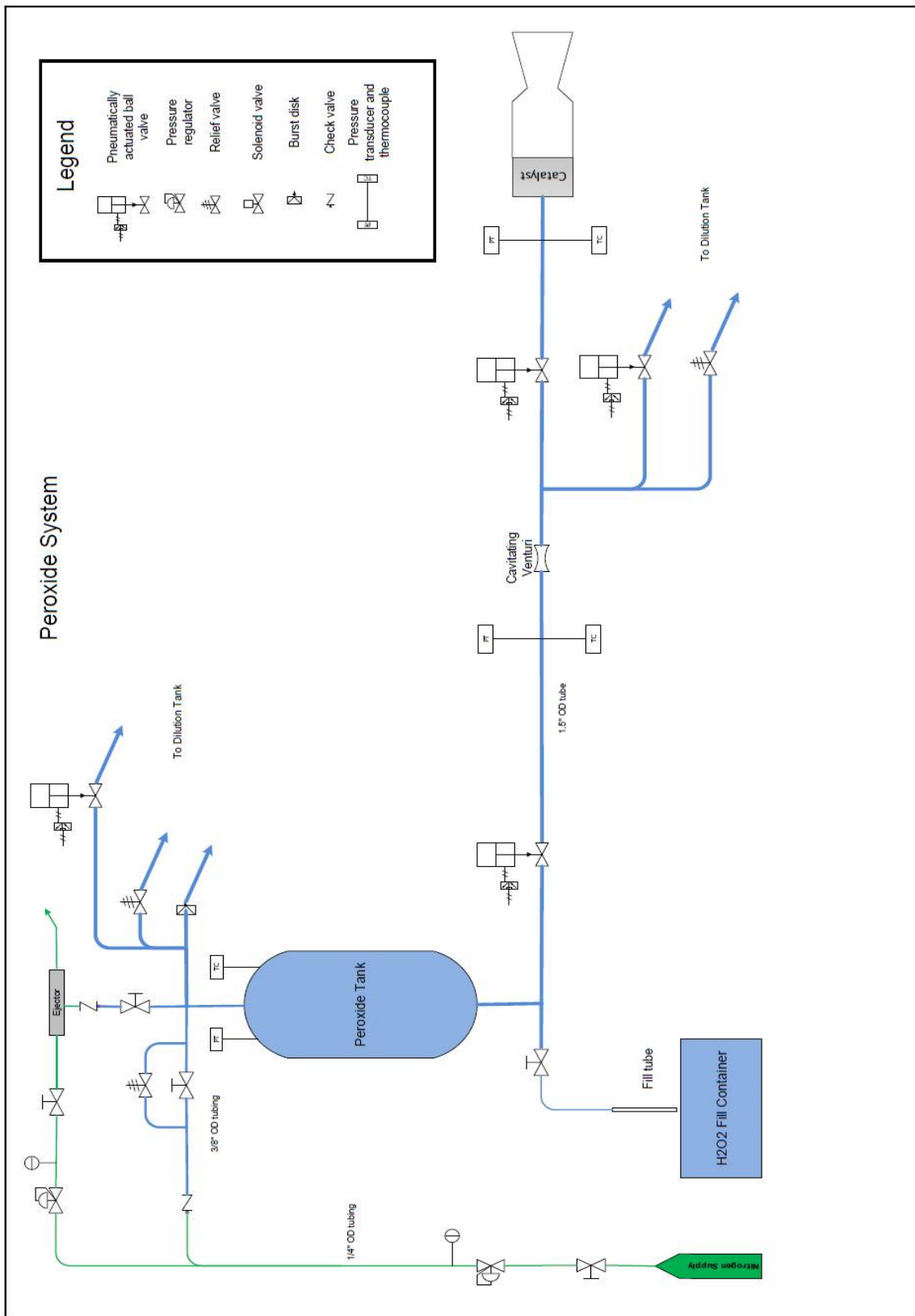


Figure 4.2.1: peroxide system P&amp;ID

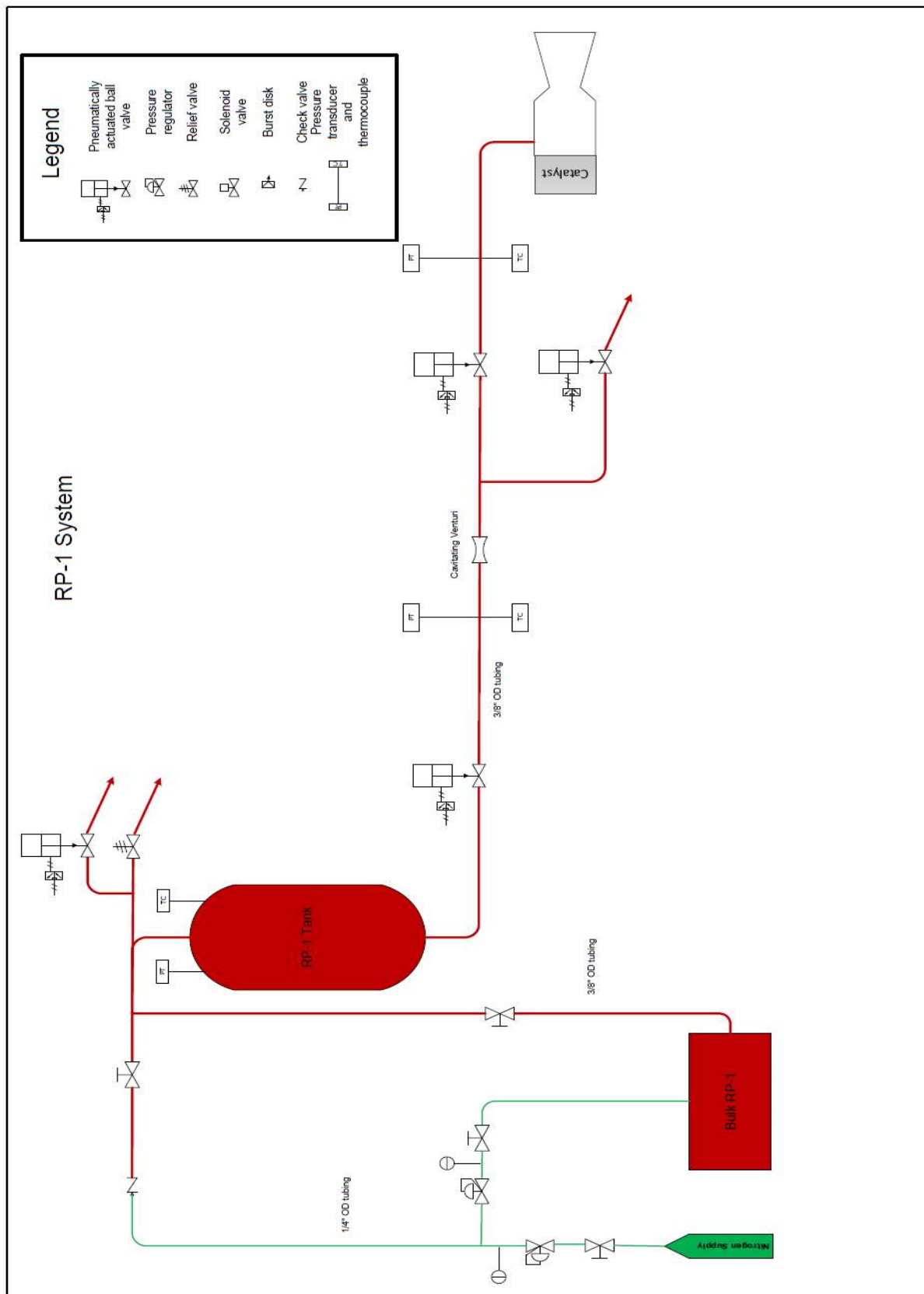


Figure 4.2.2: RP-1 system P&ID

## 4.3 Test Plan

The engine will be developed such that the engine meets or exceeds all requirements set out by the Base 11 System Requirements, as well as mission constraints obtained in Section 2. The primary performance parameters required are as followed:

- Provide stable combustion for ~60 seconds with minimal loss in system performance
- Produce 15 kN ( $\pm 0.5$  kN) thrust at sea level with mission optimized nozzle
- Provide a minimum specific impulse of 259 s

The primary components that will be tested for further development are the catalyst bed and injector. Both components are designed to be easily machinable and modular to allow for testing of different designs. The injector will be tested with different hole patterns for combustion and mass flow improvements. The catalyst bed will be tested with different catalyst configurations to ensure steady decomposition of 90% hydrogen peroxide for 60 seconds with allowable catalyst consumption and pressure drop creep. Additionally, different combustion chamber lengths will be tested using spacers between the combustion chamber inlet and injector. Testing different combustions chamber lengths will optimize combustion chamber volume with respect to the combustion performance of the engine.

# 5.0 Range Safety Systems

## 5.1 Trajectory Control

To ensure the WI Space Race rocket does not fly over or land in a populated area, the rocket will only be launched in ideal conditions, and with the launch rail set to a (small) angle to allow the rocket to ascend on a nominal trajectory (See Figure 5.1.1). Additionally, the flight computer (and ground tracking) determines its trajectory based on current GPS (if still under COCOM limits) and IMU readings. If the trajectory is predicted to deviate from the nominal trajectory, the Flight Dynamics Officer and Safety Officer will assess the situation and command an abort accordingly.

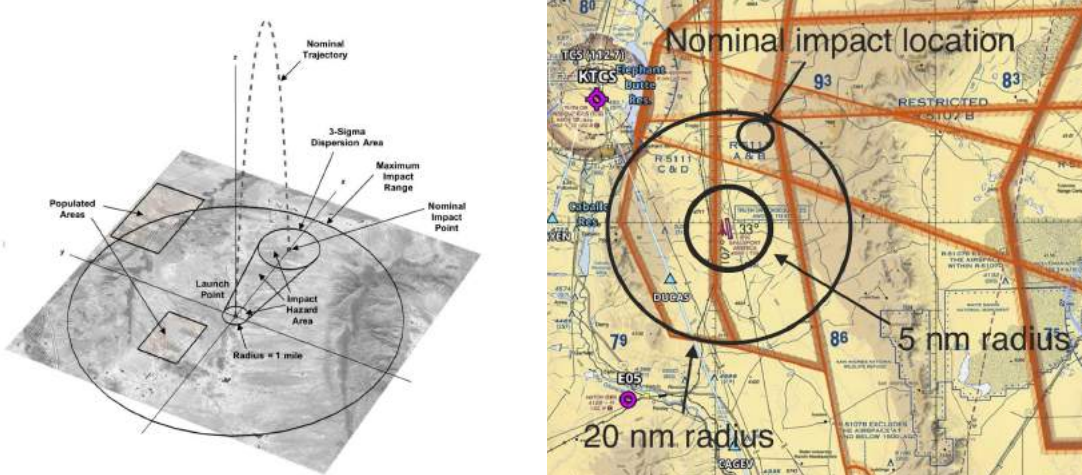


Figure 5.1.1: Left: Nominal trajectory outlined by Base11. Right: WI Space Race's proposed trajectory.

## 5.2 Drift Predictions

Upon descent, the rocket will follow a ballistic trajectory until 30 km in altitude, where the drogue parachute will deploy (outlined in Section 10.1 Parachute Sizing and Deployment Altitude). During this phase of flight, the rocket will still have substantial vertical velocity (See Figure 5.2.1). At approximately 15 km in altitude the rocket decelerates rapidly to a velocity of  $\sim 100$  m/s. It is at this point where drift predictions become important. The rocket will take approximately 300 seconds to impact after drogue deployment. Winds at high altitudes can be as high as 100 mph (50 mph is typical). This means the rocket could drift as far as  $\sim 7$  km during this phase. To remain within the maximum impact range, the rocket must not travel more than 10 km horizontally in any direction during the boost, coast, and ballistic phase.

To ensure the rocket stays within the maximum impact range, and lands within the nominal impact range, the Flight Dynamics Officer (FIDO) will use winds aloft data on days leading up to, and at the time of launch to give a calculate the predicted impact location and nominal launch rail angle. If winds are not favorable (strong westerly, or southerly winds), The FIDO will then give a “no-go” command for launch and the mission will be scrubbed.

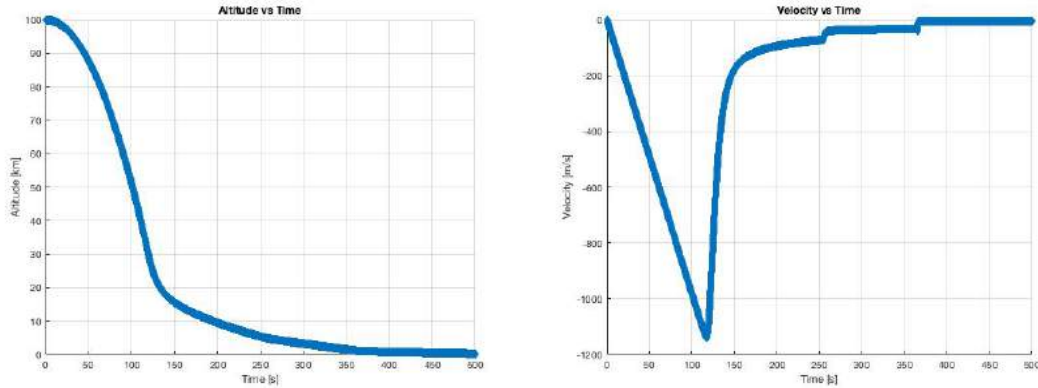


Figure 5.2.1: Left: Altitude vs Time during descent phase. Right: Vertical Velocity vs Time during descent phase.

## 5.2 Propulsion Aborts

Propulsion aborts are aborts occurring during the ‘firing’ mission phase, where the engine is active and thrust is present. A propulsion abort results in immediate engine shutdown and propellant dumping; the system then proceeds to the ‘coasting’ state as normal and triggers normal recovery operations (with, if necessary, recomputed altitude thresholds for parachutes).

# 6.0 Airframe Structure

The structure is designed as a semi-monocoque, the load is distributed through both skin and skeleton of the vehicle, while additionally relying on pressure tanks to bear load in their respective regions. There are three distinct portions of the rocket, the main body, the nose cone, and the fins, each having different design approaches tailored to their purpose, see Figure 6.0.0. The main body consists of a stressed skin atop a welded frame. The nose cone is a hollow casting with integral reinforcements. Lastly, the fins are similar to standard riveted wings. Each of these sections and their constituents will be discussed below along with loading cases and manufacturing methodologies.

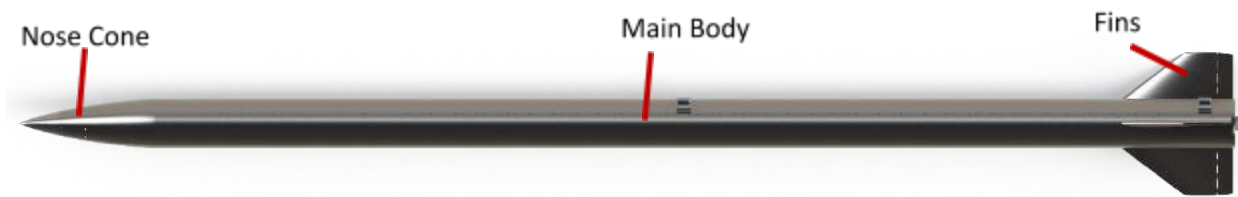


Figure 6.0.0: Breakdown of WI Space Race Rocket Airframe Sections

## 6.1 Main Body

A true monocoque (see Figure 6.1.0) would be the ideal solution for our rocket, as it simplifies the design and can minimize weight. To calculate possibilities for a true monocoque, the skin is idealized as a solid tube, which is assumed to be the only structural member. Two loading conditions are of importance—self-loading using an acceleration equal to the maximum acceleration of the rocket which occurs near burnout, or at a lower acceleration but fully laden by propellant. For the former it is approximated with a maximum acceleration of 4 G's near burnout with only the dry weight of the rocket; for the latter we assume 2 G's with a fully loaded rocket. Additionally, a moment is added to account for pitching moments due to maneuvering and weather, and a torque is added due to maneuvering. The former is approximated as a cross wind gust of 50 m/s and a pitching maneuver with the fin control surfaces at 5 degrees, while the latter uses the 5 degree control surface approximation for torque generation. Approximations made are reasonable for a general sizing of the structure. It is important to note that general approximations are made because as the structure is refined, the weight and the required control surfaces will change, altering the trajectory and vehicle acceleration, which redefines the parameters of the approximations. With a tube that is 7.62 m long with 33.528 cm outside diameter of 6061-T6 aluminum, this presents a tube wall

thickness of 0.254 cm for a safety factor of 50, with buckling of the thin-walled tube under compression being the limiting factor. The safety factor is kept large due to reality imperfections, such as stress concentrations of jointing and lack of straightness. This clearly shows that a true monocoque could work, and having a resultant mass of 55 kg, this would be an effective solution.

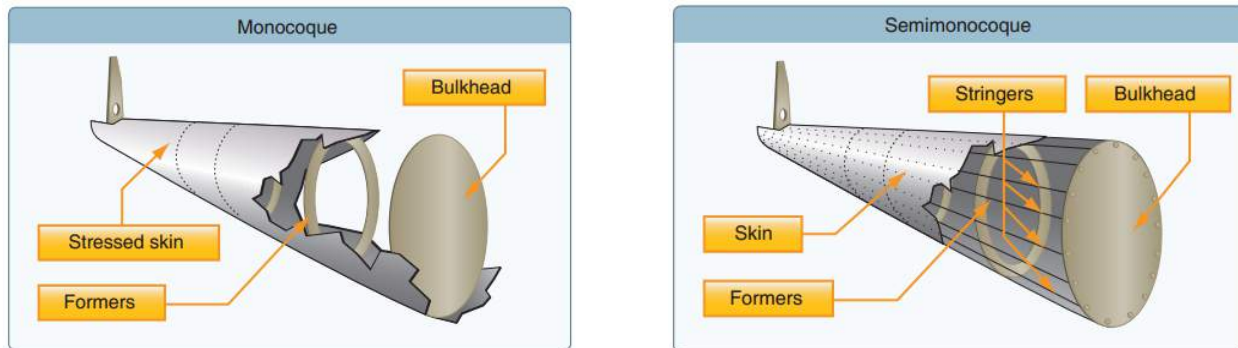


Figure 6.1.0: Diagram of Semi-Monocoque versus Monocoque [AIRSTRU]

However, this design assumes a perfectly distributed loading over the body. In reality, such a design poses problems for internal connections as large stress concentrations are created by the point loads from the connections, along with the fact that direct connections to a wide tube is difficult or impossible for small internal components. Additionally, there is difficulty creating such a structure in sections, a necessary facet to easy transportation of the final rocket. Therefore, an internal skeleton is required to support the connection between internal components and to create a sectioned vehicle, shifting the design from a true monocoque to a semi-monocoque. Normally the internal skeleton/reinforcements of aircraft vehicles are made from formers and stringers specialty crafted of sheet metal and riveted together. However, these are more difficult to produce when not in mass production, so tube stock will be used instead. Therefore, an internal frame of tube stock will be built to support the inter component connections that will work in conjunction with attached skin to carry the total structural load. In addition to the frame and the skin, some internal components can assist in load carrying, such as the main pressure vessels, so some of the structural loading will be offloaded to them.

## 6.1.1 Frame

To connect internal components of the vehicle and support some of the overall load, a skeleton structure will be used. The skeleton consists of tube stock and since weldments are a good fastening method for tube stock, they will be utilized. Welding tube stock creates a frame structure, which is monolithic and stiff, ideal for sectional development and to reduce excessive deflections in such a long and slender rocket. Aluminum is chosen as it has a high strength-to-weight ratio and is a common aircraft material. From the aluminum family, 6061 is chosen due to its ability to weld and moderately high strength-to-weight ratio of 115 kN·m/kg.

There are a few main sections of the frame. The first connects the engine to the oxidizer tank and the second surrounds the oxidizer tank. The third connects the oxidizer tank to the fuel tank and the fourth surrounds the fuel tank. The fifth connects the fuel tank to the pressurant tank and the sixth surrounds the pressurant tank. Finally, the seventh connects the pressurant tank to the nose cone. The following reviews each section.

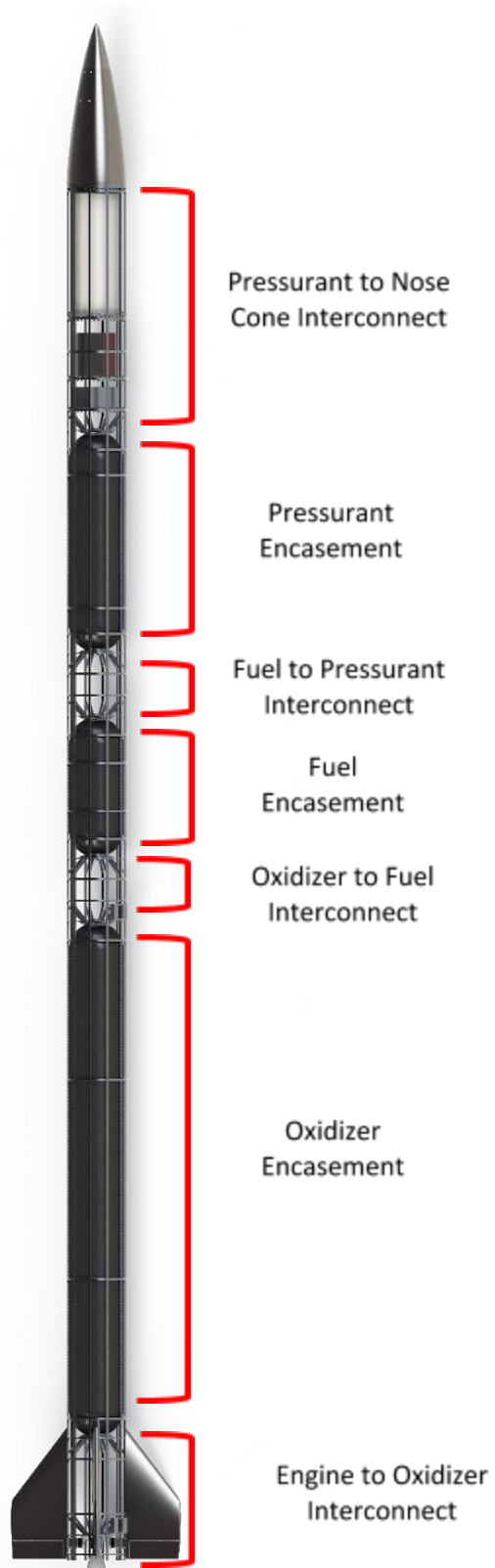


Figure 6.1.1.0: Breakdown of the Skeleton/Frame Sections

### 6.1.1.1 Engine to Oxidizer Tank Interconnect

The engine to oxidizer tank frame is utilized to connect the main engine, the fins, and the lower launch lugs to the structure. As depicted in Figures 6.1.1.1.0 and 6.1.1.1.1, it consists of 10 main struts to take the load of the engine at full thrust, two plates (Figure 6.1.1.1.2), one on each end, acting as mount surfaces for the engine and oxidizer tank, corner struts reinforcing each plate (Figure 6.1.1.1.3), curved sections to reinforce the main struts, and 10 strut-like components used for mounting the fins to. Each of the components is made of 6061 aluminum. The slender members are 0.5 in wide square stock with 0.125 in thick walls, including the curved members, which will be heated and bent to shape as necessary. The plates are 0.25 in thick, 13.2 in diameter and have slots cut in them for the struts to sit in. They also have weight reduction/stiffening holes punched into them, a center hole for the tank or engine to sit in, and a set of holes to be used for bolting. The final frame, post-welding, will be heat treated to the T6 condition to increase strength.

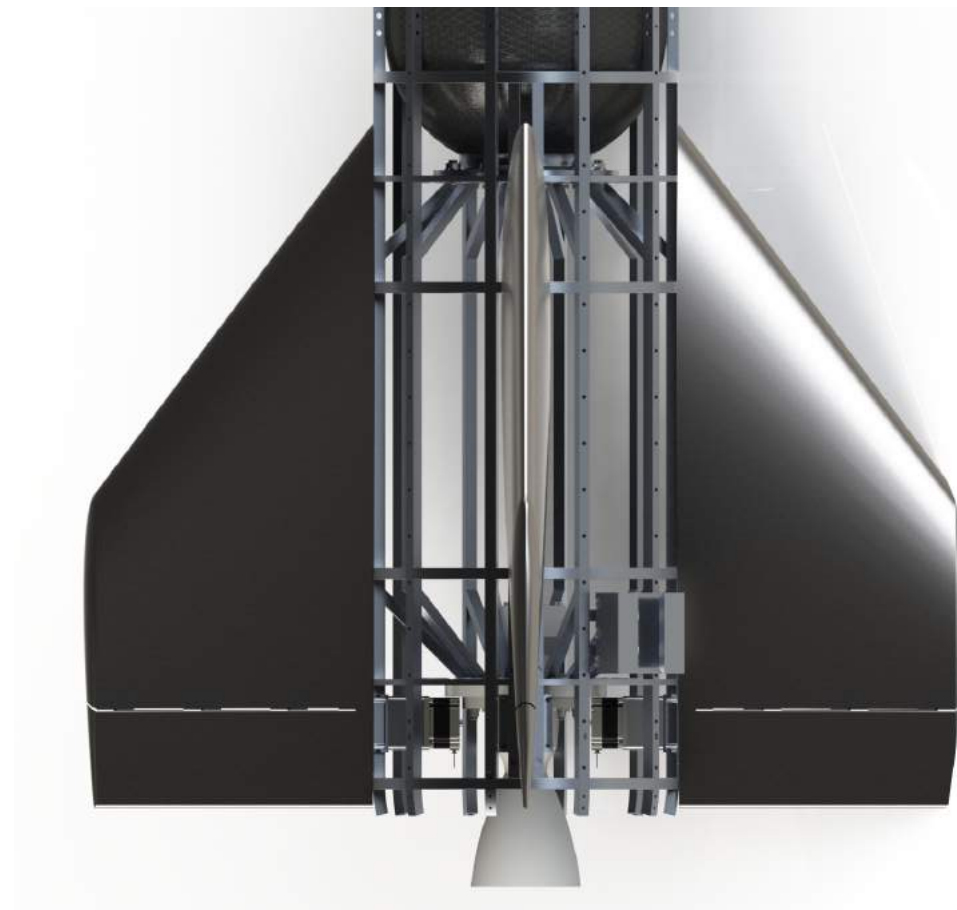


Figure 6.1.1.1.0: Engine to Oxidizer Tank Interconnect: Frame

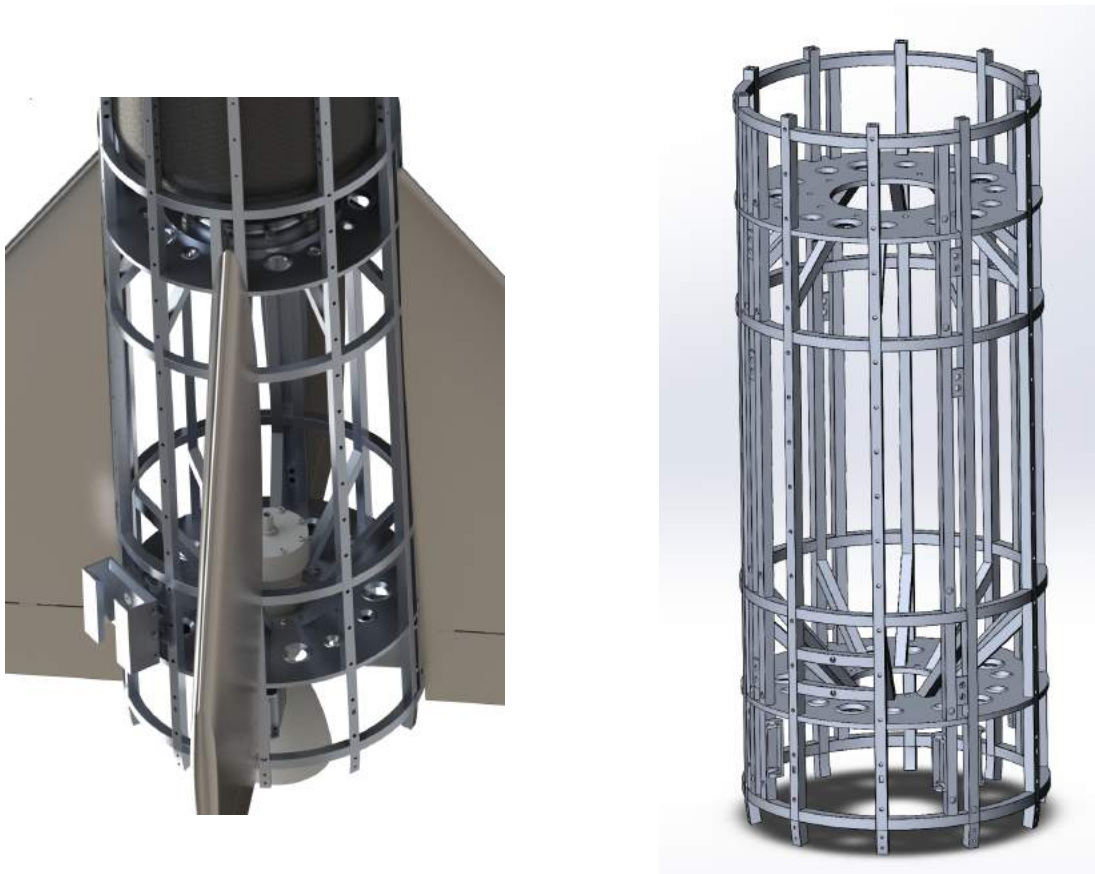


Figure 6.1.1.1.0: Engine to Oxidizer Tank Interconnect: Frame

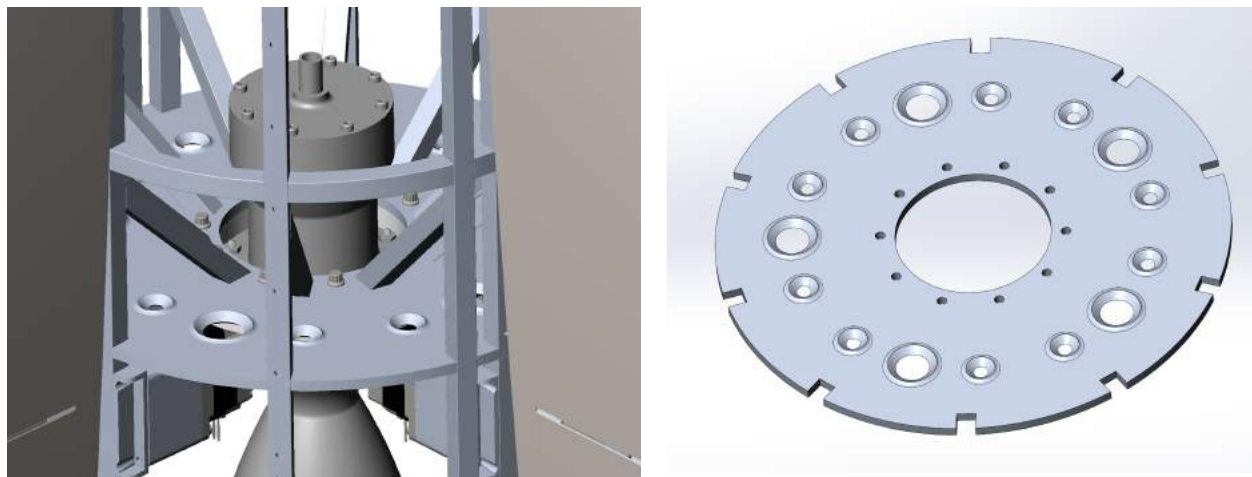


Figure 6.1.1.1.2: Engine to Oxidizer Tank Interconnect: Mounting Plate



Figure 6.1.1.1.3: Engine to Oxidizer Tank Interconnect Corner: Reinforcements

Corner reinforcements are cut and placed at a 45-degree angle, as it is optimal for load distribution, and provides reinforcement adjacent to the bolted area. There are, in addition, two angle brackets used to mount the fin actuation motors and three small strut interconnects with holes to bolt the main mounts of the fins to, per fin section (Figure 6.1.1.1.4). The curved square stock pieces create two rings at one third and two thirds the length of the main struts to force higher buckling modes (they prevent buckling about the center point of the strut, or in effect, halving the length). Another two curved square stock pieces are used to mount the lower launch rail guide via two bolt holes (Figure 6.1.1.1.5). Also, curved square stock is used as a

frame for a boat tail (Figure 6.1.1.1.6). It may be useful to note that the nominal inter-strut spacing leaves approximately 3 in of gap, allowing for a human hand and arm to be inserted between to work on internal components before the skin is applied. Finally, rivet holes are drilled in the outside of the tubes to fasten the skin to the frame.

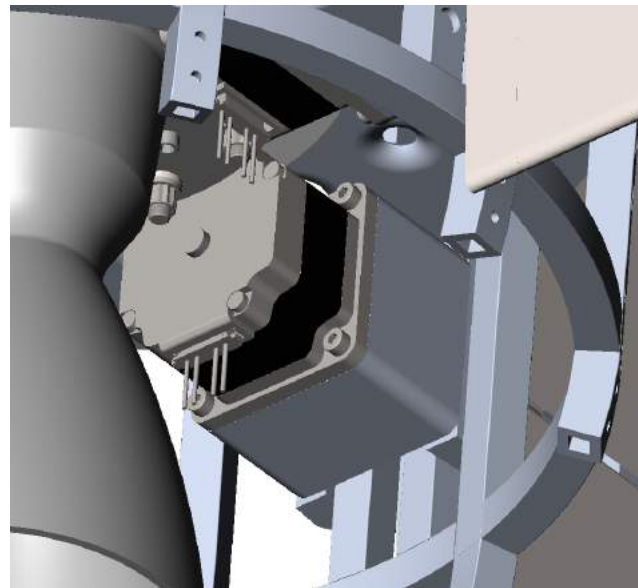
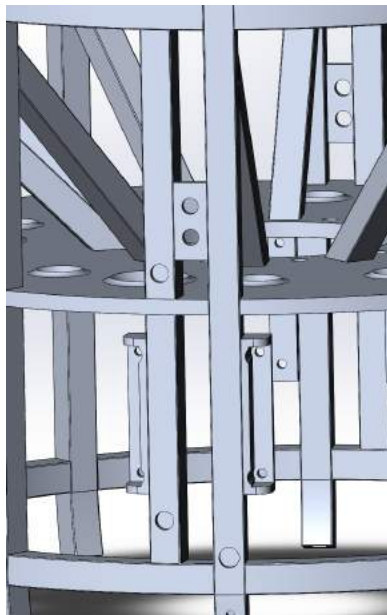


Figure 6.1.1.1.4: Engine to Oxidizer Tank Interconnect: Fin Stepper Motor Mount and Fin Main Mounts

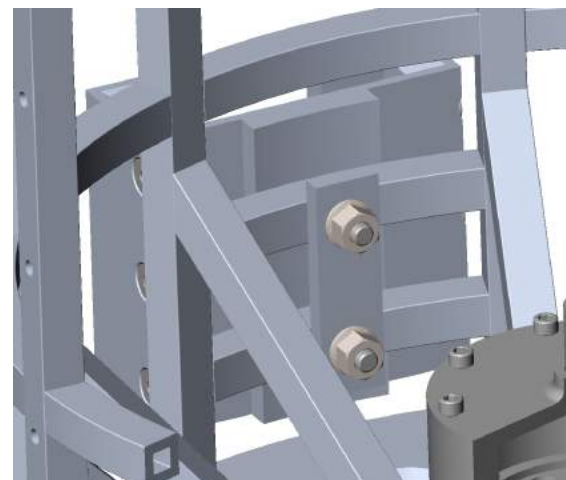
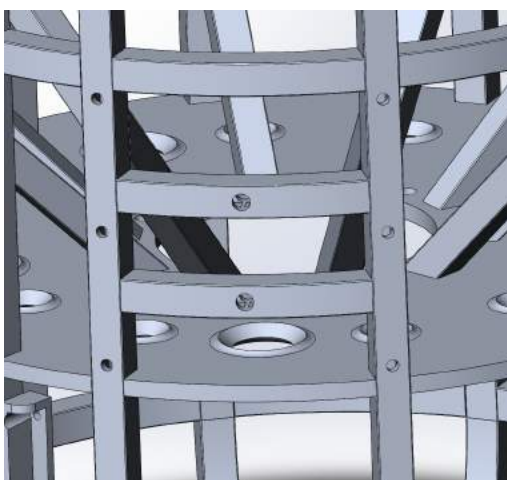


Figure 6.1.1.1.5: Engine to Oxidizer Tank Interconnect: Launch Lug Mount

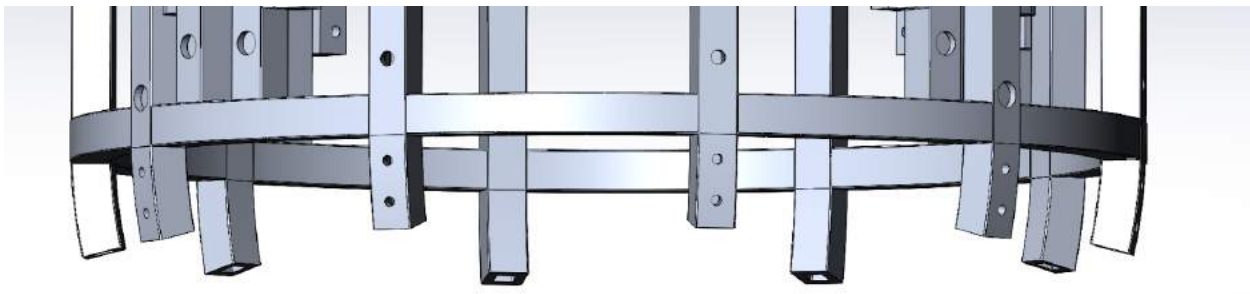


Figure 6.1.1.1.6: Engine to Oxidizer Tank Interconnect: Boat Tail Frame

Mechanics of materials calculations give a minimum safety factor of 3.4, constrained by the bending of the angled corner reinforcement members when loaded fully by the force of the engine. This loading case is an approximation for what happens at lift-off and the larger safety factor is desired due to an assumption of doubly intense loading for impacts, if the ignition is considered an impact. Although the engine does not fire at full thrust initially and takes time to fire up, the difficult-to-determine explosive nature of the firing calls for extra safety. Hot firing the engine can present more accurate data on initial kick and force, leading to an ability to refine these structural requirements. Also, these computations yielded a maximum displacement in the order of fractional millimeters, rendering them negligible. The engine to oxidizer tank was run in a SOLIDWORKS finite element analysis (FEA) with a pressure on the engine mounting plate equal to the engine thrust over the distributed area (Figure 6.1.1.1.6). Albeit not a great simulation tool, SOLIDWORKS FEA will give a reasonable ballpark estimate, and through it a safety factor of approximately two was found, again, limited by the angled reinforcements. This number was validated to an order of magnitude using an inhouse two-dimensional frame simulation script.

Taking an average safety factor of 2 for this section of the design is reasonable; however, it might be a little low if weld stress concentration factors are taken into account, especially for the aluminum (which has a fatigue limit in cyclic loading). Also, given the fact that it acts as a motor cowl, it will become very hot if the engine is not cooled completely. This means that the strength of the aluminum will decrease with the increasing temperature. These last two points present reasons to increase the safety factor. To do so, more angled members could be used, but before design modifications are done, hot fire testing is advised to obtain more proper loading data. Future work on this section includes model updating for more components, a three-dimensional frame analysis inclusive of vibrational analysis, ANSYS simulations for both static and vibrational loading, heating analysis, and model validation via testing (static and shaker table).

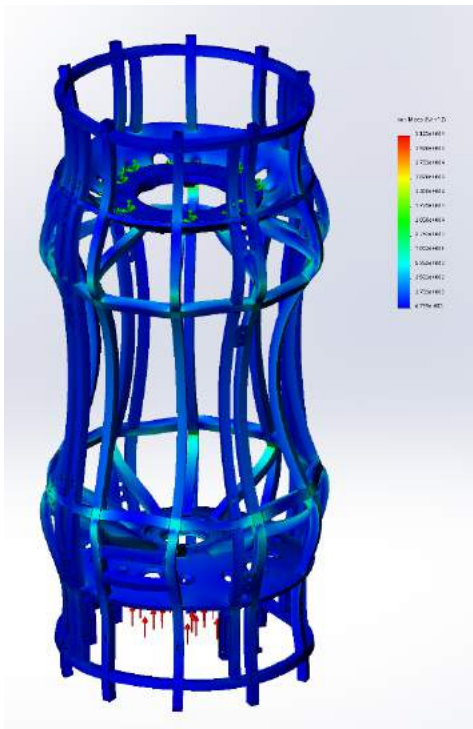


Figure 6.1.1.1.6: Engine to Oxidizer Tank Interconnect: SOLIDWORKS FEA

Mounting of the Engine will occur by increasing the diameter of the flange used to tie the combustion chamber to the injector/catalyst bed and adding a bold circle for fastening. This will then attach to the engine mounting bracket using 10 12-point, high torque nuts and bolts locked into place with wedge-lock locknuts. Mounting aluminum directly to the engine would be ill advised as it would act like a giant heatsink. While this is good for cooling the engine, it is very bad for the low temperature aluminum frame. Therefore, there will be 1 in of stacked nonporous alumina ceramic sheets (max temperature of over 2900°F and 300,000 psi compressive strength), interlaced with an ultra-high-temperature ceramic fiber insulation mat. This can be seen in Figure 6.1.1.1.8.

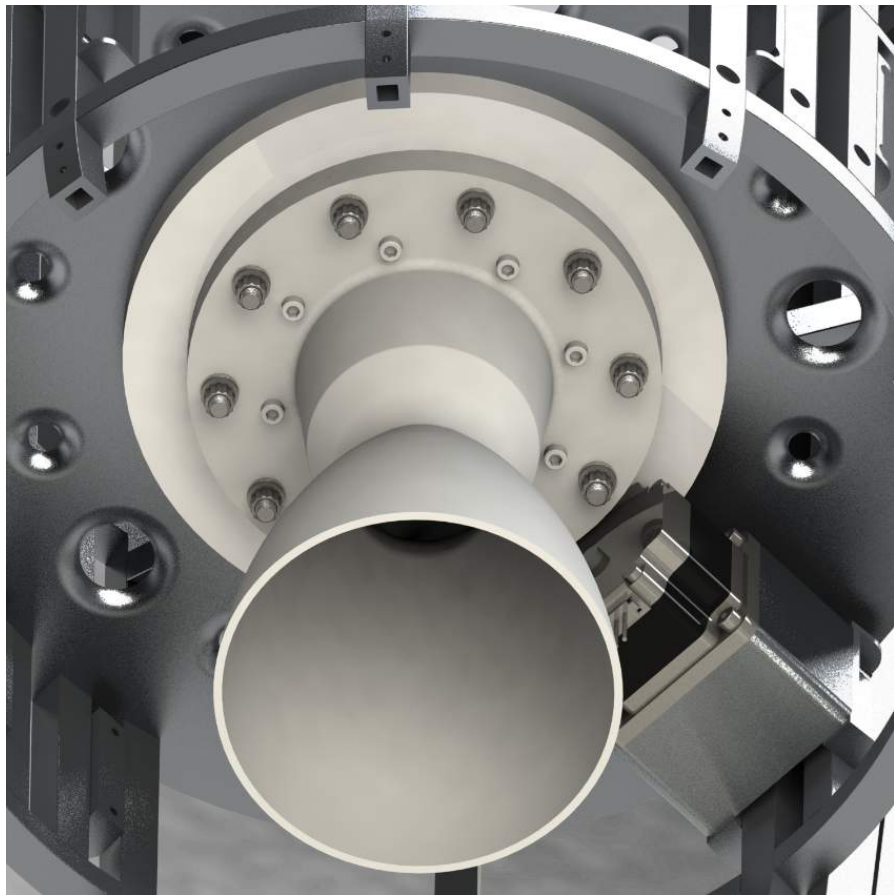


Figure 6.1.1.1.8: Engine Mount

### 6.1.1.2 Oxidizer Tank Encasement

A frame is placed around the oxidizer tank, as seen in Figure 6.1.1.2.0, following the design presented in Section 6.1.1.1. Unlike the oxidizer tank to engine interconnect, it is not designed to take heavy loading, it is intended as a rivet securing point for the skin—to prevent direct contact between the pressure tank and the flowing air which causes skin heating, a frame is placed between the skin and the tank to act as a buffer. However, under loading conditions used in Section 6.1.1.1, it shows a minimum safety factor of approximately 22, limited by compression loading, and a negligible maximum deflection of hundredths of millimeters. This safety factor value would be less and limited by buckling if it were a free beam, but if the backing pressure vessel is taken into account as an elastic foundation, it has a significantly increased buckling load (aided by the two rings connecting the struts in the middle of the frame). This safety factor is quite high and unnecessary for the section as the pressure vessel and skin are intended to also carry load, but it is the minimum reasonable tube cross section to rivet to. Therefore, it is over designed but its size is limiting by fastening constraints. Finally, it is mated to the previous frame via tailor-made tube

connectors, something that fits inside both of the nearly abutting tubes of the different frames. These tube connections (Figure 6.1.1.2.1) are stand-alone pieces not meant for high load transfer but are intended to prevent excessive vibrations of cantilever beams sticking out of the frames. With the connectors most likely being cast, their manufacturing tolerances will dictate whether interference fits, adhesive, or screws will be used to fasten them.

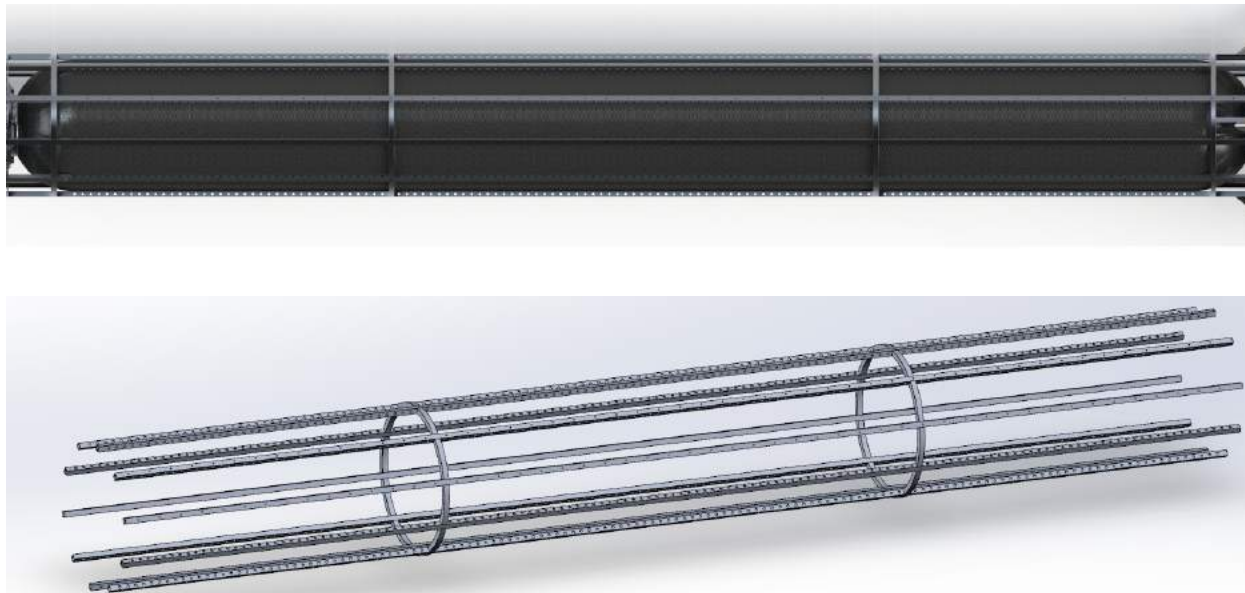


Figure 6.1.1.2.0: Oxidizer Tank Encasement: Frame

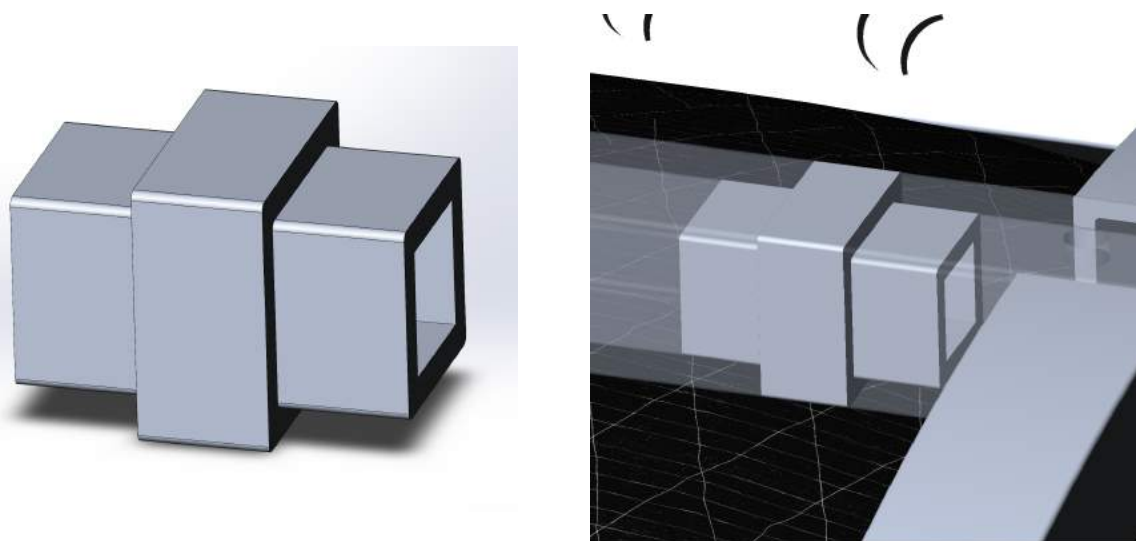


Figure 6.1.1.2.1: Oxidizer Tank Encasement: Frame Connector

### 6.1.1.3 Oxidizer Tank to Fuel Tank Interconnect

Very similar to the base design discussed in Section 6.1.1.1, the oxidizer tank to fuel tank interconnect frame has 10 main struts, two tank connection plates each having 10 tube stock angle supports supporting next

to the tank fasteners, and two struct-connecting rings of bent tube stock (Figure 6.1.1.3.0). The wall thickness of the tubes is 0.0625 in and the plates' thickness is 0.125 in. These can be thinner than the engine to oxidizer tank interconnect thicknesses due to a smaller mass load above the frame and working under the assumption that the lower frames, skin, and oxidizer tank would absorb the majority of the impact loading shock from ignition/lift-off. Additionally, the upper launch lug is optimally placed near the center of gravity of the rocket, which falls near this frame region. Thus, the second launch lug is mounted to this frame utilizing two curved tube pieces with bolt holes drilled in their centers, as presented in Section 6.1.1.1.



Figure 6.1.1.3.0: Oxidizer Tank to Fuel Tank Interconnect: Frame Connector

Simulation loading for this section consisted of the same loading as presented in Section 6.1 with the exclusion of the aft structure (65 kg) and propellant (225 kg). This yielded a safety factor of approximately 9, constrained by shear in the angled reinforcement members. Also, a negligible maximum displacement of hundredths of millimeters was determined. This calculation did not account for the plate effect on reduction of loading in the angled support, so when repeated using SOLIDWORKS FEA (again, not ideal but gives a ballpark estimate), a safety factor of approximately 32 was found (Figure 6.1.1.3.1). These both present acceptable safety factors but are higher than desired for a rocket. Here the safety factor was approximately 80 for the main strut members, showing that the number or thickness of them could be significantly reduced and still be structurally sound. Although this would reduce weight, the number of weldment points for the corner reinforcements could decrease, reducing the overall strength of the design. Therefore, minimal alterations would be made to the design other than drilling weight-saving holes in the main struts. If weight-saving is needed, this assembly is a good place to start modifying; the great dispersion of safety factors show that the design could be optimized greatly (possibly with

generative design). As described in Section 6.1.1.1, continued analysis would aid in this process for future work.

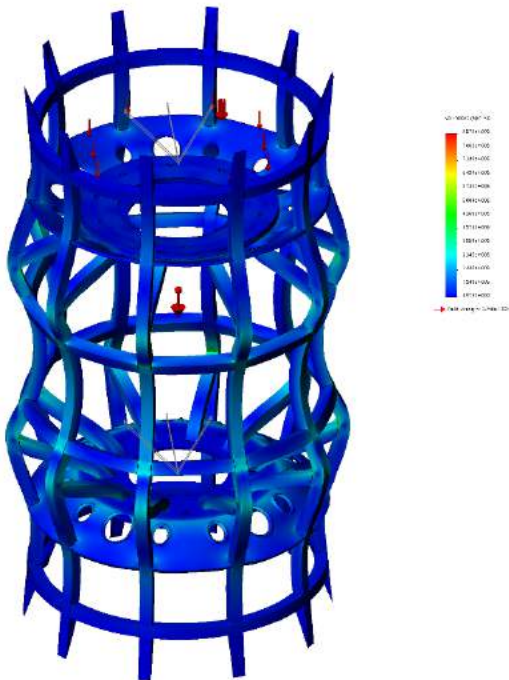


Figure 6.1.1.3.1: Oxidizer Tank to Fuel Tank Interconnect: SOLIDWORKS FEA

### 6.1.1.3 Fuel and Pressurant Tank Encasements and Interconnect

The frames surrounding both the fuel tank (Figure 6.1.1.4.0) and pressurant tank (Figure 6.1.1.4.1) are exactly as described in Section 6.1.1.2, except they are shorter. The frame connecting the fuel and pressurant tanks is exactly as described in Section 6.1.1.3, sans launch lug (Figure 6.1.1.4.1). Because the loading decreases significantly at this section of the rocket since the masses below the point can be ignored, each safety factor is significantly over what is necessary. This presents room for significant improvement. However, the similitude in design aids in ease of manufacturing, which may weight design change decisions.

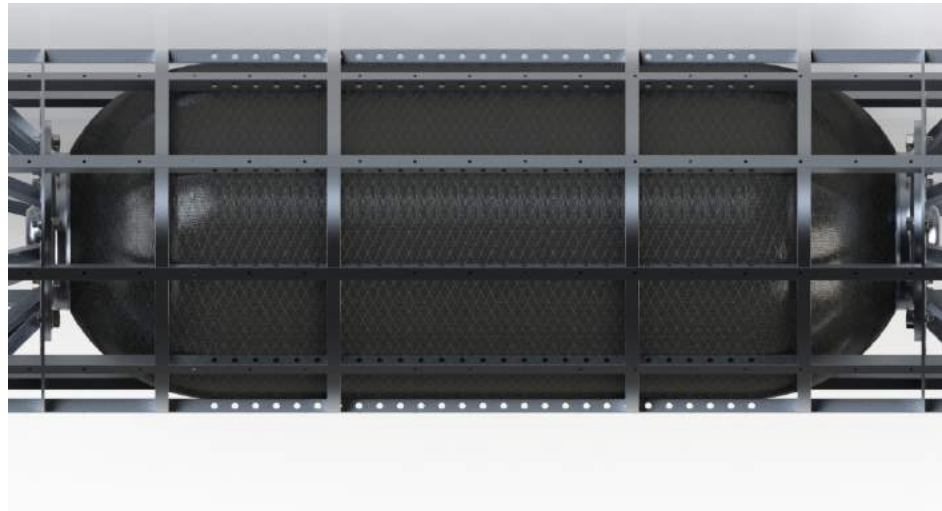


Figure 6.1.1.4.0: Fuel Tank Encasement: Frame

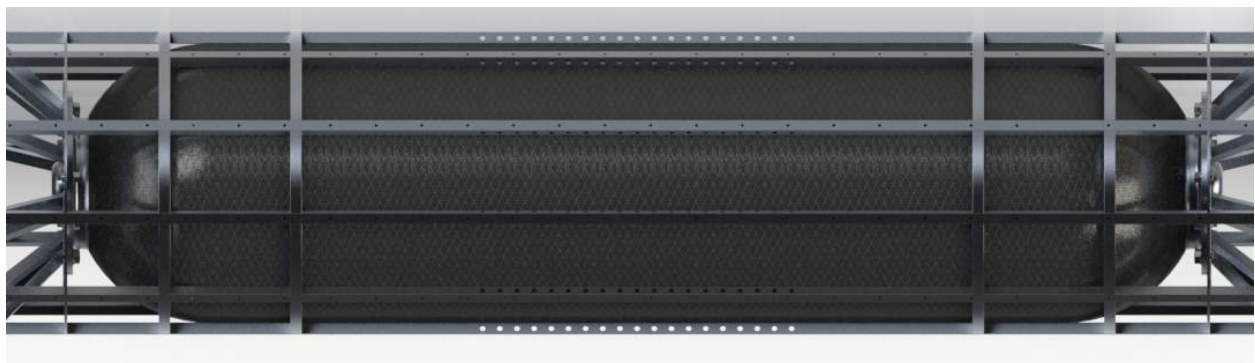


Figure 6.1.1.4.1: Pressurant Tank Encasement: Frame



Figure 6.1.1.4.2: Fuel to Pressurant Interconnect: Frame

#### 6.1.1.4 Pressurant Tank and Nose Cone Interconnect

The frame connecting the pressurant tank to the nose cone is very similar to the design presented in Section 6.1.1.3, with some exceptions (Figure 6.1.1.5.0). First, there is no upper plate nor corresponding angled reinforcement struts. Second, there is no launch lug mount. Third, it has an extended length with three internal curved tube rings. These rings are 0.75 in wide by 0.5 in tall with 0.0625 in wall thickness and have three bolt clearance holes drilled in the top of each. These are meant for bolting mounting plates to (Figure 6.1.1.5.1). The mounting plates are split such that they can be easily removed or replaced if necessary. Additionally, the plates have holes cut throughout their face for a combination of weight reduction and versatile mounting. The bottom is for mounting an electronics enclosure, the middle is for mounting the payload and the top is for mounting the parachute. The payload and the electronics enclosure will be interfaced via a damper system (most likely a simple rubber grommet damper). The parachute system also has holes for eyebolts; the parachute cords will be attached to the eyebolts (Figure 6.1.1.5.2). Future analysis is similar to what was discussed in previous sections, but this will include vibration isolation for the payload and electronics (which cannot be done yet as their mass and shape are not finalized).

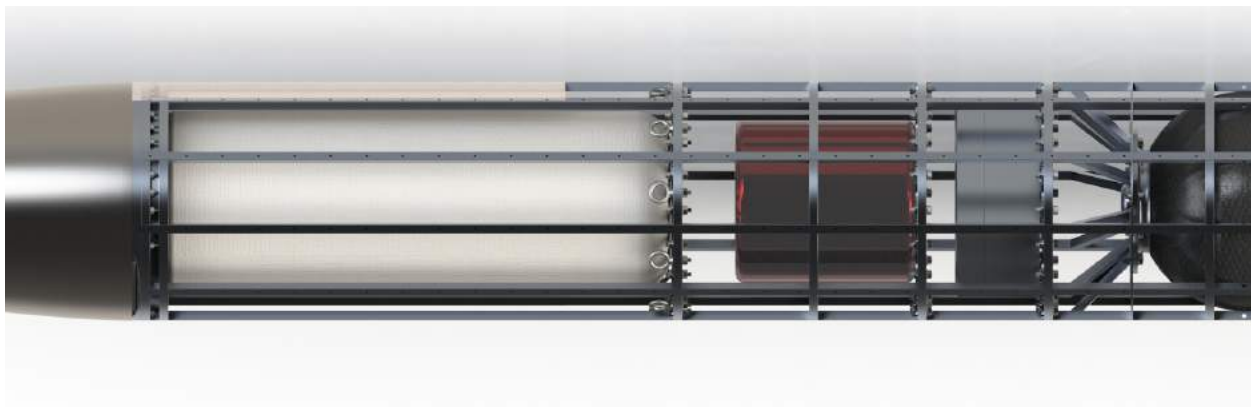


Figure 6.1.1.5.0: Pressurant Tank to Nose Cone Interconnect: Frame

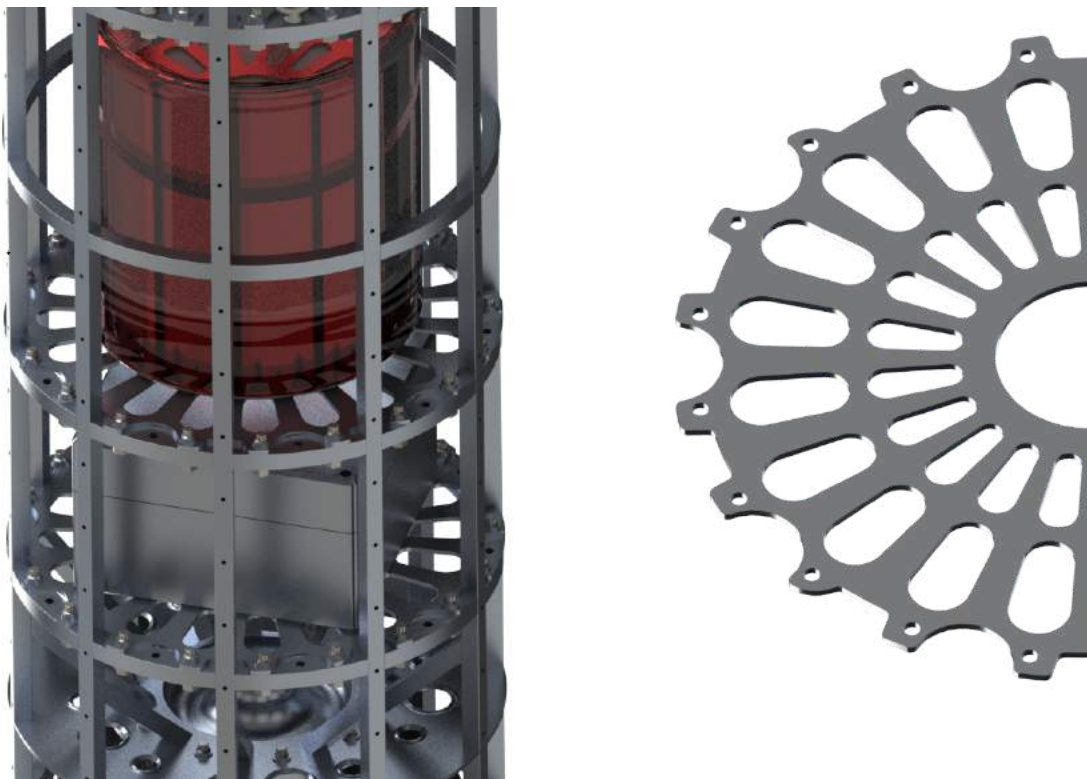


Figure 6.1.1.5.1: Pressurant Tank to Nose Cone Interconnect: Mounting Plates



Figure 6.1.1.5.2: Pressurant Tank to Nose Cone Interconnect: Parachute Mounting Plates

## 6.1.2 Fuel, Oxidizer, and Pressurant Tanks

Little star is preliminarily designed to be a pressure-fed rocket. This means that the storage of the fuel and oxidizer is done under pressure such that delivery of propellant to the engine is provided by the differential pressure between the tank and the combustion chamber. Such a design relieves the need for pressure boosting turbomachinery along the propellant

delivery pathway, reducing overall design complexity. However, this reduction in complexity comes with a consequence, a weight addition in the form of pressure vessels. Because the fuel and oxidizer need to be at a high pressure, their storage containers need to be capable of these conditions. Thicker walls and more reinforcements account for the extra strength needed and the extra weight added. Additionally, to ensure the stored fuel and oxidizer maintain their pressures throughout their depletion, a third component, a pressurant, is used. The pressurant is nominally a high-pressure gas that is fed into the ullage of the propellant tanks during their depletion which maintains the tanks at their required pressures. The complete pressure-fed propellant system is shown schematically in Figure 6.1.2.0. The following is a breakdown of our propellant storage and feed system.

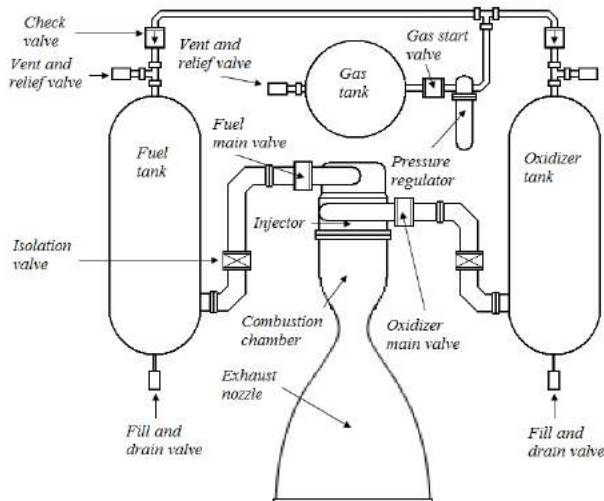


Figure 6.1.2.0: Schematic of Pressure Fed Propellant System [6.3].

### 6.1.2.1 Tank Style

High pressure tanks are often made from metals, due to their elastic properties and high strength-to-weight ratios. However, often the yield tensile strength of the metals is low, meaning that it needs bulk quantities of material to contain high pressures, adding weight to the structure. The more structural weight on the vehicle, the less efficient it is, so to reduce the weight the tanks can be constructed as a composite overwrap pressure vessel (COPV). Schematically shown in Figure 6.1.2.1.0, a composite overwrap pressure vessel is a vessel with a liner, in our case metal, that is cocooned in a composite. The composite is of a much larger strength-to-weight ratio compared to the liner, so the liner can be thin and can act as a seal for the vessel while the composite takes most of the internal pressure load. This effectively lowers the weight of the vessel while increasing its strength. Therefore, to optimize our pressure vessel weights we will be employing COPVs.

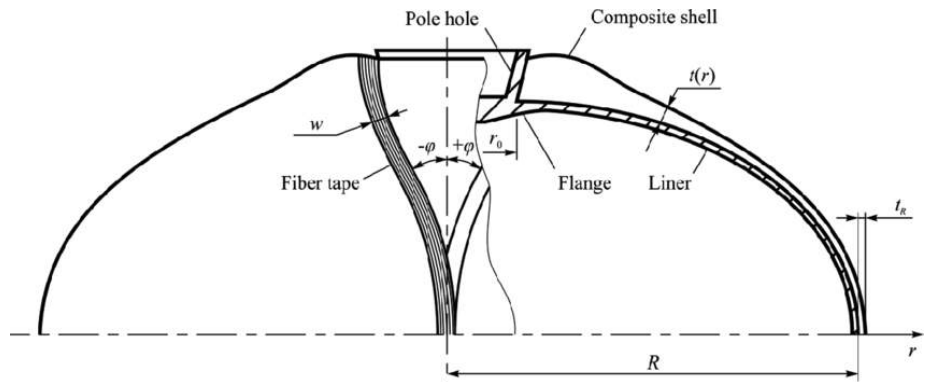


Figure 6.1.2.1.0: Schematic of a Composite Overwrap Pressure Vessel [6.4].

### 6.1.2.2 Tank Material Selection

Propellants are highly reactive substances; thus, careful attention needs to be taken to ensure compatibility between the propellant and the storage medium. There will be three substances used in the propellant system: liquid hydrogen peroxide as the oxidizer, liquid kerosene as the fuel, and gaseous helium as the pressurant. First and foremost, following competition guidelines (see Table 6.1.2.2.0), the general material allowances are determined. Hydrogen peroxide is the most restrictive substance, having full compatibility with aluminum and limited (Teflon liner required) compatibility with 18-8 stainless steel. Kerosene is slightly less restrictive, having full compatibility with nickel, aluminum, carbon steel, and 18-8 stainless steel. Helium, being an inert noble gas, is fully compatible with nickel, aluminum, carbon steel, copper, and 18-8 stainless steel, among others. Although Inconel is compatible with hydrogen peroxide (see Table 6.1.2.2.1) aluminum is preferred, following Table 6.1.2.2.2. Therefore, aluminum is the desired oxidizer tank material, with 6061 as the variant due to its reasonable compatibility, formability, weldability, strength, and ductility with temperature variations (Table 6.1.2.2.3). To simplify manufacturing, a consistent tank material is chosen between the oxidizer and fuel since both are loaded similarly. The pressurant will be at a significantly higher pressure than the fuel and oxidizer and it has no compatibility restrictions, so aluminum 2219, aluminum 7075, or Inconel 718 would be acceptable material choices. However, to keep the manufacturing systematic, aluminum 6061 is selected for the pressurant tank.

Table 6.1.2.2.0: Material Compatibility per Base 11 Space Challenge Competition Guidelines [6.25]

Service	Metals, O-Rings, Hose Liners, Gaskets and Packings								
	Nickel	Aluminum	Carbon steel	Copper	18-8 Stainless	O-Rings	Gaskets	Packings	Hose Liners
Dynamic	Static								
Pneumatic									
Air	S	S	S	S	S	1,2,3	4,10	4,8,9,10	4,10
Helium	S	S	S	S	S	1,2,3	4,10	4,8,9,10,28	4,10
Nitrogen	S	S	S	S	S	1,2,3	4,10	4,8,9,19,28	4,10
Oxygen	S	S	L	S	S	NONE		4,8,9,10	4,10
Hydraulic									
Water	S	S	S	S	S	1,2,3	4,10	4,7,9,10	4,10
Hydraulic Fluid	S	S	L	S	S	1	4,10	4,7,8,10	4,10
Oil	S	S	S	S	S	1,5	4,10	4,8,9,10	4,10
Cryogenic									
Nitrogen	S	S	U	S	S	NONE	4,10	4,7,9,10	4,10
Oxygen	S	S	U	S	S	NONE	4,10	4,7,9,10	4,10
Other Fluids									
Hydrogen Peroxide	U	S	U	U	L	24	4,10	4,7,10	4,10
Gasoline	S	S	S	S	S	1	4,10	4,8,9,10	4,10
Kerosene	S	S	S	U	S	1,5	4,10	4,8,9,10	4,10
Methyl and Ethyl Alcohol	S	S	L	S	S	1,2	4,10	4,7,10	4,10
Acetone	S	S	S	S	S	2,3	4,10	4,7,8,10	4,10
<hr/>									
Code									
S - Satisfactory	6 - Fluorosilicone								
L - Limited	7 - Flexitallic with teflon filler								
U - Unsatisfactory	8 - JM-76								
1 - Buna-N	9 - Flexitallic with Teflon filler								
2 - Butyl Rubber	10 - Kel-F								
3 - Neoprene	19 - Fluorolube grease (GR 362)								
4 - Teflon	28 - High Density Polyethylene								
5 - Viton-A (SR270-70)									

Table 6.1.2.2.1: Inconel 718 Compatibility with Hydrogen Peroxide [6.5].

Class 1 is completely compatible, class 2 is compatible up to 4 hours at 160°F or 1 week at 70°F, class 3 is compatible less than 1 minute at 160°F or 1 hour at 70°F, and class 4 is not recommended [6.6].

Material	90% H <sub>2</sub> O <sub>2</sub>	98% H <sub>2</sub> O <sub>2</sub>	Temperature	Notes
718	Class 2	Class 2	70 F	Surface Finish must be better than 10 rms
718	Class 4	Class 4	151 F	

Table 6.1.2.2.2: Aluminum Compatibility with Hydrogen Peroxide (at 70°F) [6.7]. Class 1 is completely compatible, class 2 is compatible up to 4 hours at 160°F or 1 week at 70°F, class 3 is compatible less than 1 minute at 160°F or 1 hour at 70°F, and class 4 is not recommended [6.8].

Material	90% H <sub>2</sub> O <sub>2</sub>	98% H <sub>2</sub> O <sub>2</sub>
Aluminum 355	Class 2	Class 3
Aluminum B356	Class 1	Class 1
Aluminum 1060	Class 1	Class 1
Aluminum 1160	Class 1	Class 1
Aluminum 1260	Class 1	Class 1
Aluminum 2014	Class 4	Class 4
Aluminum 2017	Class 4	Class 4
Aluminum 2024	Class 3	Class 4
Aluminum 5254	Class 1	Class 1
Aluminum 5652	Class 1	Class 1
Aluminum 6061	Class 2	Class 2
Aluminum 7072	Class 1	Class 1
Aluminum 7075	Class 4	Class 4

Table 6.1.2.2.3: Aluminum 6061-T6 Material Properties at a Range of Temperatures [6.9].

Temperature (°F)	Tensile Strength, Yield (psi)	Tensile Strength, Ultimate (psi)	Elongation at Break (%)
700	1740	3480	95
601	2760	4640	85
500	4930	7400	60
399	14900	19000	28
300	31000	33900	20
212	38000	42100	18
75.2	40000	45000	17
-18.4	41000	47000	17
-112	42100	49000	18
-321	47000	60000	22

Although aluminum 6061 is compatible with the substances contained in the tanks and has a relatively high strength to weight ratio compared to other metals, it has a low tensile yield strength. Therefore, we will be employing COPV tanks, where aluminum 6061 acts as the liner. The composite fiber will be continuously wrapped Torayca T-1000 and the matrix will be formed from 3M 5832 resin, allowing for a 70.5% fiber volume [6.10]. Properties for these materials are presented in Table 6.1.2.2.4. Torayca T-1000 is selected due to historical success in rocket COPV's (with ARDE 31-43B resin), see [6.11].

Table 6.1.2.2.4: Properties of the Composite Materials for the COPV [6.12] and [6.13].

Material	Tensile Stress, Yield (psi)	Density (lb/in <sup>3</sup> )	Tensile Modulus (psi)
Torayca T-1000	924,000	0.0654	42,700,000
3M 5832 Resin	11,300	0.0444	446,000

### 6.1.2.3 Tank Design

The pressure vessels are the main component driving the dimensions of the vehicle. If they are too wide, the internal stresses require very thick walls. If they are too thin, the pressure vessels become unwieldy in length. Therefore, a good medium is needed. An optimization of diameter to length, pressure, and weight was performed that minimized weight, skin friction from length, and lack of manufacturability of long vessels. Via pressure vessel calculations, it was found that for a construction of only aluminum 6061-T6, the wall thickness was optimized to be approximately 0.27 in at a 12 in diameter for a pressure of 1500 psi and safety factor of 1.3. The pressure was chosen to allow derating of the vessels down to operating pressure, which yields a final safety factor of over 2. Employing similitude in design, that is, only varying the length of the vessels for ease of manufacturing for each propellant type (except for the pressurant which has a wall thickness to support 2000 psi safely), this led to lengths of approximately 9.5 ft, 2.5 ft, and 4.5 ft long for the oxidizer, fuel, and pressurant tanks, respectively, allowing for losses, ullage, etc. (approximately 5%), see Figure 6.1.2.3.0. Because the oxidizer tank is the largest and heaviest when loaded, it is placed on the bottom of the rocket (this also helps with the oxidizer delivery because the large oxidizer-to-fuel ratio calls for significantly more oxidizer transport, which is better at shorter distances), followed by the fuel tank, and lastly, the pressurant tank.



Figure 6.1.2.3.0: Pressurant Tank (Top), Fuel Tank (Middle), Oxidizer Tank (Bottom)

These vessels are designed from only aluminum so a great reduction in weight is made when removing aluminum from the outside of the vessel and replacing it with the higher strength-to-weight ratio fiber overwrap. Performing a composite analysis to replace as much aluminum as possible while keeping structural integrity drove the inner aluminum (now a liner) to 0.1 in thick and the overwrap to 0.1 in thick, see Figure 6.1.2.3.1. The amount of aluminum could be further reduced but doing so increases the manufacturing difficulty of the tube significantly.



Figure 6.1.2.3.1: Fuel Tank Cutaway

Manufacturing would be done by either having a specialty extrusion company extrude a tube of the thickness and diameter needed, or we can purchase pre-made 0.25 in thick tubes to the diameter and length needed and machine them down to size on a large lathe. The end caps, Figures 6.1.2.3.2 and 6.1.2.3.3, will be machined out of solid billets of aluminum and they will be welded to the tubes by a certified welder, per competition requirements. The overwrap would be performed on a winding machine. Two of each vessel will be manufactured in order to proof test them.

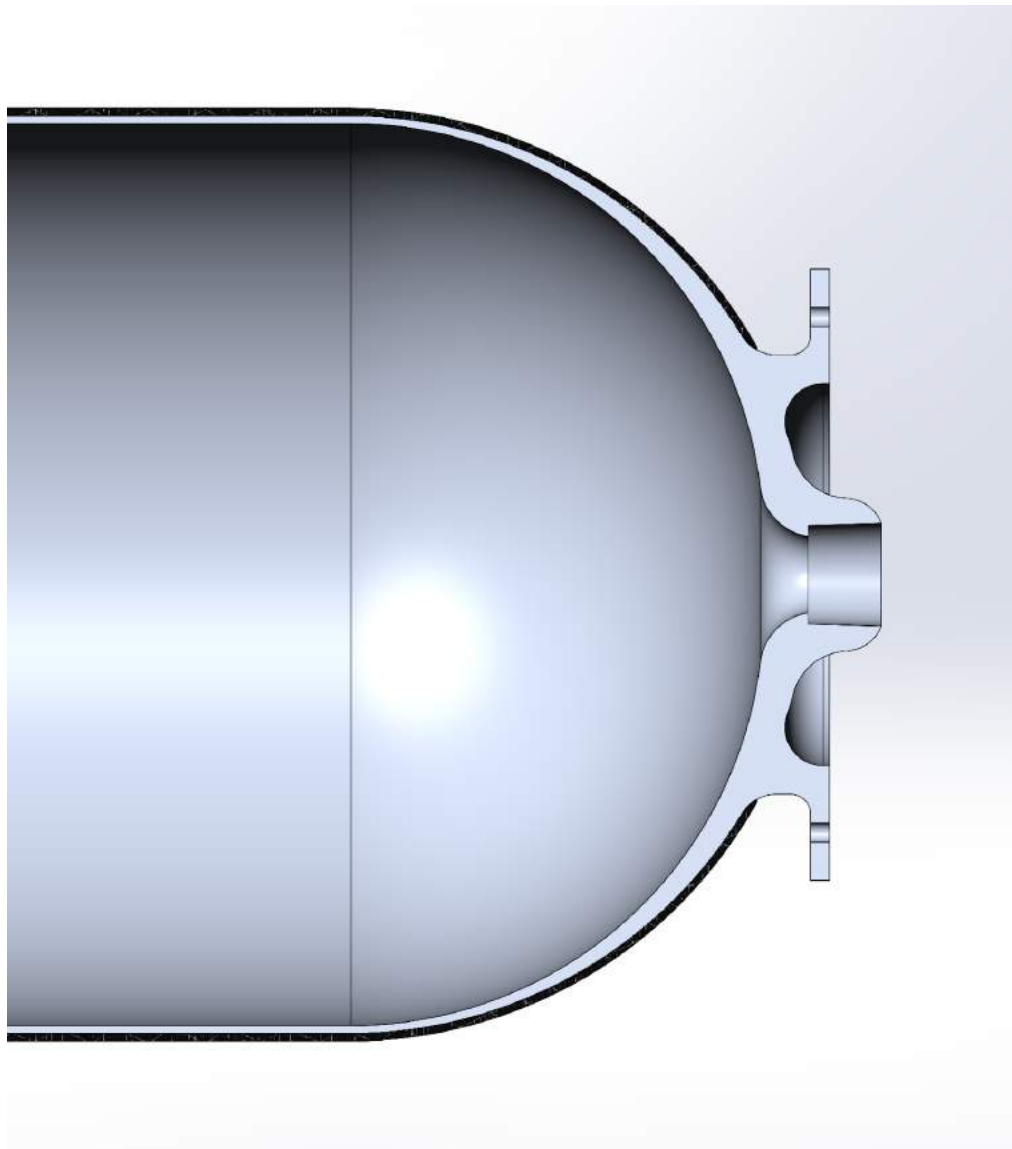


Figure 6.1.2.3.2: Fuel Tank End Cross Section

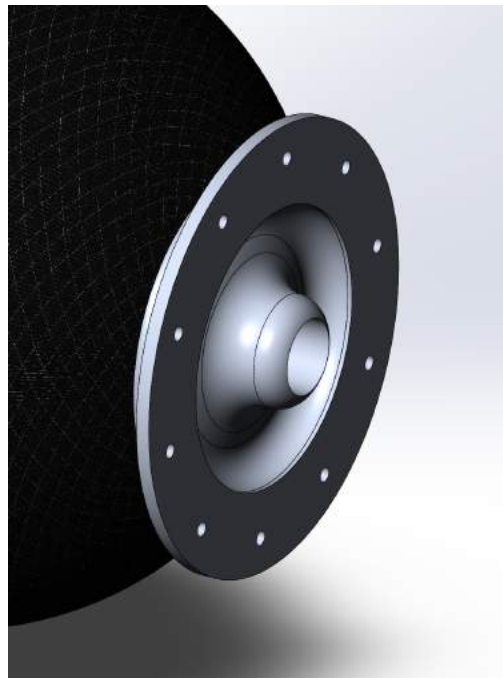


Figure 6.1.2.3.3: Fuel Tank End

The vessels will be designed and built by us, but if money permits we will have off-the-shelf vessels as backups. The backups would be: an ARDE 4929 [6.14] or ARDE 5066 [6.15] for the fuel tank, ARDE 4929 or ARDE 4816 [6.16] for the pressurant tank, and two General Dynamics 220165-1 [6.17] for the oxidizer tank.

The main pressure vessels are large and thick enough to take the load of the entire rocket. Performing an analysis similar to the one described in Section 6.1, the tank as a structural member has a minimum safety factor of approximately 100 in buckling. This does not include the internal pressure so the buckling possibility is lowered and this safety factor is undershot. This shows that the frame and skin around the vessels are mainly for insulation purposes. Since the glass transition temperature is near 300°F for the overwrap, the insulation is very necessary to ensure safe operation when under skin heating.

### 6.1.3 Skin

The skin is 0.0120 in thick Ti-6Al-4V (annealed) sheet designed to withstand the higher skin heating temperatures present. From experimental data on a similar rocket, the skin heating can cause skin temperatures in excess of 900°F, a temperature that would remove heat treatment and almost all strength from aluminum alloys. Therefore, a higher temperature compatible annealed titanium alloy or Inconel would work well for the skin to keep structural integrity, see Figure 6.1.3.0. The titanium alloy has a higher strength-to-weight ratio, see Figure 6.1.3.1, so it is used. The major downside to titanium alloys is the cost, but through [6.18] we could source all of the sheet needed for under \$10,000.

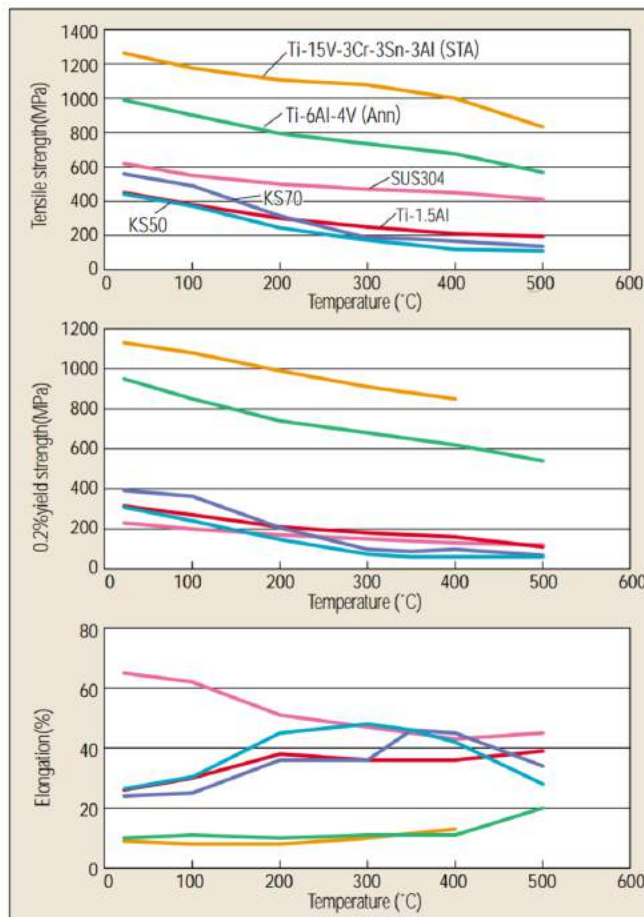


Figure 6.1.3.0: Temperature Effect on High Temperature Materials [6.19]

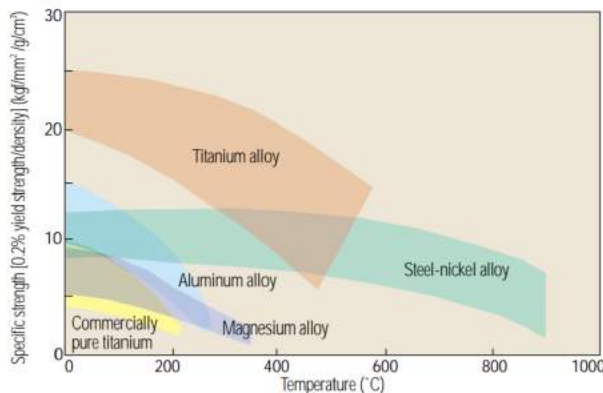


Figure 6.1.3.1: Specific Strength (Strength-to-Weight) of Possible Materials [6.20]

The skin is cut to fit a half shell of the rocket, to create only two overlap points on the surface, see Figure 6.1.3.2. It will be mainly riveted to the underlying frame but select panels near important maintenance points will be fastened by thread-locked machine screws so as to be able to remove those panels for access points. Following the analysis performed in Section 6.1, the limiting safety factor is approximately 2.2 in buckling at room temperature. Additionally, the safety factor for the tube in compression without buckling is 32 at room temperature and 20 at approximately 900°F, meaning that the skin could theoretically carry the full load of

the rocket. Since the skin is not the only structural member, its thickness could be reduced in future iterations to save money and weight. Reducing down to 0.004 in thickness would still have a safety factor of 10 in compression, but would cause a buckling action under full loading if it is considered a free tube. However, as it is well constrained, the approximation of the skin as a free tube is quite off and should be reconsidered, meaning that a reduction down to 0.004 in is feasible.

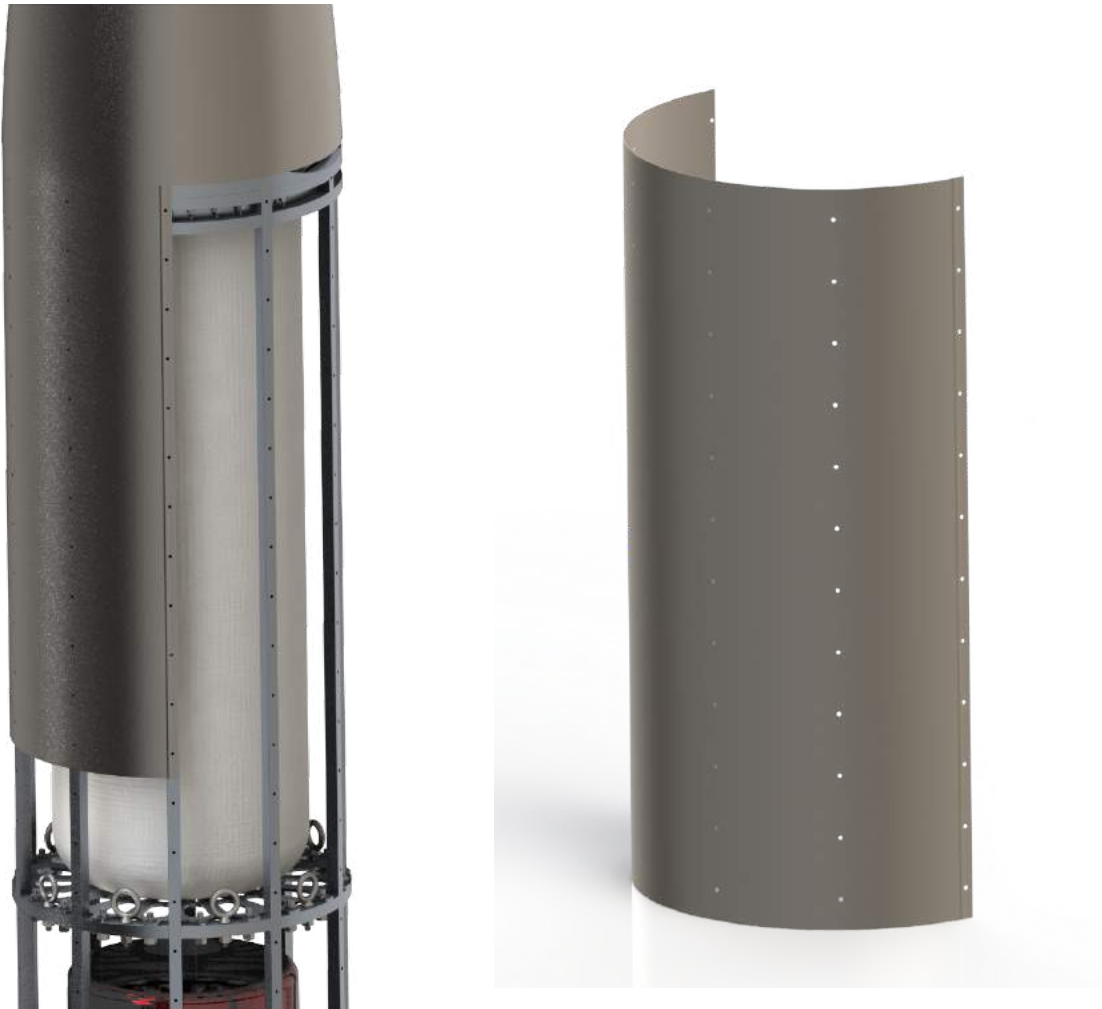


Figure 6.1.3.2: Main Body Skin

## 6.2 Nose Cone

Aerodynamic optimization of the nose cone drove the use of the Von Kármán shape. Building a nose cone around this, it was optimized at 36 in long with the major diameter equaling that of the main body. Normally a nose cone is jettisoned entirely as a whole or two halves. However, as the competition disallows total ejection of any part, there are two options: eject the nose cone but keep it tethered to the rocket or have the nose cone open up but keep it directly attached to the rocket. The former presents a danger of having a heavy metal object falling right next to the parachute system of the main rocket upon descent. This could cause tangling issues or worse. Therefore, the latter option of keeping the nose

cone attached when opening it presents a safer, albeit heavier and more complex, alternative.

For the nose cone (Figure 6.2.0), it was decided to use a design that split down the middle (Figure 6.2.1). The design thus consisted of three major components. Two cone halves and one monolithic ring used to attach the two halves together and to the main rocket body. Each cone half is hinged on its base's outer corners. The hinge is buried in both the cone body and the main rocket connector. The main rocket connector is connected to the rocket body by bolts. In the nose cone there is a NEA model 9103 electronic hold down and release mechanism [6.21] mounted on a swivel, holding the halves together via a bolt (Figure 6.2.2 and Figure 6.2.3). It acts electronically such that upon activation, the hold on the bolt is released. At this time, a spring with 30 lbf/in constant, compressed 1 in and kept between the release and the bolt is allowed to extend, forcing open the two halves. The halves release at a linear velocity of approximately 1.5 ft/s and as they are opening, a locking arm mechanism extends and engages at full stroke to ensure the halves stay open (Figure 6.2.4). This action will occur at apogee, allowing for the spring constant to be low as there would be no air resistance/force from the rocket falling. The locked open cone halves increase the coefficient of drag, aiding in slowing the rocket as it descends and helping assure the rocket stays upright. It is important to note the necessity of the swivel features of the hold down and release mechanism. If it is not allowed to swivel, binding during release would occur. Additionally, there is a set of access hatches (Figure 6.2.5) in the tip to reset the mechanism when putting the assembly together, but through a clever design modification, ensuring mechanism alignment, these could be removed in a future iteration.

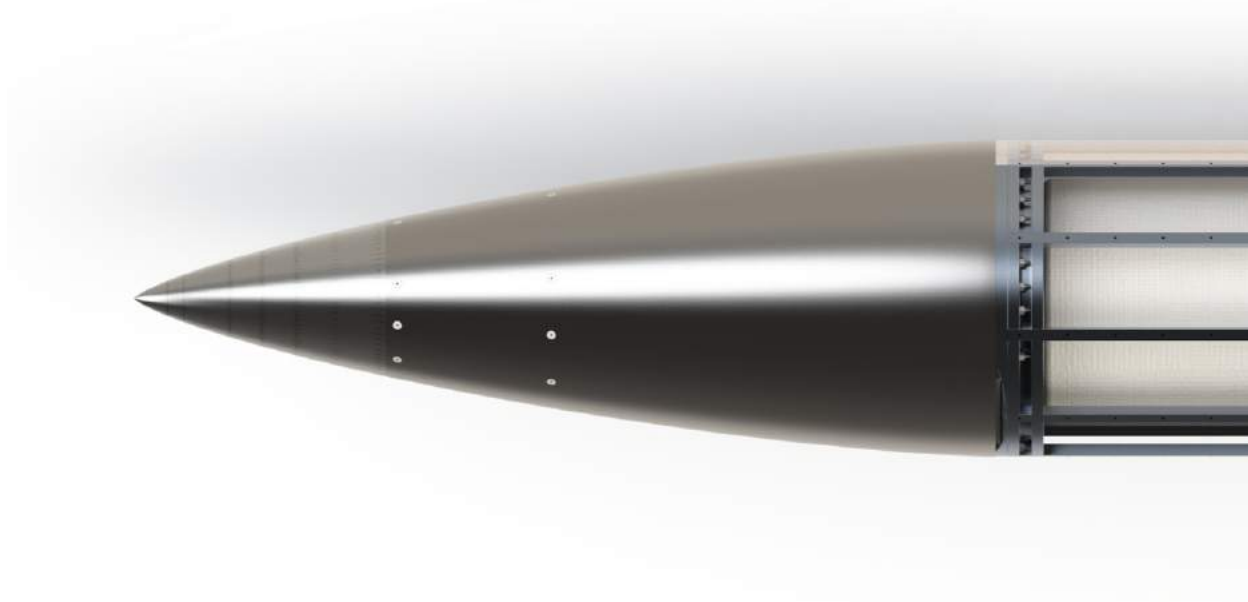


Figure 6.2.0: Nose Cone



Figure 6.2.1: Nose Cone Opened

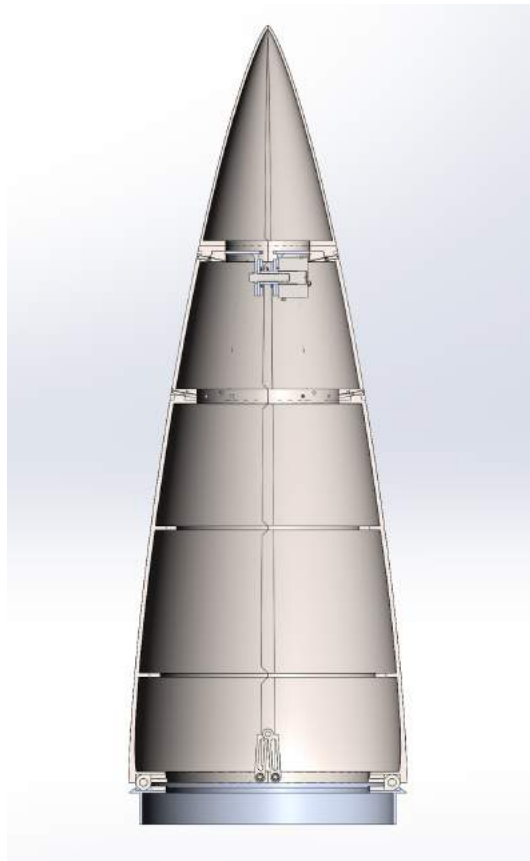


Figure 6.2.2: Nose Cone Section

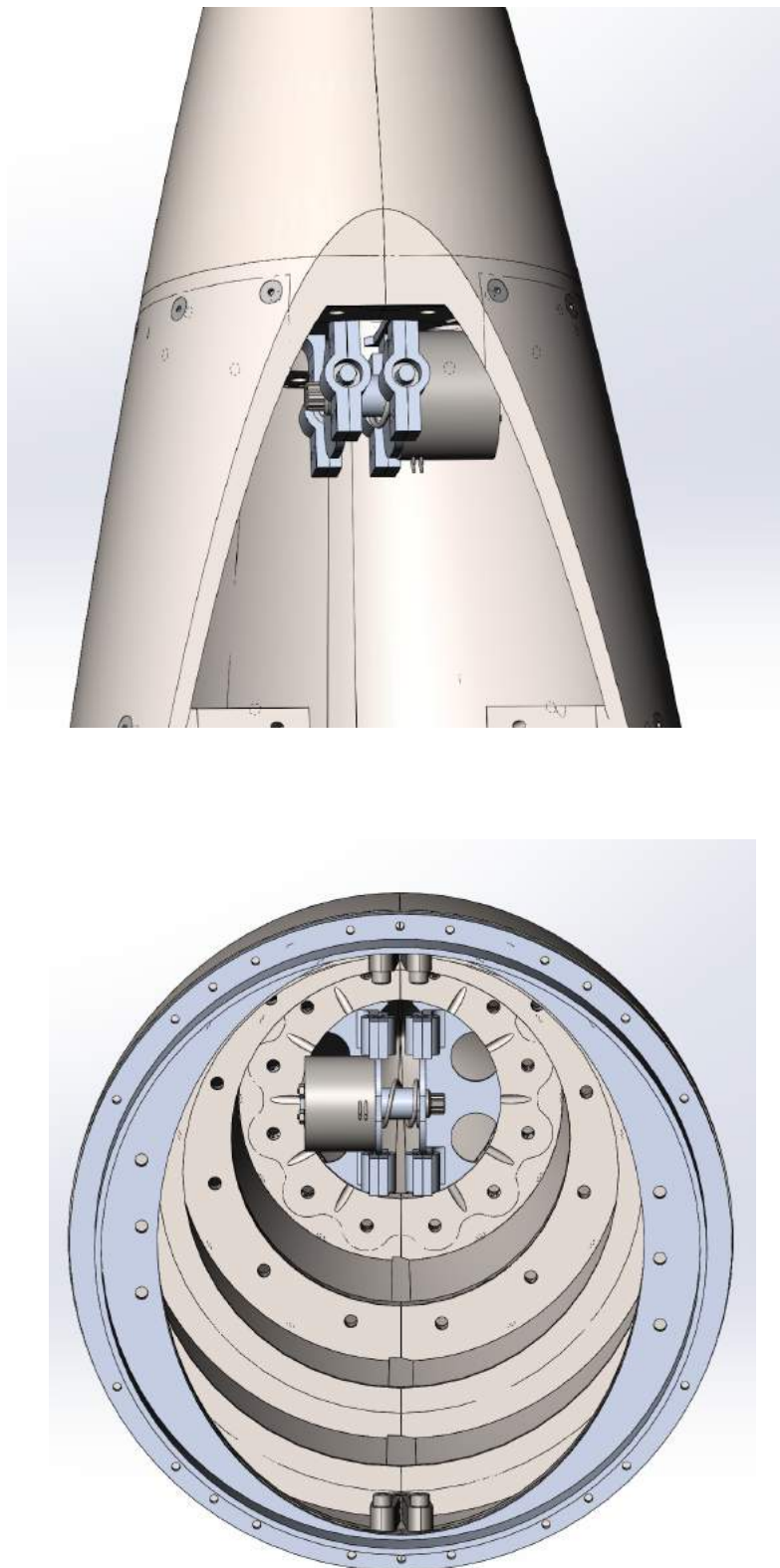


Figure 6.2.3: Nose Cone Release Mechanism

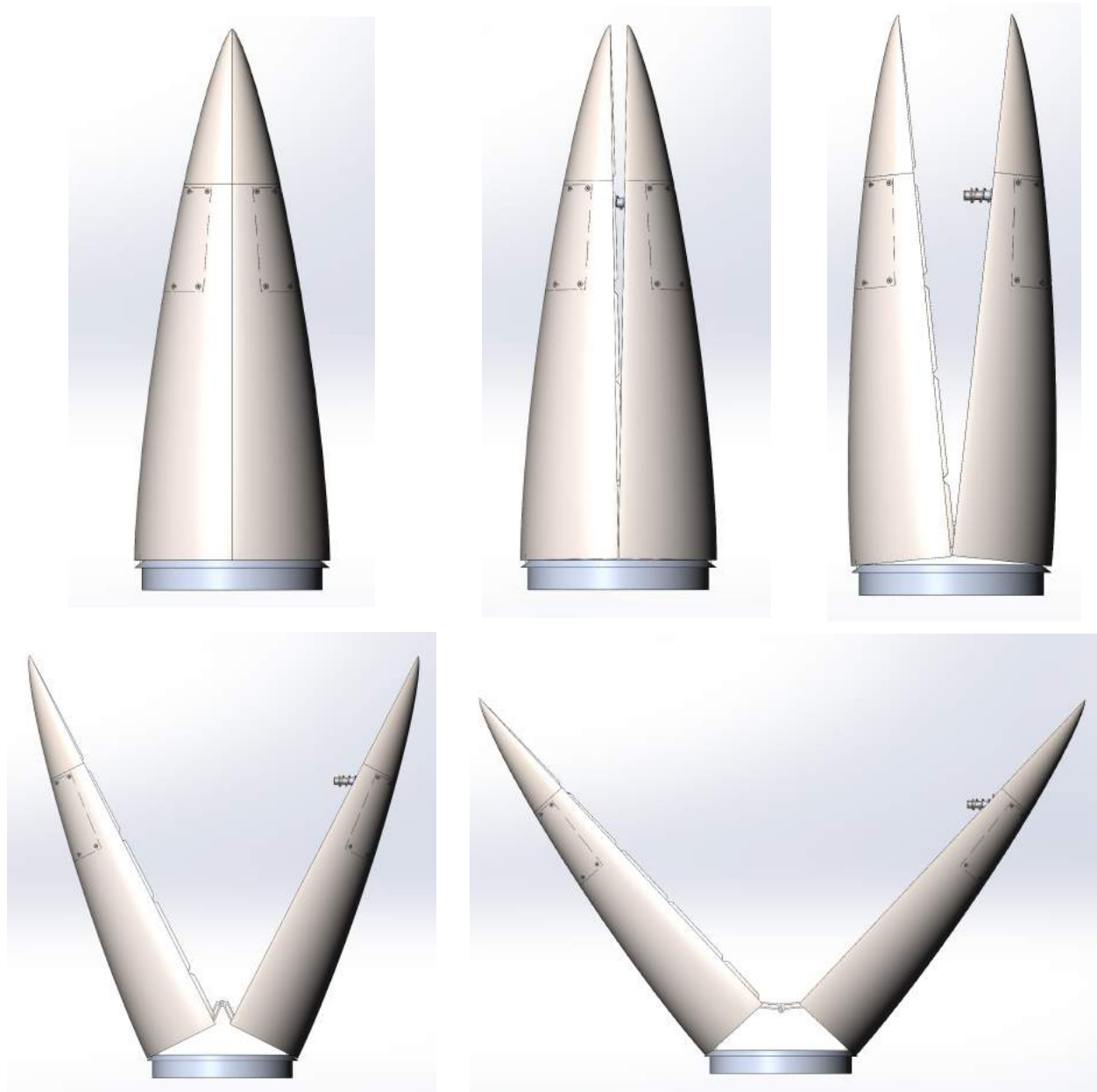


Figure 6.2.4: Nose Cone Opening

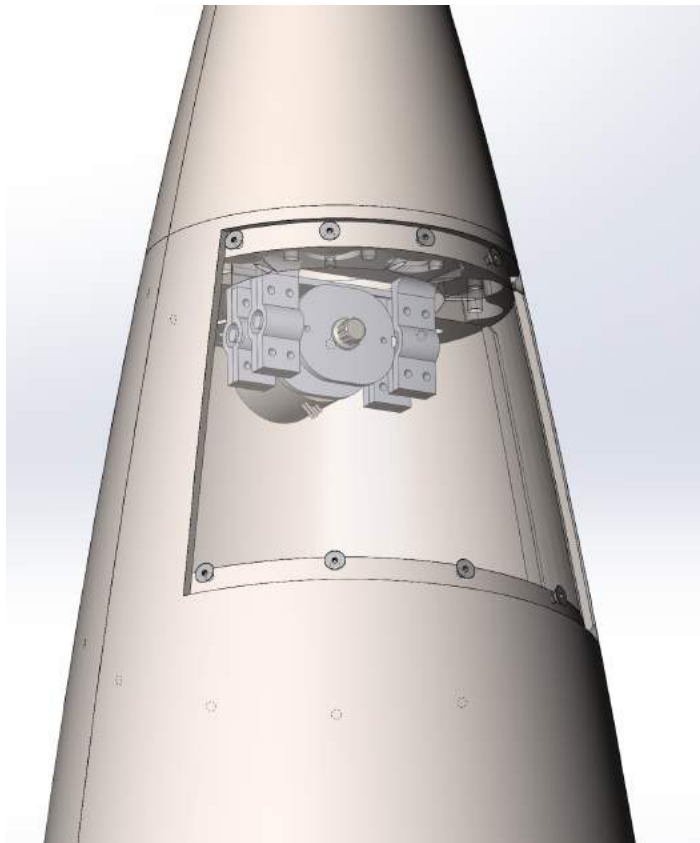


Figure 6.2.5: Nose Cone Access Panel

The nose cone halves consist of two separate halves, each with nominal thickness of 0.1875 in. The tip of the cone is made of Inconel and the main cone body is of Ti-6Al-4V. The individual halves are bolted together. The tip is made of high temperature material due to a maximum stagnation temperature of 1016°F (and a maximum normal shock temperature of 979°F at approximately 28 km and 4.2 Mach), which is straddling/above the melting point of aluminum used throughout most of the structure. However, as Inconel is heavy at the thicknesses required to ensure structural integrity at temperature, the tip is kept as small as possible. The use of a titanium alloy on the rest of the body is acceptable as the skin heating on this section should reach an approximate maximum of 900°F, a temperature where the tensile strength of the alloy should be still over 500 MPa. The cone tip and body halves are to be investment cast, including the integral stiffeners. The stiffeners prevent buckling but are currently over designed in thickness to ensure metal flow during the casting process. This can be refined via casting simulations or post-processed to remove extra material by machining and is left as future work. The final product will be polished smooth to ensure the lowest coefficient of friction, and thus, drag.

## 6.3 Fins

The fins are designed from a NACA 0006 airfoil [6.22]. Their sizing has been derived from a flight stability analysis in conjunction with minimizing drag. Four fins

are used to ease flight control, as their control surfaces can act symmetrically or anti-symmetrically with ease. The last 4 in of each fin is actuated by a direct-drive stepper motor, an oriental motor pkp264d28a2-sg18 [6.23], mounted inside the main body tube and will control both pitch and roll, making them flaperons. The structure is similar to a standard wing design, Figure 6.3.0, as it consists of ribs acting as formers, spars acting as rib alignment and main beams for bending, and skin to bear a portion of the load in a semi-monocoque design.

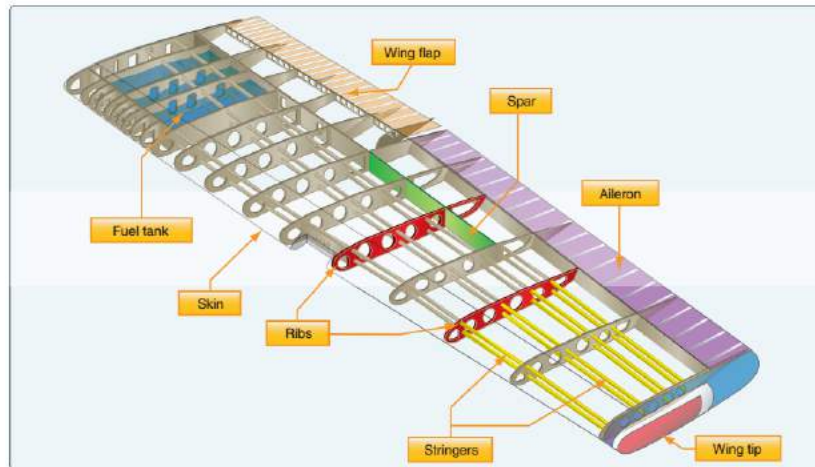


Figure 6.3.0: Standard Wing Structure [6.24]

All main internal components are of 2024-T3 aluminum, with the ribs and spars being 0.0625 in thick, the angle brackets used to connect the ribs to the spars being 0.125 in thick, and the skin being a 0.0120 in thick sheet of Ti-6Al-4V (annealed), see Figure 6.3.1. Ribs will be either stamped from a sheet or welded from a flat plate and a formed section. Spars are square tube stock with a 0.75 in width (Figure 6.3.2). Actuator components will be machined from small blocks. The 0.375 in shaft and shaft connectors are hardened steel. All connections will be made by riveting except the shaft clamps and shaft mounting components. Needle bearings will be used to ensure smooth rotation action of the control surfaces (Figure 6.3.3). The structure has been designed with stiffness in mind to alleviate flutter issues. However, a dynamic analysis will need to be performed on the fins to ensure flutter or vibrations will not be an issue.

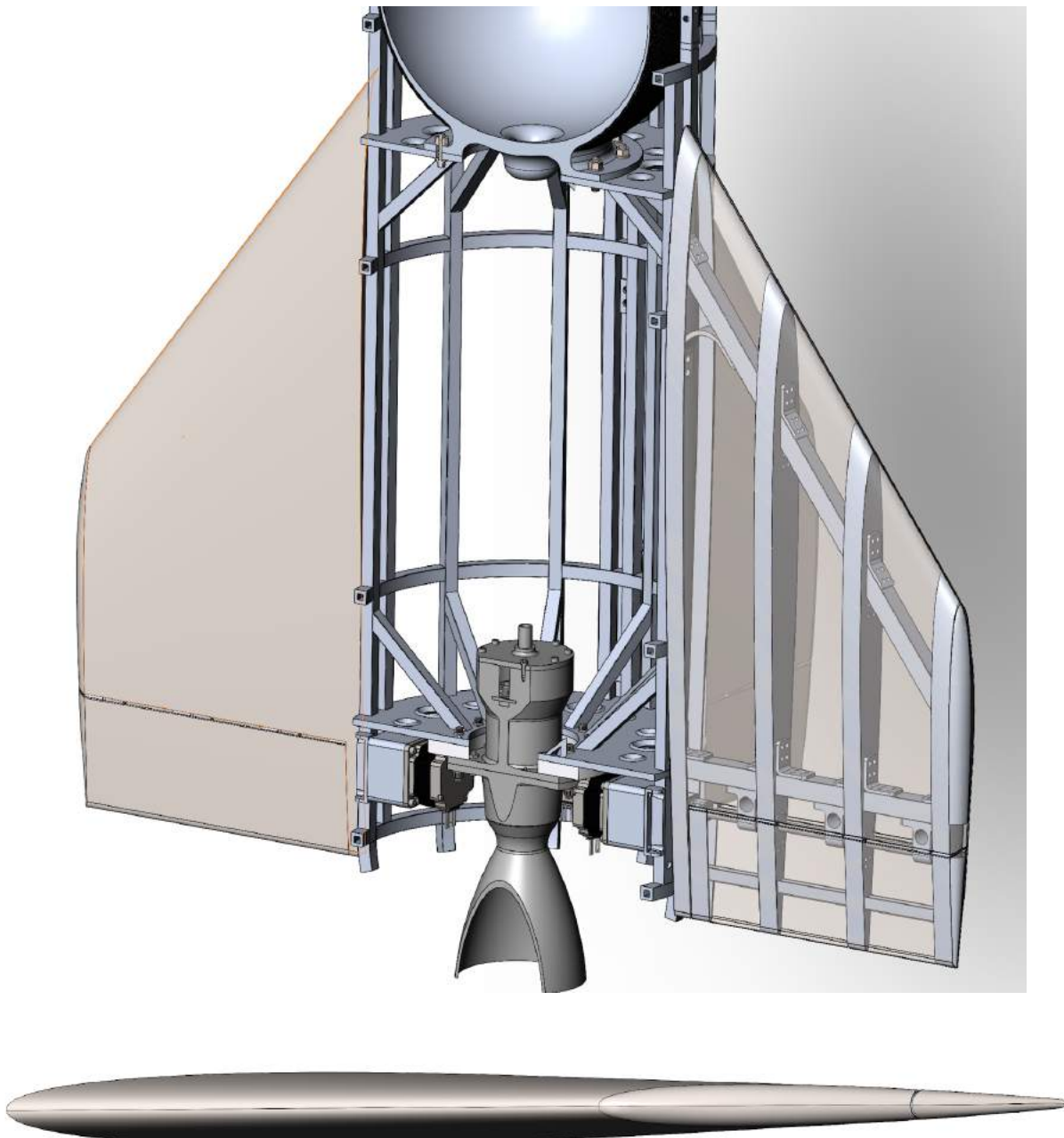


Figure 6.3.1: Fins

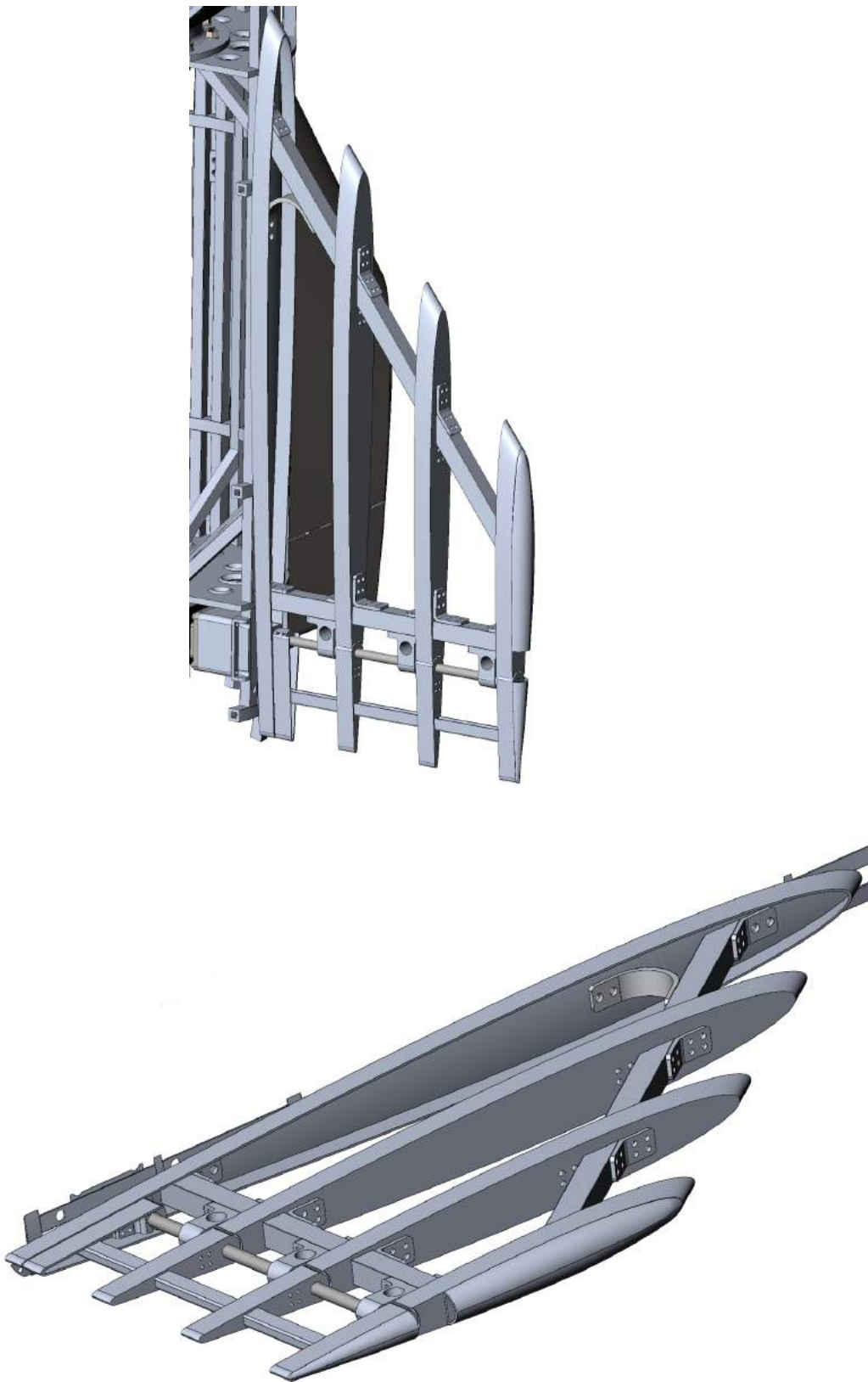


Figure 6.3.2: Fin Internals

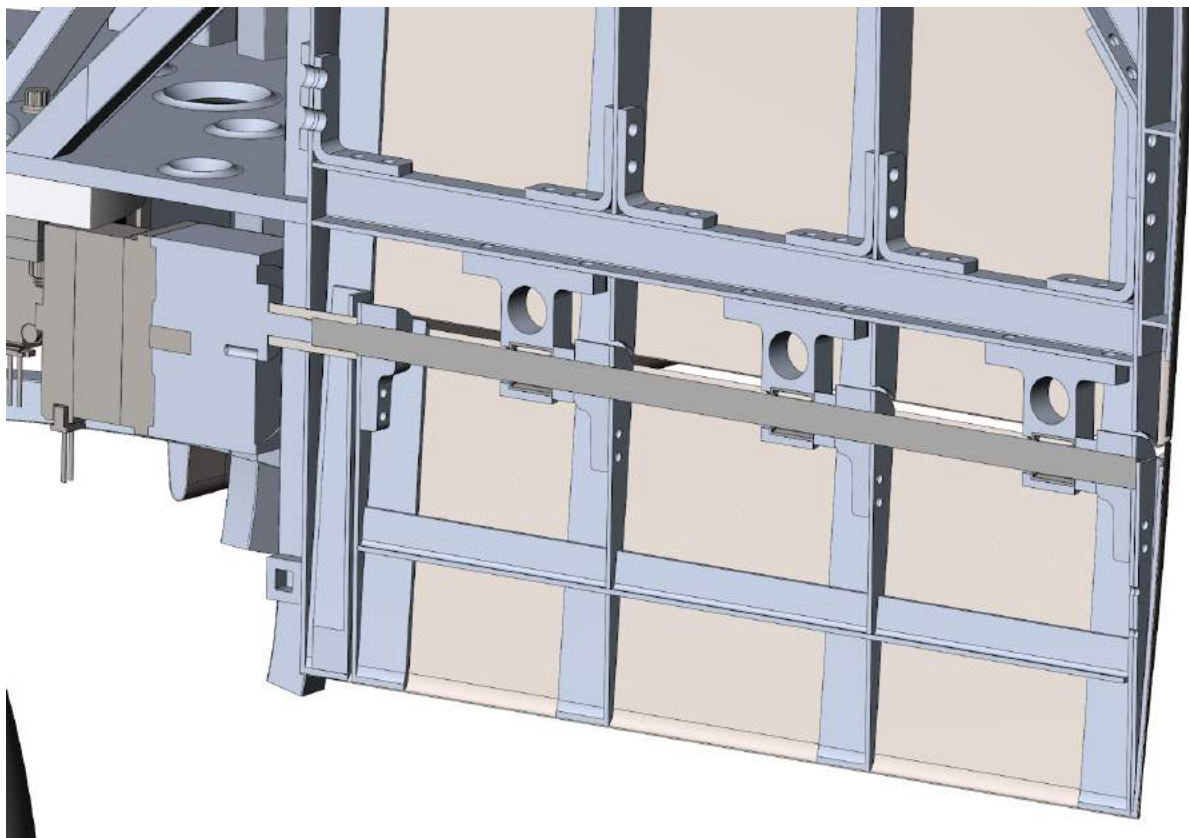
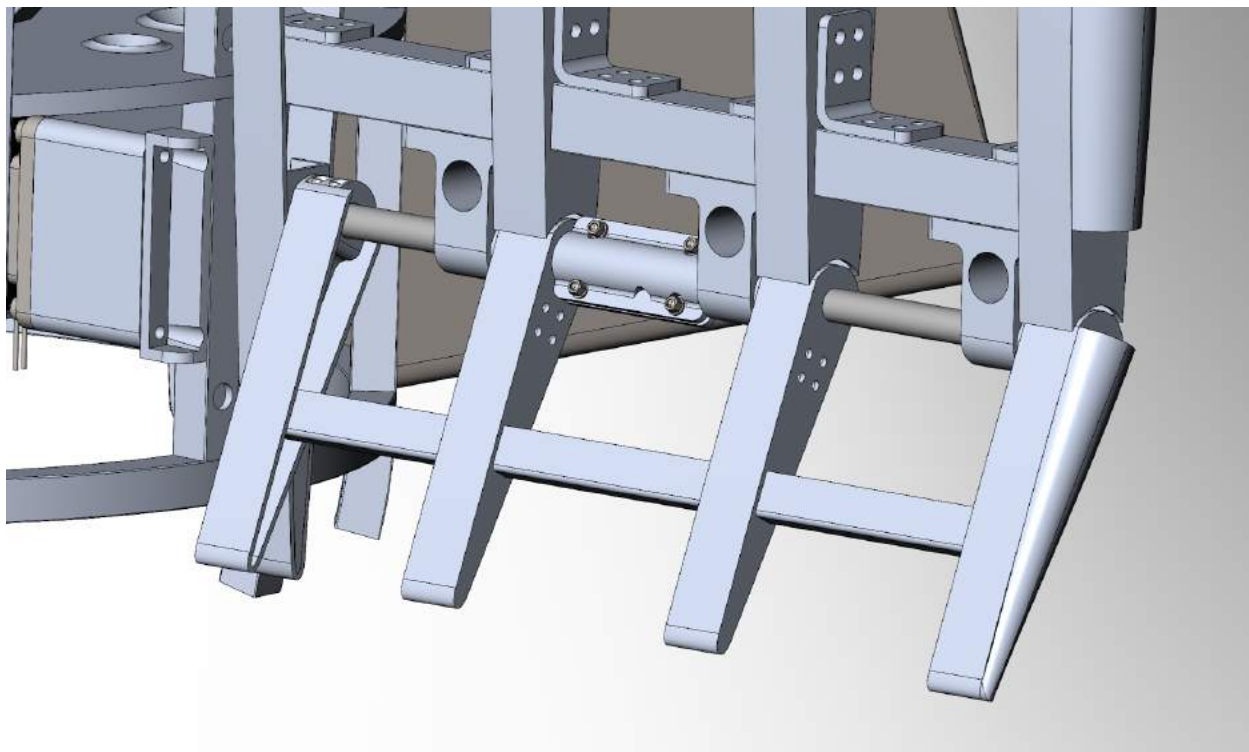
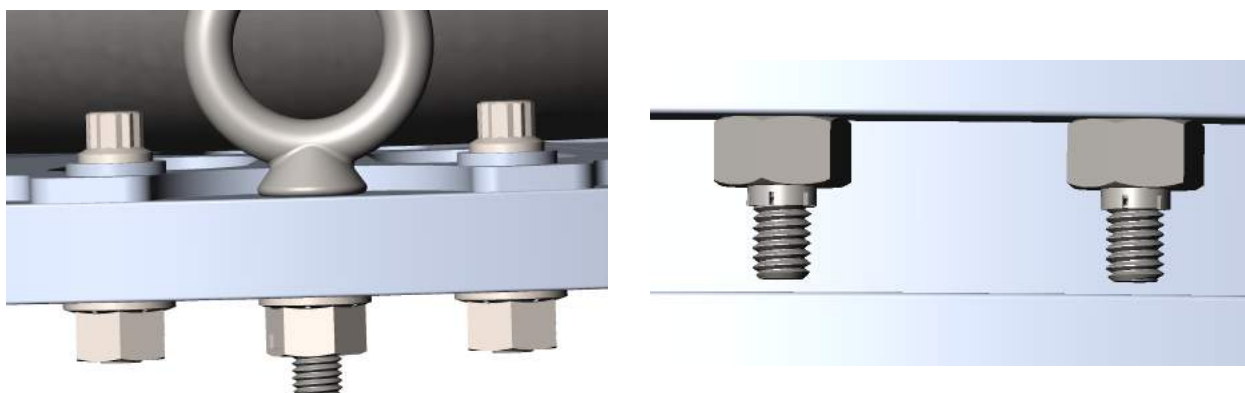


Figure 6.3.3: Flaperon

## 6.4 Fastening

When using tube stock, the ideal fastening method is a weldment, due to the lightweight nature (minimal extra material is added during the process) and rigidity of the connection. Keeping in mind the local metallurgical changes, such as grain growth and coarsening, which leads to reduced local strength and stress concentrations, welds will be used. Reduction of weld problems will be mitigated by prepping the weld surfaces correctly, properly performing the welds without inclusions (most likely robotically), post-grinding protuberances, and post-weld heat treating the entire structure. Most welds will be performed by gas tungsten arc welding (GTAW) (alternatively referred to as TIG).

Threaded fasteners are a good option to maintain the ability to remove them if necessary. However, this ability comes with the possibility that they will accidentally remove themselves under vibrational or cyclical loading. Thus, locking mechanisms will be used on all threaded fasteners. For fasteners that thread into a tapped hole, thread-locking compound will be used, such as Loctite. For general fasteners under reasonable vibrational loading that use a nut for fastening, locknuts will be used. Specifically, grade G distorted-thread fasteners with flanges are very strong, lock in place under moderate vibrations, and have a flange to distribute their load. For extreme vibrations, i.e., mounting the engine, wedge lock washers will be used. These are produced by NORD-LOCK and have exceptional capabilities under extreme vibrations. Unlike normal lock washers, these work well, but like most lock washers, they will damage the working surface. This means they are limited to use on steels instead of the softer aluminum to ensure proper adherence. All bolts will be alloy steel with tensile strengths of around 140,000 to 170,000 psi. They are preferred to be fine threaded where applicable. Each will be torqued to a prespecified torque to ensure proper bolt tension, and each in-house tapping will be having a long enough engagement to prevent tear out. These calculations are left to future work due to their tailored nature; once the design is iterated through, these will be determined. See Figure 6.4.0 for some in-use examples of threaded fasteners with locking mechanisms.



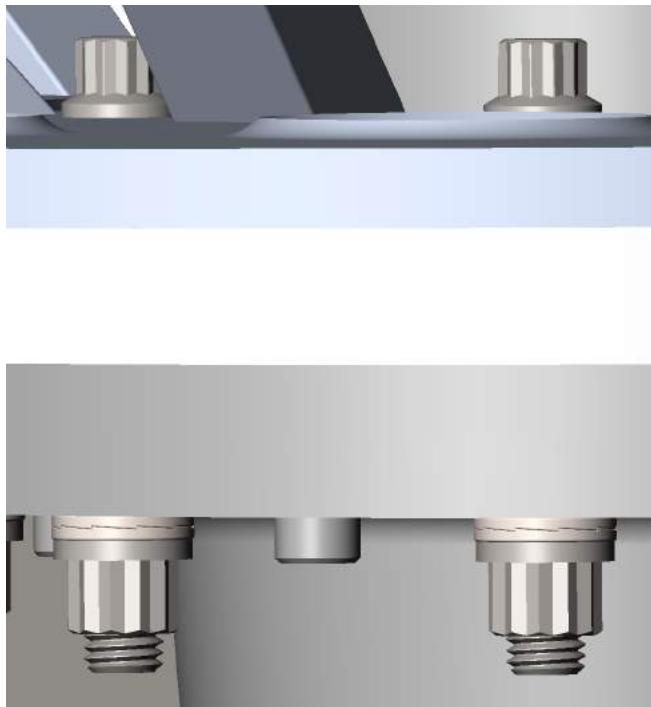


Figure 6.4.0: Threaded Fastener Examples with Locking Devices

Rivets will be used extensively throughout the structure. The main use will be on the skin and in the fins. The majority of the rivets will need to be blind as they are to be fastened into an enclosed tube stock; however, where thicker rivets are needed, solid rivet are to be used. It is important to note that the blind rivets do not sit flush so they will increase aerodynamic drag. To alleviate this, flush riveting could be used but that would require access to both sides of the rivet and such a change is left for future work.

# 7.0 Flight dynamics

## 7.1 Proposed Flight Dynamics Design

Throughout the duration of flight, there are many disturbances that cause the rocket to become unstable. These disturbances may include thrust instability, wind, and launch rail disturbances during initial takeoff. To compensate for these disturbances, roll, pitch, and yaw will be controlled during the entirety of flight. This is accomplished by dynamic control surfaces attached to bottom of each of the rocket's fins. These will be controlled using four servo motors that will operate as the rocket deviates from its vertical trajectory.

Control surfaces will become ineffective at  $\sim 30$  km in altitude. To ensure the rocket maintains a vertical trajectory to 100 km, roll stabilization will be implemented after engine burnout. This will be achieved by deflecting the control surfaces to induce an angular rate, which gives the rocket added longitudinal stability due to its angular momentum. This maneuver will occur at approximately 20 km in altitude when the onboard accelerometer detects engine burnout. Performing this maneuver post-burnout is important because centripetal acceleration is unwanted in the pressure fed system, which could "push" the propellant to the side walls of the tanks, thus causing the engine to shut down prematurely.

## 7.2 Equations of Motion

To obtain the transfer function, which is the equation that represents the intrinsic behavior of the vehicle when it acted on by a disturbance, it is essential to derive the equations of motion. The equations of motion represent the linear and angular accelerations on each axis which are affected by external forces and moments. The following section will describe these equations using the nomenclature found in tables 1 and 2.

Table 7.2.1: Summary of nomenclature used to describe equations of motion.

Axis	Name	Linear Velocity	Small Angular Displacement	Angular Velocity
X	Roll	U	$\Phi$	P
Y	Pitch	V	$\Theta$	Q
Z	Yaw	W	-	R

Table 7.2.2: Summary of nomenclature used to describe equations of motion.

<b>Axis</b>	<b>Moment of Inertia</b>	<b>Force</b>	<b>Moment</b>
X	$I_x$	$F_x$	L
Y	$I_y$	$F_y$	U
Z	$I_z$	$F_z$	N

The angular velocities of the rocket will be measured by gyros fixed to the three axes, which provide near continuous data to the controller to calculate the new desired fin positions. Applying Newton's second law, the summation of all the external forces on the rocket must be equal to the time rate of change of its momentum, and the summation of the external moments must be equal to the time rate of change of its angular momentum. The external forces consist of thrust, lift, drag, and gravity, and the external moments are produced by lift and drag throughout flight. Although the mass of the rocket will change due to fuel being consumed, the mass of the rocket was assumed to be constant to obtain the general equations of motion. The effect of propellant sloshing and aeroelastic deflection of the body will be discussed later. With these initial assumptions, the equations of linear motion were derived using the techniques found in Aircraft and Missiles by John H. Blakelock (see Equations 1-3).

$$\sum \Delta F_x = m(dU/dt + WQ - VR) \quad (1)$$

$$\sum \Delta F_y = m(dV/dt - UR - WP) \quad (2)$$

$$\sum \Delta F_z = m(dW/dt + VP - UQ) \quad (3)$$

The change in forces represents the deviation away from equilibrium due to disturbances. To obtain the equations of angular motion of the rocket, the momentum of the element of mass due to the angular velocity is equal to the tangential velocity of the element of mass about its center of gravity. Representing J as the product of inertia, the following angular equations of motions were developed (see Equations 4-6).

$$\sum \Delta L = (dP/dt)I_x - (dR/dt)J_{xz} + QR(I_z - I_y) - P Q J_{xy} \quad (4)$$

$$\sum \Delta U = (dQ/dt)I_y + PR(I_x - I_z) + (P^2 - R^2)J_{xz} \quad (5)$$

$$\sum \Delta N = (dR/dt)I_z - (dP/dt)J_{xz} + PQ(I_y - I_x) + QRJ_{xz} \quad (6)$$

Equations 1-6 represent the nonlinear equations of motion that will be used to monitor the stability of the rocket in time. These equations were then further broken down and linearized to describe the longitudinal and lateral dynamics.

As a pitching moment occurs about the Y axis, it causes a rotation about this axis, as well as a change in the forces applied in  $F_x$  and  $F_z$ . In other words, a pitching moment does not cause a yaw moment, rolling moment, nor a change in force along the Y axis. Therefore, the angular velocities in roll and yaw as well as linear velocity along the pitch axis can be set to zero. When P, R and V are taken to

be zero as per the preceding justification, equations 2, 4 and 6 are eliminated. As a result, the simplified longitudinal equations can be used. The lateral equations of motion can also be derived in a similar approach, now with a yawing moment about the Z axis. Equations 2, 4 and 6 are used to describe the lateral dynamics. Due to bending of the rocket in flight, the dynamics pose many non-linearities. As a result, the disturbances are modeled to be small perturbations from the equilibrium position, and the small-angle approximation assumption is made between the disturbed angle and reference position. This assumption is used to obtain the linearized equations of motion.

Using the fundamental equations of motion, the applied forces and moments are expressed as the forces and moments caused from disturbances. These equations will be used to form the transfer function of the rocket's pitching, yawing and rolling moments.

## 7.3 Roll Stabilization Technique

Roll stabilization control is implemented during the boost phase of flight (engine on), which will be approximately the first 25 km. As the controller receives constant flight data from the inertial measurement unit (IMU), the stability control algorithm will calculate the desired fin deflections to correct for the desired orientation. Four servo motors will be controlled by the flight control algorithm delivered by the flight computer. During this initial duration of flight, the algorithm will correctively change the control fin positions to change the rocket's roll, pitch and yaw moments to prevent instability of the rocket's orientation.

As mentioned in prior sections, during initial flight we will maintain control over pitch and yaw dynamics, while also bringing roll rate perturbations to zero. A roll control algorithm will be implemented maintaining a set-point roll rate equal to zero, in addition to having decoupled pitch and yaw motion separately controlled. Focusing on the pitch and yaw control system, the difference between the current pitch angle from disturbances and the rocket's ideal angle of projection will be computed. The set-point of the rocket's angle of projection will be zero to correct the rocket to a vertical position. In order to maintain stability, the control algorithm will use closed-loop feedback control to compensate for the disturbances administering a pitch and yaw motion on the rocket.

We could use of a roll rate gyro to reduce the roll rate during initial flight. The roll rate gyro results in a Type 0 system that will cause steady-state error in roll rate during the presence of constant disturbances causing rolling moment. To ensure the desired roll rate is controlled, a gyro with its input axis along the longitudinal axis of the rocket will be used. As a result, the feedback received will be a signal proportional to the roll angle about the longitudinal axis of the rocket.

## 7.4 Aerodynamic Fin Control Approach

Aerodynamic fin control will be responsible for control of yaw and pitching moments after engine cut-off, as well as the recovery period. Initially, the proposed

algorithm for stability prevents roll, pitch and yaw. After engine cut-off, only pitch and yaw will be controlled allowing the rocket to have rolling motion. Rolling motion will be achieved by differential movement of the controlled fins at the bottom. During this duration of flight, the set-point of rolling rate will no longer be zero, and will now have a desired rate of change as reference for the controller.

As seen in Figure 7.4.1, the reference position is set to zero. As several disturbances are encountered during flight, this will cause a change in the orientation about y-axis represented by  $\dot{\theta}$ . Using feedback control, the change in angle will be inputted back to the controller. To maintain the desired pitch angle, the control algorithm will calculate the desired moment needed to obtain the set-position, which will be sent to the servo motors to change the position of the fins. This process will also be used for both yaw and rolling moments.

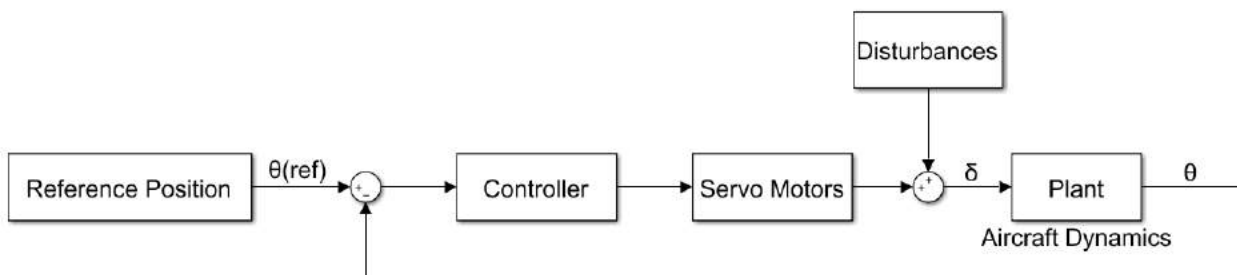


Figure 7.4.1: General block diagram of flight stabilization for pitching moment. This block diagram represents how the controller will be implemented in order to compensate for several disturbance during flight. The set-point of each reference position will be set to zero. The plant will consist of the aircraft dynamics that will consist of the pitch moment equation of motion. The input is the fin deflection angle  $\delta$  and the output is the pitch angle  $\theta$ .

## 7.5 Static Stability Analysis

To ensure mission success, stability of the rocket is a key concern. If unstable, the rocket has the possibility of flipping over mid-flight if perturbed slightly from its vertical path. While some flight vehicles exploit instabilities for increased maneuverability, our situation is the exact opposite, we want to exploit stability to safeguard against deviations from our desired trajectory. This is done by making the vehicle passively stable—a condition in which the vehicle naturally returns to its initial trajectory. Passive stability is governed by the location of the center of pressure caused by the airflow around the rocket and by the center of gravity of the rocket. The former is dictated by external geometry interacting with a freestream flow and the latter is governed by the mass distribution inside the vehicle. As the vehicle cruises, it can pitch slightly about its center of gravity due to weather or other factors. If the center of pressure is not coincident with the center of gravity, it will generate a moment during the pitching maneuver due to the equivalent pressure force applied at a distance from the rotational center. Therefore, if the center of pressure is above the center of gravity, the moment

tends to flip the vehicle but if it is below the center of gravity, it will tend to return the vehicle to its initial trajectory, creating stability.

Stability margins are measured in calibers, or the largest diameter of the vehicle, from the center of gravity to the center of pressure, positive being more stable. Using OpenRocket as a first iteration, it was determined that using a Von Karman nose cone and four trapezoidal fins, with dimensions given in Figure 7.5.0 and layout given in 7.5.1 (connected by a 13.2 in diameter and 26 ft long body tube), the stability margin starts at approximately 3 calibers around 0.1 Mach, increases to approximately 3.3 calibers at 0.8 Mach, continues to increase to 4 calibers around 1.35 Mach, at which point it starts to decrease, becoming neutrally stable at approximately 2.8 Mach. It is important to note that, as given in Figure 7.5.2 (pulled from the software's documentation [OpenR]), there is significant deviation from reality in stability beyond Mach 1 in OpenRocket. Thus, using the stability data generated in the lower Mach regime and extrapolating it following the experimental curve in Figure 7.5.2, we can assume a stability margin of approximately 3 for the majority of the flight. While this is stable, it is also overstable—it may have a tendency to pitch into the perturbation, i.e. weathercocking tendencies increase. To decrease the stability margin, the center of pressure only needs to be moved forward. This can be accomplished by smaller fins on the back, canards on the front, etc. Another important point is that the center of gravity used in OpenRocket differs from that of the CAD model. The more accurate CAD model gives the center of gravity as 194 in from the tip while the OpenRocket model has it as 226 in from the tip for the dry rocket. This only increases the stability margin. However, the center of gravity of the dry rocket in CAD is above its midpoint, making it unstable in other ways. Lastly, this analysis would be well suited for software such as the Fluent package of ANSYS but we are currently constrained to the student edition. The student edition restricts the number of elements allowed making the computation impossible to run. This should be alleviated in the future by joining up with other teams that have full access to the software.

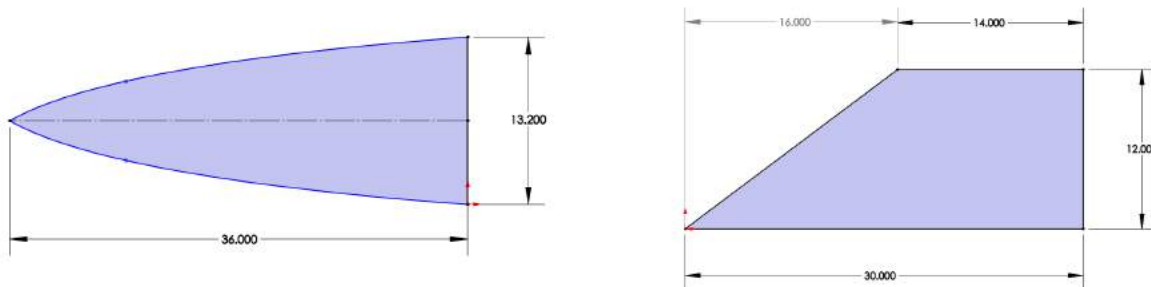


Figure 7.5.0. Dimensions for the Von Karman Nose Cone and Fins Used (in inches)



Figure 7.5.1. Rocket Layout used in the OpenRocket Simulation

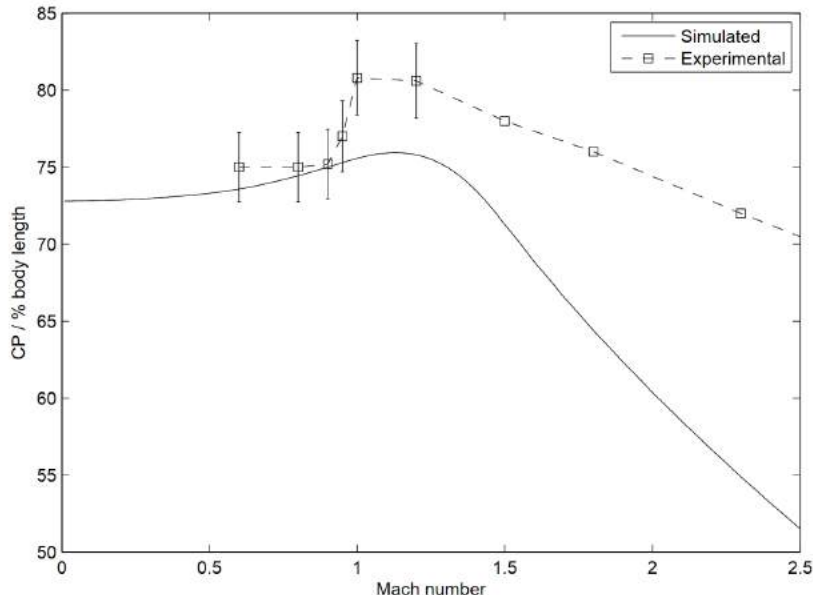


Figure 7.5.2: Experimental versus Simulated Center of Pressure. The graph exemplifies the deviation from reality that the model rocketry simulators have in locating the center of pressure. The solid line is simulated in OpenRocket [7.1].

## 7.6 Dynamic Stability Analysis

To ensure our rocket maintains stability during transonic and supersonic speed, the control system will adjust the positions of the control fins to correct for the rocket's deviations away from the desired flight path. To analyze this behavior, there are several parameters and control techniques that were evaluated to explain the behavior of the rocket's motion after experiencing external disturbances.

The damping ratio is used to determine the oscillatory response of the system. The controller design will aim for a critical damping ratio, resulting in zeta equal to one. The closer the damping ratio is to 1, the quicker the response to steady-state, in addition limiting oscillations in the system. As a result, the rocket would turn to equilibrium (set-point of 0) faster.

To ensure that this is accomplished in the controller design, a lead-lag compensator will be used as the controller design. In the frequency domain, the open-loop transfer functions for the various rocket moment dynamics will be analyzed, forming the transfer functions between each angle deflection caused by disturbance, and the output of the rockets angle (see Figure 1). Creating a bode plot, an analyzing the gain and phase margin, the system of response will be evaluated to determine the speed of response. With a lead compensator, positive

phase can be added to the system thus increasing the desired damping (see equation 7).

$$\zeta = \text{Phase Margin(degrees)} / 100^\circ \quad (7)$$

The lead controller has less tendency to saturate. It contains a gain, zero, and pole (see Equation 8). In a lead compensator, the magnitude of the zero is less than the magnitude of the pole. This design approach replaces a real pole at larger value, thus increasing the speed of the response without decreasing stability. To account for steady-state error, a lag controller (see Equation 9) will be used in parallel with the lead compensator.

$$\text{Lead (s)} = K(s - z)/(s - p) \quad z < p \quad (8)$$

$$\text{Lag (s)} = K(s - z)/(s - p) \quad z > p \quad (9)$$

## 7.7 Selection of Aerodynamic Shapes

Selection of the aerodynamic shapes for the vehicle are of utmost importance to optimizing the flight trajectory by minimizing drag. For instance, if the drag coefficient is increased from 0.1 to 0.2 on the nose cone, it could easily prevent us from hitting our 100 km altitude mark possibly by kilometers. Therefore, a study was performed to find a suitable nose cone shape and wing shape. It is pertinent to note that through OpenRocket simulations, the body tube maintained the maximum drag coefficient of all components, starting at 0.4, increasing slightly during the transonic region, and decreasing to approximately 0.33 afterwards.

### 7.7.1 Nose Cone

There are many nose cone types, most having specialized flight regimes they are optimized for. As our rocket will be operating from 0 to approximately 5 Mach, it is important to use a shape that is effective over the full flight range. Studying Figure 7.7.1.0, it is noted that the Von Karman nose cone, a Haack series with a specific parameter set to zero, is in average, optimal over our flight regime. This is because it is mathematically designed for minimized drag given a length and major diameter [7.2]. Therefore, it is selected.

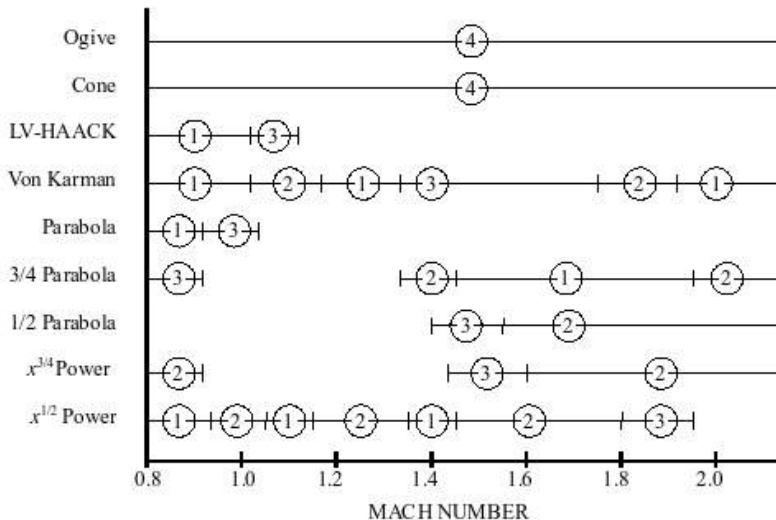


Figure 7.7.1.0: Nose Cone Types and Their Effectiveness at Different Mach Numbers with 1 Being Good and 4 Being Poor [7.3].

The Von Karman shape is defined by the Haack series,

$$\theta = \arccos \arccos \left( 1 - \frac{2}{xL} \right)$$

$$y = \frac{R}{\sqrt{\pi}} \sqrt{\theta - \frac{\sin \sin(2\theta)}{2} + C \sin^3(\theta)}$$

where  $R$  is the major radius,  $y$  is the radius at position  $x$ ,  $L$  is the total length, and  $C$  is a coefficient. For a Von Karman  $C = 0$  [7.4]. This was utilized to generate our nose cone shape for a total length of 36 in and a major radius of 6.606 in. Using an OpenRocket simulation, the nose cone selected starts at a coefficient of drag of 0.02 and peaks at 0.12 when passing through the transonic region (maximum peak occurred around 1.11 Mach). Possibly blunting the nose or adding a drag-reducing aerospike could bring this value down but that is left for future work.

## 7.7.2 Nose Cone

Fins can be used in a few ways, statically straight to ensure a straight flight, fully or partially/sectionally dynamic to maneuver the vehicle, or permanently canted to automatically spin stabilize the vehicle. Although spin stabilization is useful to help ensure a straight flight, the complications of sloshing fuel forced us to reject the idea when in fueled flight. Because we desire some control over the vehicle, the statically straight fins will not be used. This leaves only actuated fins, and since actuating only part of a large fin is easier than the whole fin, we chose to actuate a section of a static fin to act as our control surface.

To optimize efficiency, an airfoil shape is employed. When picking the airfoil shape, minimizing drag is key while still keeping efficacy of the fin. Therefore, the NACA 0006 was selected as it is symmetric (does not induce unwanted lift effects), thin, has minimal drag, but can still be effective at maneuvering at low angles of attack. The shape can be seen in Figure 7.7.2.0, and the coefficients of lift and drag for different conditions are given in Figure 7.7.1.1.

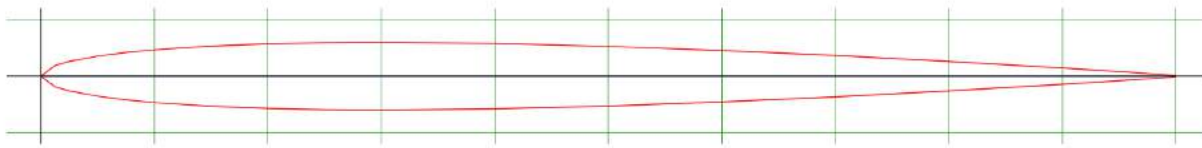


Figure 7.7.2.0: NACA 0006 Profile [7.5]

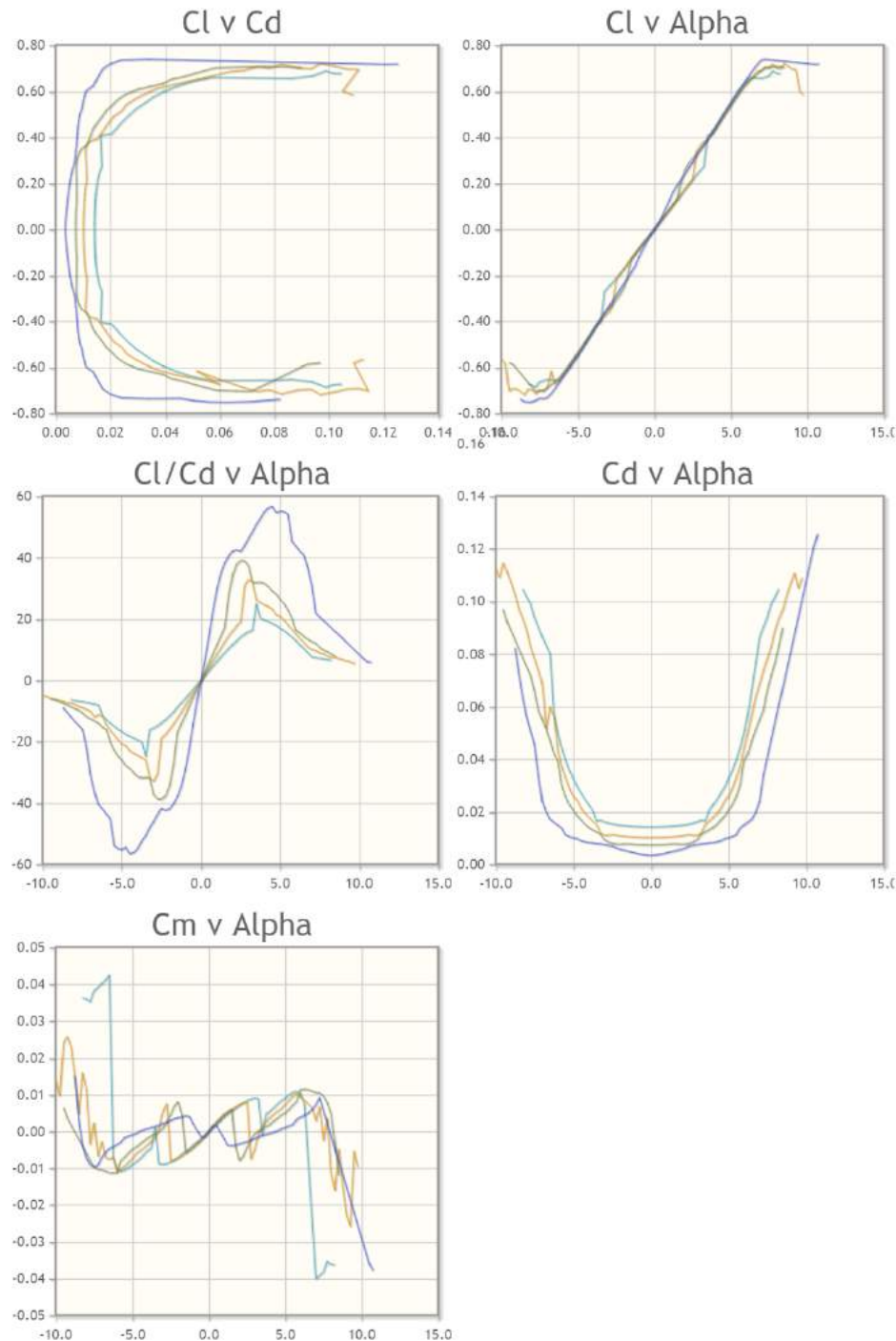


Figure 7.7.2.1: NACA 0006 Aerodynamic Coefficients [7.6]

# 8.0 Electronics and Altitude Monitoring

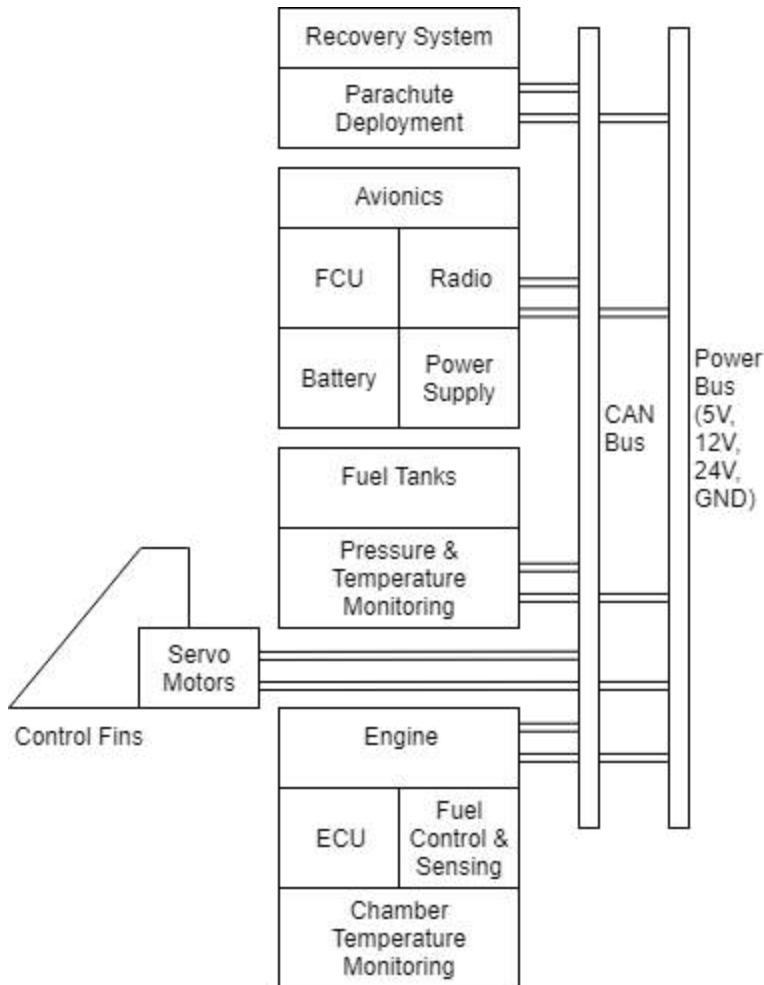


Figure 8.0.1: Simplified diagram of our rocket's electrical systems

## 8.1 Flight Computer

Our control systems have three main responsibilities:

1. Send telemetry down a link and listen for any command messages coming back up from the ground.
2. Sequence the mission (burn, coast, recovery, etc.) based on sensor data and external commands.

3. Run the active stabilization control loop at a high enough rate with sufficiently bounded latency and jitter.

We've evaluated multiple options for flight computer hardware, initially considering the BeagleBone, Raspberry Pi, single-board computers with ARM SOCs. However, our control loop does not need to run faster than 100 Hz; running too fast would be detrimental — destabilizing the system and introducing flutter. Given this relatively slow control rate, using a high-performance ARM microcontroller is sufficient.

We are targeting a Cortex-M microcontroller, with STMicroelectronics as the preferred vendor. The STM32F4xx and STM32F7xx lines both have sufficient compute capacity. Our current preference for the flight controller is the STM32F413, a good balance between compute capability and large peripheral count (3x bxCAN peripherals, 10x USARTs).

If we need to upgrade during development to a larger STM32 microcontroller to handle increased requirements, STM32 chips are code and peripheral compatible within a family (eg, F4) up to specific chip peripheral options. Custom circuit boards will be designed to interface the main flight computer with sensors, actuators, and their supporting equipment in a mechanically and electrically robust fashion.

Harnessing all engine monitoring sensors and control actuators back to a central microcontroller is prohibitively complex and expensive. As a result, we've decided to delegate engine monitoring and low-level control responsibilities to a smaller microcontroller localized to the engine assembly. This engine controller will communicate with the main flight computer via CAN, vastly reducing harnessing requirements and decreasing signal degradation in analog signal paths for pressure transducers and thermocouples. We're targeting the STM32F413 microcontroller, the same model used on the flight controller. The system design of this engine controller can be found in section 8.1.1.

Assuming we have 15 to 20 pressure transducers and a similar number of thermocouples on the engine monitoring system and we transmit data as single-precision floating point numbers (worst case; most sensors have far less resolution than a single-precision float and we could send data as fixed point), then transmitting data to the main flight computer at 10 Hz requires a bandwidth of  $10 \text{ Hz} \times 20 \text{ channels} \times 4 \frac{\text{bytes}}{\text{channel}} = 6.4 \text{ kilobits/s}$

Even in low-speed mode, CAN has a maximum bandwidth of 128 Kbps, far greater than the computed necessary bandwidth. We can easily send engine telemetry back to the main flight computer, with plenty of bus bandwidth to spare for commands and other data.

### **8.1.1 Engine control and monitoring**

The control for the engine will be partitioned off onto a separate, dedicated Engine Control Unit (ECU). It will be solely responsible for monitoring and controlling the engine with four essential input signals: temperature, pressure, flow

rate, and vibration. It will be the only access to engine ignition. The main Flight Control Unit (FCU) will send commands over the CAN bus to request certain amounts of thrust from the ECU, which has full control over the fuel lines and can disregard these requests if they endanger the engine or the rocket. Further details of the ECU and FCU firmware and operation can be found in sections [9.1.1](#) and [9.1.2](#).

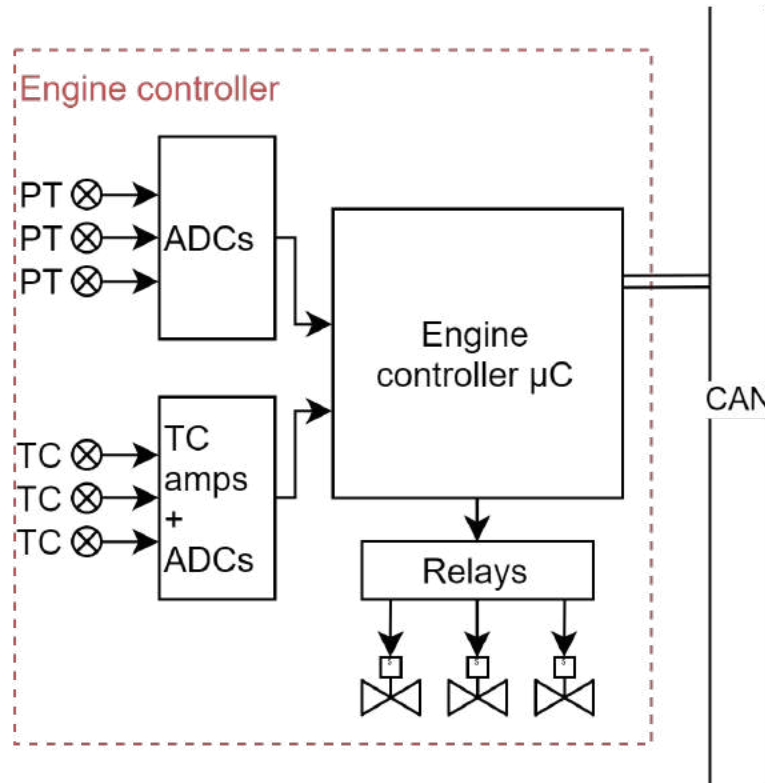


Figure 8.1.1.1: Engine Controller Architecture.

The controller will be directly connected to all of the sensors monitoring the fuel lines around the engine, and a sensor measuring chamber temperature itself. As shown in the P&ID diagram in section 3.6, the engine controller will be connected to sensors monitoring the fuels lines near the engine.

Sensing in the environment around the engine is challenging, with high vibrations and temperatures, and potentially corrosive fuel. We will ensure all sensors in contact with kerosene or peroxide fuel will not react or corrode in contact with them. We chose sensor ranges carefully, to be about  $\frac{2}{3}$  greater than potential input to avoid sensor saturation and invalid data. We carefully evaluated them to be fail-safe to enable detection of spurious data.

### 8.3.1.1 Pressure Transducers

We propose to use MLH series Honeywell heavy duty pressure transducers [8.1] to measure pressures in fuel lines and tanks. With a range of 50 to 2000 psi, they offer good output linearity across this large range. To reduce the

possibility of noise, we will sample from small ADCs mounted next to these sensors at 100Hz via RS485 lines routed to the ECU.

### 8.3.1.2 Temperature Measurement and Thermocouples

We chose to use grounded Chromel-Alumel (K type) thermocouples [8.2] in all of our extremely high or low temperature measurements due to their wide temperature range, fast response, and common availability. These are shown in the PI&D in [Section 3.6 Valves and Plumbing](#) as the sensors on fuel lines next to the chamber. We will use integrated thermocouple to digital converters such as the MAX31855 [8.3] instead of conventional cold-junction compensators because of their simple operation and usage. Secured on a custom PCB, we will encapsulate them inside an insulated box as the outside temperature could pull them out of their operating region.

The chamber temperature will likely be too high for thermocouples to function, even for extremely high temperature tantalum sheathed platinum/rhodium probes. If chamber temperature is required, high temperature infrared pyrometers could potentially be used. We are unsure if they would function in the engine plume environment, but they would be tested and used if they are reliable.

### 8.3.1.3 Valve Control

The two main valves controlling the fuel lines will be electro-pneumatic valves, with actuating pressure from the helium tank as shown in figure [[3.6 Valves & Plumbing](#)]. Larger solenoid valves will control pressure out of the helium tank and the helium tank fueling input for remote pressurization or depressurization. We will drive all solenoids using custom boards featuring integrated power MOSFETs, flyback diodes, and galvanically isolated gate drivers. We will also add voltage stiffness with on-board electrolytic capacitors potted for vacuum exposure. The galvanic isolation will prevent any ESD or noise from turning on the MOSFETs and thus opening the valve when not intended.

## 8.1.2 Backup Systems Controller

The backup systems controller is an Arduino variant (most likely, an Arduino Due) with a CAN interface. In the case of main flight computer failure during powered and unpowered flight, it will take control of critical sensors, instruct the engine controller to gracefully shut down via CAN, and handle recovery system deployment.

## 8.2 Power Supply

We ran total power estimates for the rocket, and divided rocket run-time into four stages: engine run time, controlled descent time, nominal recovery time, and

emergency recovery time. At each stage, different systems will be operating at different levels of capacity and output. Nominal recovery time, during which the radio is transmitting frequently, was chosen to be around three hours. If the rocket has still not been recovered in that time, it will go into emergency recovery mode, transmitting less frequently. Power estimates were run so that this emergency period could last a minimum of two days.

Table 8.2.1: Table of power requirements over the rocket's flight and recovery

Rocket Power State	Time (Hours)	Average Power Required (W)	Total (Wh)
Engine Run Time	0.017	87.15	2.91
Stabilized Descent Time	0.12	59.43	14.52
Nominal Recovery	3.00	0.42	2.49
Emergency Recovery	48.00	0.03	3.169

From these estimates, the minimum power needed is 15.4 Whrs. When selecting our batteries, we allowed for large safety margins as this is a rough estimate of the power requirements.

We choose to use high output polymer lithium-ion cells to power the rocket during flight and during recovery. Although they require multiple layers of protection to mitigate thermal runaway they have much higher energy densities, low cost, and high current output than NiCd batteries or Li-Ion cells. Similar types of lithium polymer pouch cells have been tested in vacuum conditions, and if restrained properly they do not suffer significant changes in energy output and storage abilities.

Four Polymer Li-Ion 6050140-10C [8.4] 3.7V cells, each with a 40A discharge rate, will be placed in series to create a main battery with 14.8V nominal voltage. The total energy storage of the system will be 59.2 Whrs, more than three times the calculated 15.4 Whrs needed by the rocket. Each cell will be slotted into and constrained by an aluminum enclosure to create a structurally sound battery that will also allow any heat generated by the batteries to easily dissipate.

Electrical protection, isolation, and management will be more complex. An on board commercial 4S PCM [8.5] will be used to balance cell charge, monitor batteries and protect them from over-discharging. By managing charging inside the rocket next to the batteries, we will avoid issues with voltage drops over long charging cables from and to the rocket. Finally, in case of PCM failure, a 40A fuse will prevent any over discharge of the cells and the thermal runaway that could result.

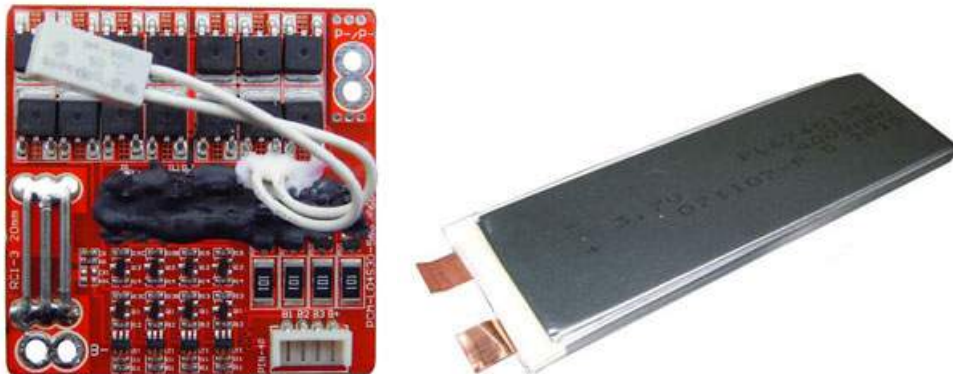


Figure 8.2.1: PCM module and the high power lithium polymer cells we will be using

At this battery voltage of 14.8V, we found DC/DC conversion efficiency using common commercial parts rated to our anticipated maximum current requirements. On the rocket, DC/DC buck or boost converters at the properly rated currents will supply the voltage lines of 3.3V, 5V, 12V and 24V and will be mounted to a custom PCB. The maximum possible output current seen by the battery was determined to be 27 amps. Actually reaching this amount of current draw during flight is unlikely. Even at this value, our batteries will be able to output the required current with a safety margin of 1.52.

Table 8.2.2: Table of maximum current requirements at each voltage level to estimate maximum battery discharge requirements

<b>Voltage Level</b>	<b>Max Wattage Needed (W)</b>	<b>DC/DC Converter Efficiency</b>	<b>Max Battery Current Required (Amps)</b>
3.3V	3.3	83% [8.6]	1.12
5V	99.6	88% [8.6]	20.96
12V	36	95% [8.7]	3.41
24V	17.28	89% [8.8]	0.87

We will thoroughly test all of the cells at various pressures and temperatures to ensure battery operation across the flight. Although they have already been tested at 11.6 kPa and -20C to ensure transportability as part of the UN38.3 certification, we will further test them at the 1.12 kPa and -40C they will briefly experience at around 100 Km. At these conditions, cell voltage and internal series resistance will be measured to ensure nominal battery operation. Afterwards, we will inspect them for any degradation.

## 8.3 Electrical Ruggedization

While traveling through 100 km of atmosphere and back, the rocket will experience large variations in temperature and pressure. This range of temperature at times will be outside of the regular industrial electrical component rating of -40 °C to 85 °C, but only for a short duration of time.

Thus, we will secure the majority of the avionic components in a thermally and electrically insulated aluminum chamber. Inside the chamber, we will use lightweight fiberglass blankets, isolating the entire chamber from the extreme thermal changes and vibrations. This chamber will not be airtight, however, and will allow the pressure inside to vary with external pressure. Certain components, especially vented electrolytic capacitors, are more sensitive to pressure changes. Any electrolytic capacitors will be potted with epoxy to stop ruptures in the vacuum environment. Even inside this insulated box, water condensing in the interior of the rocket presents a major issue. Electronic grade silicone sealant will be used to protect any components or PCBs that are not already waterproof to prevent shorts or other issues.

We will carefully choose and test components that are necessarily external to the core avionics like sensors, antennas, mechanical actuators and power drivers. Utilizing thermal models of the rocket, the exact temperature ranges each sensor and actuator undergoes will be determined. From this information we can select and test high or low temperature tolerant components at the ranges they will experience.

### 8.3.1 Harnessing

Harnessing in the rocket presents a unique set of challenges and requirements. Most of the connections throughout the rocket will be teflon coated wire, as they provide a larger range of operating temperatures and are less brittle than PVC when cold. We will mitigate electrostatic discharge and electrical noise in all signals through the rocket with copper shielding in wiring and containment boxes for the various avionic components.

We will carry the voltage mains, ground return, and the main CAN bus along a primary cable bundle through the rocket. The differential CAN signal will be routed using a twisted pair of wires with an overbraid to reduce noise and crosstalk. We chose two separate Beldon 83322E PTFE cables to route the CAN bus and the power through the rocket. The teflon allows the cable to withstand -65C to 200C, assuring that there will be no issues with insulator cracking or melting.



Figure 8.3.1.1: Belden shielded PTFE cable will route the CAN bus and power through the rocket

Additional teflon sleeving and insulation will be used near fuel tanks to reduce cracking or flexibility if there are any issues with extreme cold. PTFE coaxial cable will be carefully routed from the radio inside the avionic compartment to the antennas. A single ground return line will be routed, and care will be taken to eliminate potential ground loops within the system.

We will adhere to harnessing standard NASA-STD-8739.4 in the actual construction of the rocket. We will use crimp connections wherever possible. To test the harnessing system, we will be constructing a wooden mock-up of the rocket with all of the cables needed in place. This way cable resistances, parasitic impedances and potential interferences can all easily be tested and simulated on the ground. Decoupling capacitance will be installed as needed through the rocket to prevent voltage drops from line inductance, especially on the input voltage lines of sensors used.

## 8.4 Position and Altitude monitoring

Our control loop, recovery system, and potential pad umbilical ejections all require inertial data. To obtain these measurements, we're using a 9 degree of freedom inertial measurement unit. There are a wide range of devices available on the market; we evaluated Xsens, Analog Devices, and KVH. We've decided to use Xsens MTi-series products due to their good performance and reasonable pricing, as well as their factory tuned high-quality onboard Kalman filter which outputs attitude Euler angles and quaternions with no additional computational overhead on our part.

To obtain better safety, robustness, and accuracy guarantees, three IMUs will be used: one MTi-30 and two fallback hot-standby MTi-3s. During sampling, data is read from all three IMUs and assessed for consistency. Obviously erroneous measurements (eg, gyro range clipping) are discarded and the inconsistent IMU disabled. If all three IMUs are active, voting is performed with an approximate similarity measure; the majority sample is taken as ground truth.

To provide accurate altitude measurements after the COCOM limits are reached, two different barometric altimeters will be used. First, for low altitude

measurements, we will use an Xtrinsic MPL3115A2 [8.9] altimeter in addition to GPS altitude measurements. After around 50 km, this altimeter will not be reliable as the pressures outside the rocket will simply be too low. Thus, a second, ultra-low pressure sensor will be included to give altitude estimates once the rocket is above 50km. We chose a Honeywell ASDX [8.10] series pressure sensor to provide these estimates. We will need to verify that this sensor will function at the low temperatures it will experience with thorough testing.

## 8.4.1 Telemetry

The telemetry system consists of three parts: The telemetry downlink operating on the 33-cm band, command uplink on the 70-cm band, and an APRS data redundancy downlink on the 2-meter band.

### 8.4.1.1 Flight and Ground Antennas

Several antennas will be used in order to maintain a continuous connection with the rocket. The table below shows the antennas that will be flown onboard the rocket.

Table 8.4.1.1.1: Onboard antennas

Antenna	Gain (dBi)	Polarization	Purpose
900 MHz Half Wave Dipole [8.11]	2	Vertical linear	Primary telemetry downlink and backup uplink
434 MHz Half Wave Dipole [8.12]	2	Vertical linear	Primary telemetry uplink
144 MHz Half Wave Dipole [8.13]	2	Vertical linear	APRS redundancy downlink

The next table shows the antennas that will support the ground station. All directional antennas will be attached to an antenna tracker, which is explained in more detail in section 3.1.

Table 8.4.1.1.2: Ground antennas

Antenna	Gain (dBi)	Polarization	Purpose
900 MHz Patch Antenna [8.14]	8	Right Hand Circular	Long-range telemetry downlink
900 MHz Dipole Antenna [8.15]	5	Vertical linear	Short-range telemetry downlink

434 MHz Yagi Antenna [8.16]	10	Vertical linear	Long-range telemetry uplink
-----------------------------	----	-----------------	-----------------------------

### 8.4.1.2 Telemetry Downlink

The primary radio downlink utilizes the XBee-PRO SX [8.17] operating on the 33 cm radio band. The radio broadcasts with 1W of power and a medium data-rate speed of 13.75 kilobytes per second [8.18]. We can confirm that the radio will be able to transmit throughout the duration of the flight using a link budget. The table below defines the terms used in the equation.

Table 8.4.1.2.1: Definitions of link budget equation terms

Name	Symbol
Received Power (dBm)	$P_{out}$
Transmitted Power (dBm)	$P_t$
Transmitter Antenna Gain (dBi)	$G_t$
Transmitter Loss (dB)	$L_t$
Free Space Path Loss (dB)	$L_{fs}$
Miscellaneous Loss (dB)	$L_m$
Receiver Antenna Gain (dBi)	$G_r$
Receiver Loss (dB)	$L_r$

The Link Budget equation is:

$$P_{out} = P_t + G_t - L_t - L_{fs} - L_m + G_r - L_r \quad (8.1)$$

To calculate the free space path loss, use the following equation:

$$L_{fs} = 20 * \log_{10}(\text{distance}) + 20 * \log_{10}(\text{frequency}) + 32.44 \quad (8.2)$$

Using a maximum distance of 150 km at a transmitting frequency of 928 MHz, we can calculate the free space loss to be 135.3 dB.

Values from Table 8.4.1.2.1 can now be added into equation (8.1) in order to calculate the received power in addition to a 3 dB receiver loss caused by the polarization mismatch [8.19]. The received power is calculated to be -98.06 dBm. This is within the receiver's -106 dBm sensitivity limit [8.18].

In the case of a failure in the primary command uplink system, the XBee-PRO SX on-board the rocket is capable of receiving commands from the ground system.

#### **8.4.1.3 Command Uplink**

The primary command uplink system will use the LoRa RFM96W module transmitting on the 434 MHz amateur radio band. This radio will transmit at 100 mW at a bandwidth of 34.25 bytes per second. Similar to section 2.5.2, we can establish a link budget to ensure that the radios will be able to transmit and receive data from a distance of 150 km.

Using equation (8.2) and a frequency of 434 MHz, the free space path loss can be calculated to be 128.7 dB.

Values from Table 8.4.1.2.1 can now be added into equation (8.1) in order to calculate the received power. The received power is calculated to be -96.72 dBm. This is within the receiver's -148 dBm sensitivity limit [8.20].

The LoRa radio has additionally been successfully tested by a team member on a high altitude balloon at a line-of-sight distance of 120 km.

#### **8.4.1.4 Telemetry Protocol**

All telemetry and command messages will be sent using the following format:

\$WISR, ID, COUNT, < DATA >\* CHECKSUM

Table 8.4.1.4.1: Command message format breakdown

<b>Identifier</b>	<b>Purpose</b>
\$WISR	Callsign
ID	Signifies which data points are being transmitted in the packet
COUNT	An incrementing counter showing the packet order
<DATA>	Comma-separated list of data points
CHECKSUM	A CRC-CCITT-16 checksum [8.21]

The total length of each transmitted packet will not exceed 256 bytes.

### 8.4.1.5 APRS Data Downlink

In addition to the onboard telemetry system, we will be running a Tracksoar V2, which is a fully commercial off the shelf (COTS) data acquisition and telemetry system. It will be powered by 2x AA batteries and will run independently from all of the onboard avionics and telemetry. The onboard sensors will report temperature, pressure, humidity, location, and altitude.

The system will be transmitting its data via APRS with an expected line-of-sight range of over 400 miles [8.13]. Packets will be received and uploaded to the internet via publicly run local receivers.

### 8.4.1.6 Doppler Analysis

To ensure we won't have link loss during thrust due to Doppler shift, we calculated frequency shifts and compared them to the maximum allowed deviation in the radio datasheets. We can compute Doppler shift as

$$f = \left(\frac{c}{c+v}\right) f_0$$

where  $f$  is observed frequency,  $f_0$  is transmitted frequency,  $v$  is the velocity of the rocket relative to the receiver, and  $c$  is the speed of light.

Based on calculations in [Section 2.5: Predicted Performance](#), the peak speed of the vehicle is 1263.46 m/s. We then find the shifts for our radio bands:

**Table 8.4.1.6.1:** Doppler analysis

Radio	$f_0$ (nominal)	$f$ (shifted at peak $v$ )	$\Delta f$
LoRa uplink	434 MHz	433.998 MHz	1.629 kHz $\approx$ 3.75 ppm
XBee downlink	928 MHz	927.996 MHz	3.911 kHz $\approx$ 4.21 ppm

LoRa's spread spectrum encoding is extremely robust to frequency shifts and has been tested extensively for CubeSat applications [8.22]; a shift of 3.75 ppm will not affect the rocket's ability to receive command messages. For the XBee downlink, the XBee has an RF selectivity of 900 to 930 MHz, and, at medium data rate, an IF selectivity of  $\pm 250$  kHz at 30 dB and middle data rate; our doppler shift is extremely compared to these figures and should not affect performance.

## 8.4.2 In-Flight Altitude Prediction

In order for our apogee to be as close to the 100 km target as possible, the flight computer will actively determine if engine shutoff must occur before all of the rocket's fuel has been burned. Once an apogee of greater than 100 km has been

predicted, the flight computer will trigger an engine shutoff and vent any excess propellant. It will perform this prediction using the rocket's instantaneous velocity, acceleration, and altitude. For this purpose, we will need a pitot tube [8.23] to measure the rocket's speed/velocity relative to the surrounding air mass.

# 9.0 Software

## 9.1 Rocket Embedded Software

Our rocket's embedded system architecture has two main parts, the Flight Controller and the Engine Controller. Each subsystem has its own computer that runs its own custom firmware for autonomous operations. The Flight Controller firmware is in charge of advancing the rocket through the various stages of the mission. The Engine Controller firmware monitors the rocket's engine health and can control the various elements of the engine following commands from the Flight Controller.

### 9.1.1 Flight Controller (FCU)

The mission is sequenced by a finite state machine, with transitions triggered by both onboard events (sensor readings and models) as well as external commands. External control is necessary in two cases:

1. On-pad, we must manually advance the state machine during fuelling, as well as giving an ignition command. Aborting during, for example, the pressurized state is also necessarily remote and manually-controlled, and triggers proper venting to return the rocket to a safe-to-approach state.
2. In-flight, aborts are mainly useful in the event of severe engine malfunction during the firing state; a manual abort here would trigger an immediate transition to coasting.

In pad states, abort often has a manual component in addition to whatever automatic responsibilities are detailed here; see [Section 12.1.6 Pad Abort](#) for more information.

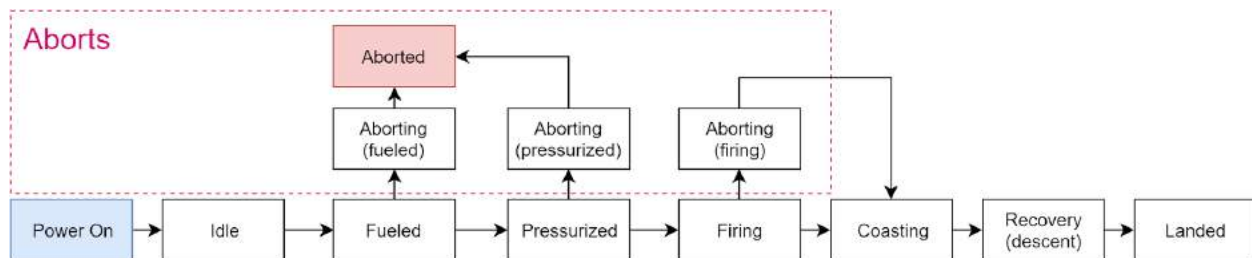


Figure 9.1.1.1: High-level state-machine overview.

Resource access and critical sections are necessary to support our complex coexisting synchronous and asynchronous tasks. We've decided to use an RTOS, using the standard ARM Cortex-M NVIC interrupt priority controller as a low-cost backend. This allows interrupt tail chaining and low-cycle-count prioritization. To

decrease overhead from repeated interrupts, we use Direct Memory Access (DMA) wherever possible.

Synchronous sensor data is sampled at a rate of 100Hz. All asynchronous systems are configured to transmit data at a rate matching or exceeding the synchronous sampling rate, so that each sampling period is guaranteed to contain a received sample from all asynchronous devices.

ECU asynchronous monitoring data via the CAN link is written in the background via DMA to buffers in RAM, firing interrupts when complete. IMU data is also asynchronously received via DMA, but we wait for all redundant IMUs to return data, with some timeout in case an IMU is offline; after acquiring all data, we use a voting system to decide which IMU to pick as ground truth for that sample. IMU sampling is additionally synchronized with the FCU's sampling periods via vendor-provided APIs and physical trigger channels.

The control loop is run once all sensor collection for a sampling period is complete. As such, it nominally runs at 100Hz, with some variance due to waiting for sensors. Based on preliminary controls analysis, small background jitter is not particularly problematic for our active stabilization systems. We can also analytically bound the maximum possible variance in execution period, assuming at least one IMU is operational, the IMUs strictly follow datasheet variances, and the ECU is operational.

During sampling periods, data relevant to telemetry is pushed onto ring buffers. This queued data is assembled into packets and transmitted periodically when the FCU has idle CPU time at a nominal rate of  $\sim$ 10Hz. Telemetry data plus additional monitoring is written locally to a redundant pair of SD cards for flight logging purposes.

Messages received by telemetry/command radios are buffered and trigger interrupts causing state transitions or actuations. Any abort messages received are propagated onto the CAN bus; arming messages relevant to ECU operation are also relayed.

### 9.1.2 Engine Controller (ECU)

The engine controller is local to the engine and handles engine-specific control responsibilities, receiving commands from the flight controller over CAN and sending back telemetry. In addition to raw telemetry, the ECU monitors and reports engine health based on expected nominal parameters of the engine and supporting components in the current state. All commands are received over CAN via the STM32's bxCAN peripheral and buffered; an interrupt processes these commands and causes internal state changes and actuations.

The ECU's firmware is bistable. In safe mode, commands resulting in potential engine ignition are ignored. Commands triggering fueling actions are accepted, as the ECU is responsible for fuel line controls.

When ground control sends an engine-arming message, the FCU will relay that message over CAN to the ECU, initiating a transition into armed state. Pre-fire aborts will trigger depressurization and fuel draining in a fashion which prevents

propellant fire or explosion; during-fire aborts trigger safe engine shutdown and fuel dumping at the maximum possible safe rate.

During nominal operation, the ECU is responsible primarily for sequencing valve actions based on high-level FCU command. The two major command functions are ignition (see propulsion section) and safe nominal shutdown (used before coasting).

## 9.2 Ground Dashboard Software

Our ground dashboard software will allow team members on the ground to view telemetry data collected by sensors on the rocket. It will also give us the ability to send commands to the rocket to sequence the mission through launch or to trigger transitions to abort states in extraordinary circumstances. The application will consist of a single page Graphical User Interface (GUI) displaying live telemetry data. The GUI will run responsively in a fixed 16:9 aspect ratio on the device of our choosing. Figure 9.2.1 provides a simple, high-level view of our dashboard software architecture as well as its interfaces with other systems and operators.

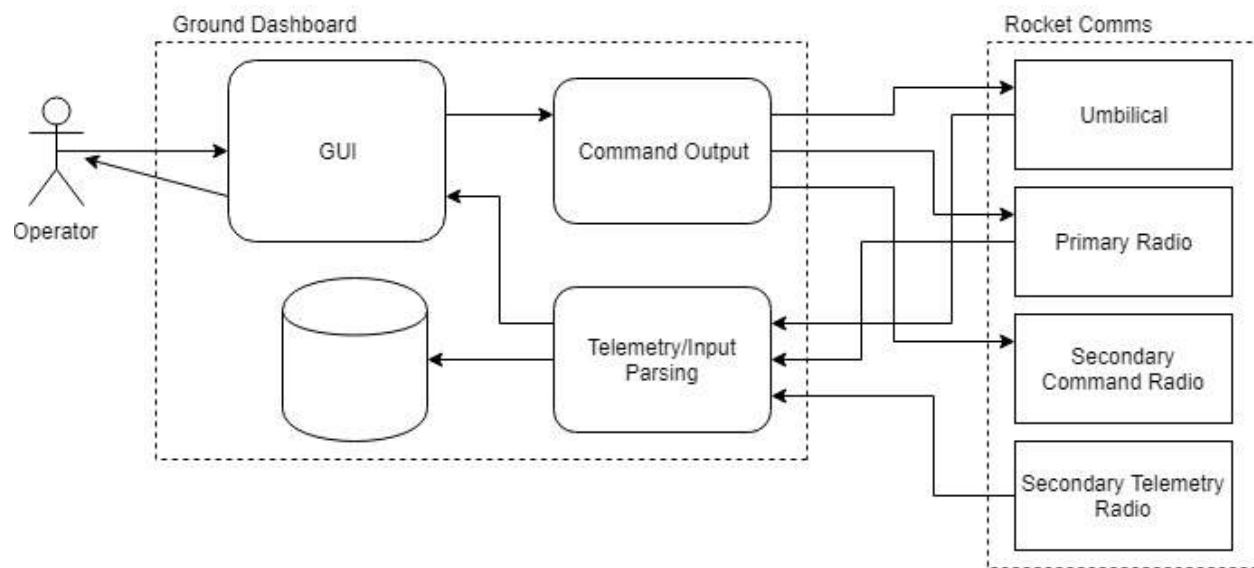


Figure 9.2.1: Dashboard software architecture block diagram

The dashboard will transmit data over a serial connection via the umbilical while the rocket is on the pad. The dashboard also interfaces with our primary radio for sending and receiving data/commands, a secondary radio that will repeat commands sent by our primary radio, and a secondary radio for receiving telemetry data. Received data will be stored in a database or more lightweight storage like a JSON file.

## 9.2.1 Technology Stack

We considered several options while deliberating on the dashboard's technology stack. We went with Node.js as our JavaScript runtime environment, using it to write all backend code. This decision was made mostly due to team member experience with JavaScript. We want the dashboard to be a project that new members or those with limited experience can contribute to right away.

We also selected Node.js for its event-driven concurrency model and non-blocking I/O. This allows our dashboard accomplish multiple tasks at once, without needing an explicitly multithreaded design. An event-driven model matches our system model well, since the reception of data and push of a command button can be viewed as events; this will result in clean code that maps nicely onto our real-world systems.

To implement the dashboard as a standalone application, we've chosen Electron, a Node.js-based toolkit for building desktop apps. The application backend will deal with system interfacing (namely, serial data transmission and reception), passing data to and from a frontend based on modern web technologies, and storing telemetry data in a database/log file for later reference.

We're building the frontend in a to-be-determined frontend framework to ease page rendering and dynamic content. Further evaluation is necessary, but we are leaning towards Vue.js, due to its popularity and relatively low barrier to entry. We don't think it's necessary to use a full framework like Angular at the moment, as we have only a single page and a somewhat unusual data architecture, which would only be hindered by a more opinionated framework.

## 9.2.2 Graphical User Interface (GUI)

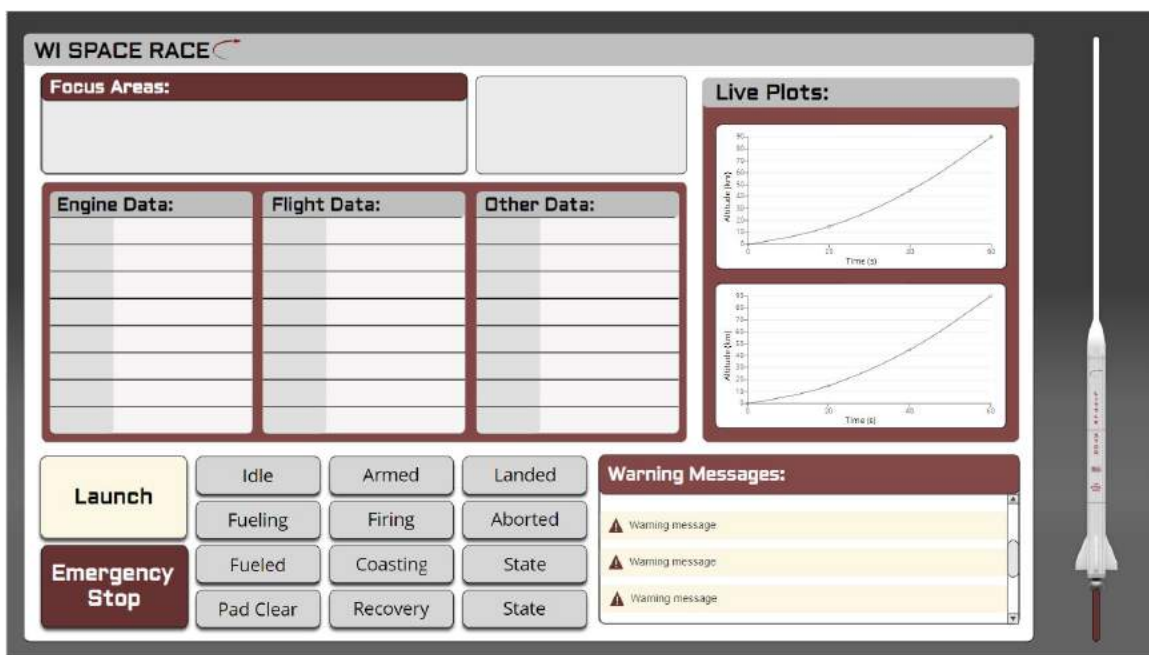


Figure 9.2.2.1: Mockup of Ground Dashboard GUI

**Focus Areas:** Displays data of interest (altitude, velocity, etc.).

**Live Plots:** Generates graphs of telemetry data during flight. Operators can specify what data they wish to display at the moment.

**Data Lists:** Displays various live telemetry data.

**Warning Messages:** Displays error messages for vehicle health data nearing out-of-bounds. We will cap the rate at which messages will be displayed per datum to avoid clutter.

**State Transition Buttons:** Allows us to send a command to the rocket to manually transition to a state when appropriate. Valid transitions will be highlighted (red), as well as the current state we are in (green). <confirmation> The buttons shown serve as an example, not our actual states. Additionally, abort states will be represented as larger buttons similar to the Emergency Stop.

**Rocket:** Represents progress to the Kármán Line. Rocket moves up the screen as our altitude increases to 100 km.

# 10.0 Recovery System

The recovery system uses a 2 m drogue and a 10 m main chute deployed at altitudes of 30 km and 1 km, respectively. The nose cone separates into two pieces at apogee, which exposes the parachute deployment system. CO<sub>2</sub> gas canisters activated by actuators, will provide a rapid release of pressure to eject the parachutes out of their housing at the desired altitude. Both parachutes will be attached by 1 inch thick kevlar webbing (each webbing rated for 2000 lbs). Parachute deployments will nominally be triggered at their corresponding altitude during descent by the flight computer. In the case of an abort, the drogue chutes will be triggered when the rocket is both decreasing in altitude and at an altitude less than 30 km. The main chute will be deployed at an altitude of less than 1000 m.

## 10.1 Parachute Sizing and Deployment Altitude

Initial parachute sizing was determined by solving the equation of motion for an object in free-fall (using a drag coefficient of 1.2). A standard “rule of thumb” for high powered rocketry is a maximum descent rate of ~7 m/s on impact. As can be seen from Figure 10.1.1, a parachute diameter of 10 m results in a final descent velocity of 5.5 m/s (12 mph).

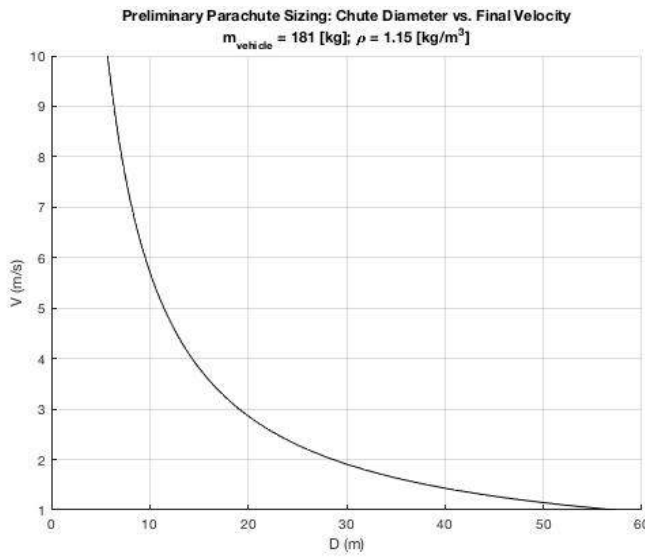


Figure 10.1.1: Initial parachute sizing calculation shows a parachute diameter of ~ 10 m is needed to ensure the rocket lands at a safe velocity (~5 m/s, 12 mph).

Additional analysis was done to determine the optimal deployment altitudes to minimize drift, while ensuring parachute/rocket structure integrity. MATLAB simulations were performed with the initial state of the rocket at apogee (100 km) and an initial velocity of 0. We quickly discovered that the impulse from deploying the drogue parachute as the rocket enters the atmosphere would result in forces that would destroy the parachute. To overcome this we will use parachute reefing to deploy the drogue parachute in a closed state at an altitude of 35 km, then open the drogue parachute at 30 km to decelerate the rocket as it enters the thick part of the atmosphere. The main parachute is deployed at 5 km (reefed), then opens at 1 km to slow the rocket down to a final velocity of 5.25 m/s. Figure 10.1.2 shows the forces that the drogue and main parachute will experience on deployment. It is important to note that these assume the parachutes will open instantaneously. Therefore, the actual impulse of opening will be much less.

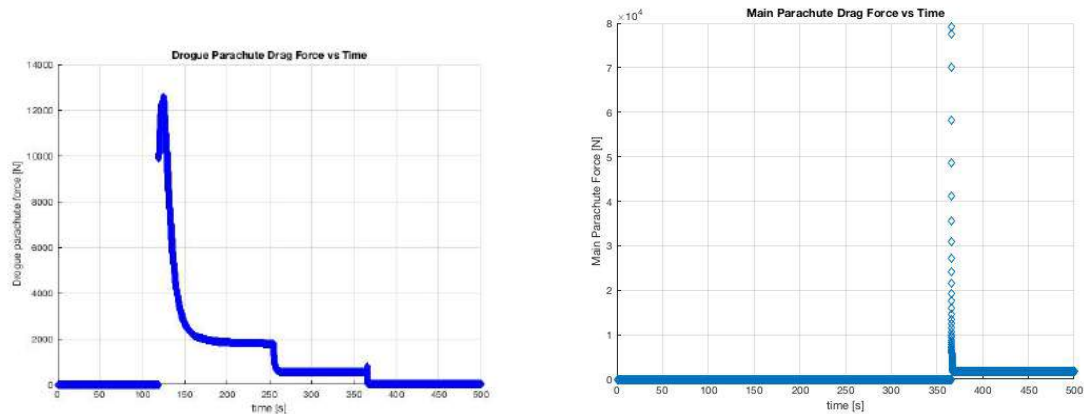


Figure 10.1.2: Left: Drogue Parachute Drag Force vs Time, Right: Main Parachute Drag Force vs Time. Results show initial deployment of drogue parachute will experience a large (~12 kN) impulsive force, then quickly reduce to 2 kN. Similarly, the main parachute experiences an extraordinarily large initial impulse (due to assumption that parachute opens instantaneously), then the force reduces to 2 kN until touchdown.

This configuration resulted in a total descent time of 494 seconds, a final descent velocity of 5.25 m/s, and nominal parachute forces of 2 kN (450 lb). More analysis is required to determine the time it takes to open the parachutes so the impulsive forces can be understood. Figure 10.1.3 shows the resulting velocity and acceleration vs time:

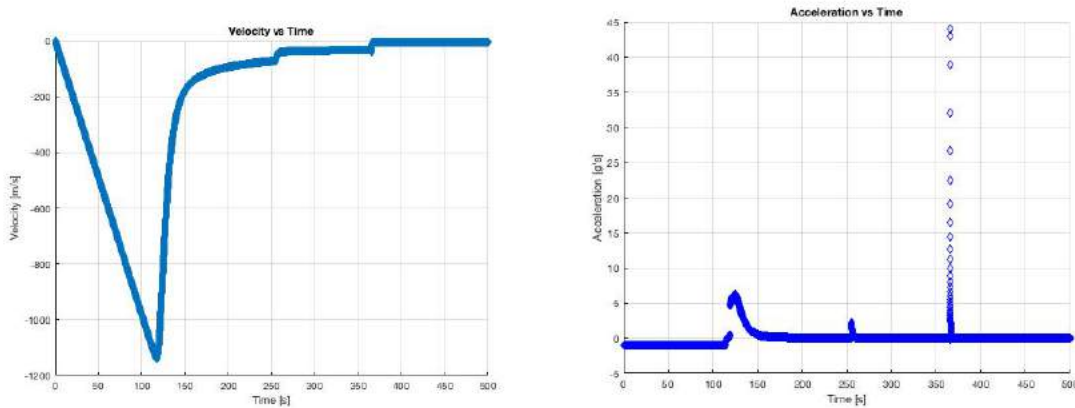


Figure 10.1.3: Left: Velocity vs Time. Right: Acceleration vs Time. Results show the effect of staging parachutes to minimize descent time (thus minimizing rocket drift), while ensuring structural integrity of parachutes and rocket. \*Note: Large acceleration spike is due to instantaneous opening of main parachute. This is not physical, however, more analysis will be done to determine actual impulse.

## 10.2 Recovery system electronics

Parachute deployment will be achieved by releasing high pressure CO<sub>2</sub> gas in the parachute canister. The gas will be released by an electric linear actuator, which opens a valve with a high flow rate. The main flight computer will determine when criteria to deploy the drogue and main parachutes are met using data from the rocket's barometers and/or GPS. After landing, recovery efforts will be conducted using a simple directional antenna setup detailed below.

### 10.2.1 Lightweight Recovery Module (LRM)

The LRM is a self-contained device intended to aid in recovery efforts consisting of a computer, battery, display, radio, and directional antenna. This device will remain on the ground. It will allow us to avoid needing to mobilize our dashboard setup and other cumbersome ground equipment. Up to and upon landing, the rocket's primary radio will continue to transmit position data. The recovery team will set out with the device towards the last known position of the rocket in an attempt to continue receiving position data. Once they close in on the location of the rocket, they will use the directional radio on the LRM to determine the direction of the signal being put out by the rocket's primary radio and thus the direction of the rocket. An Arduino UNO [10.1] hooked up to a simple display [10.2] will provide the necessary computing power and an interface for receiving GPS data. An XBee radio [10.3] with a small yagi antenna [10.4] will allow us to receive transmissions from the rocket once we have line-of-sight.

# 11 Ground Support Equipment

## 11.1 Launch Rail

As discussed in earlier sections, launch rail safety will be a major priority. To form a common basis amongst our team, we plan to use the provided 60 ft. Microcosm Launch Rail, as shown in Figure 11.1.1. We have formed the following pre-launch plans, operations, and design around this basis.

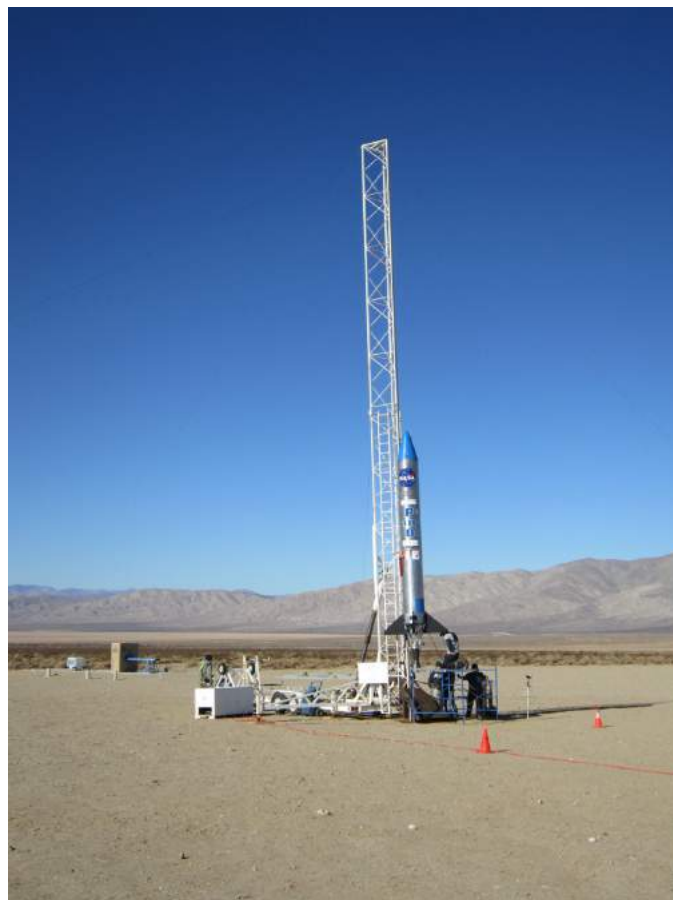


Figure 11.1.1: The Microcosm Launch Rail. The rail is able to be rotated 90 degrees horizontally.

### 11.1.1 Launch Lugs

We designed the launch lugs according to the specs designated by the website. They will have removable sides, as shown in Figure 11.1.1.1, so we can lay our rocket over the rail and then fasten the sides of the lugs to the main piece of the lug.

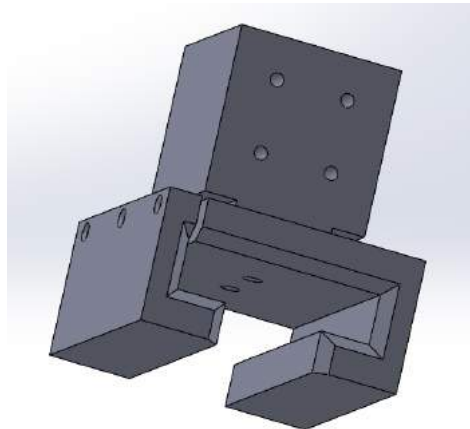


Figure 11.1.1.1: A 3D model of one launch lug, displaying one of two removable sides.

We will machine two launch lugs, one attached to the center of gravity of the rocket, the other to the bottom. For fasteners, we will be using #6 flat head machine screws.

## 11.1.2 Mounting the Rocket

For mounting the rocket, we are going to use an engine hoist, as pictured in Figure 11.1.2.1.



Figure 11.1.2.1: An example of a manual hoist that we will use to lift the rocket onto the rail.

After assembly, we will use the hoist to lift the rocket, laying horizontally, off its assembly stands. We will have one person on each end, guiding and turning the rocket so that it can be aligned with the launch rail, which will also be in a horizontal position, and then we will lower the rocket and attach it to the rail. The fact that we will be working in the sand has been considered, meaning we will replace the fixed caster wheels with lawn tractor tires, for more traction.

### 11.1.3 Electrical Umbilicals

Once we are a go for pressurization, no one will be allowed near the rocket. Instead of having our systems running on battery power for however long the rocket sits on the pad, we will have a built in electrical umbilical system. We will be using the Cooper Industries Umbilicals and disconnects [11.1], as shown in Figure 11.1.3.1. These specific connectors are designed specifically with launch vehicles in mind.



Figure 11.1.3.1: An example of an umbilical connector that automatically close once disconnected.

Our plan is to have these installed on the side of the rocket, close to our internal power supply, pointing normal to the launch rail. Our plan is to plug in the connector while the rocket is still laying horizontally on the rail, and then having the connector wire running to our ground power supply. To make our system less complex, we will let the rocket yank the connector out when it leaves the pad. To provide strain relief on the electrical cord, kevlar cord will be tied around the connector and then tied off to a static part of the launch rail. This will prevent the wires from getting damaged on disconnect. This process has been flight tested last year, at the MRL rocket competition.

## 11.2 Antenna Tracking Station

In order to allow the directional antennae to be pointed at the payload for the duration of the flight, an automated antenna tracker is being designed. It will use two high-power servos to actuate an antenna arm along the pan and tilt axes.

The antenna tracking station uses the position and altitude of itself and the rocket in order to calculate the necessarily pan & tilt offsets needed to keep pointing at the rocket. In order to calculate the ground distance between the station and the rocket, we will be using the haversine formula. This formula takes the "great-circle" distance between two coordinates, which takes the Earth's shape into account. The formula is broken into three parts and is as follows [11.2]:

$$a = \sin^2(\Delta\phi/2) + \cos \phi_1 \cdot \cos \phi_2 \cdot \sin^2(\Delta\lambda/2) \quad (11.3)$$

$$c = 2 \cdot \text{atan}2(\sqrt{a}, \sqrt{1-a}) \quad (11.4)$$

$$\text{distance} = R \cdot c \quad (11.5)$$

Where  $\phi$  is latitude,  $\lambda$  is longitude, and  $R$  is the earth's radius. The correct tilt angle can be calculated by taking the inverse tangent of the distance and the difference in altitude. Likewise, bearing angle can be calculated via the following equation:

$$\theta = \text{atan}2(\sin \Delta\lambda \cdot \cos \phi_2, \cos \phi_1 \cdot \sin \phi_2 - \sin \phi_1 \cdot \cos \phi_2 \cdot \cos \Delta\lambda) \quad (11.6)$$

Using these offsets in conjunction with orientation data supplied by the IMU, the tracking station can actuate its pan and tilt servos to point at the rocket. The following figure shows how data flows from the antenna and is processed by the auto-tracking station.

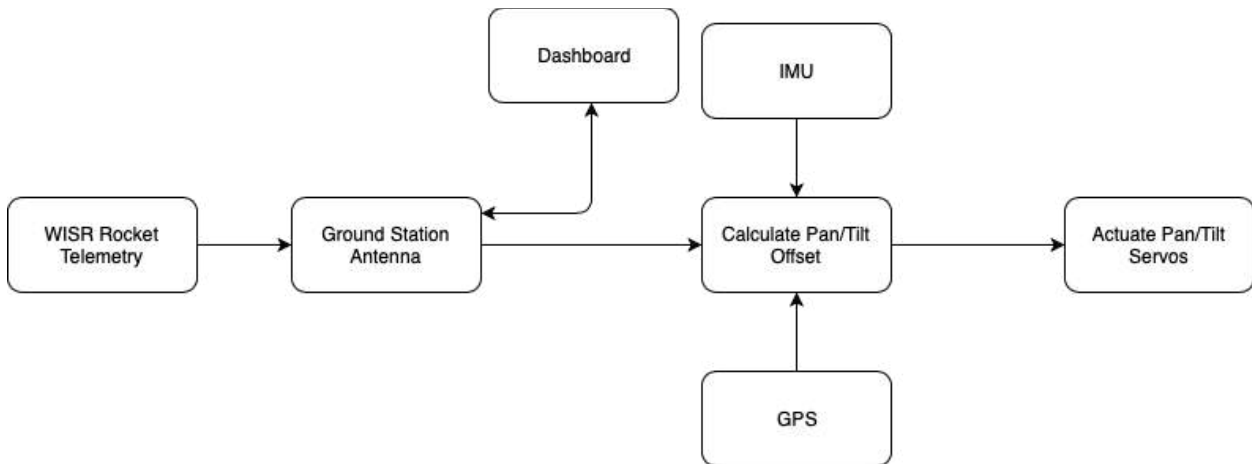


Figure 11.2.0: Block diagram showing the auto-tracking process

This process will be performed every time a valid packet is received by the ground station. In cases where the exact coordinates are not contained in the received telemetry packet, the ground station will estimate the rocket's coordinates using IMU data and the signal RSSI. Figure 11.2.1 shows a similar antenna tracker, designed and built by a team member for high altitude balloon tracking.



Figure 11.2.1: A station used for tracking high-altitude balloon payloads

### 11.3 Fueling Operations

For fueling, we will designate personnel that will be allowed on the pad during the fueling process. The rest will be evacuated to a safer location. This team will be trained in materials handling and safety and emergency procedures. Since we will be using peroxide, which will burn skin on contact, the team will be equipped with full body protective suits, rubber overboots, face shields, and rubber gloves, so no skin will be exposed.

For fueling equipment, two transfer tanks will be designed to hold the liquid HTP and RP-1. The tanks will be placed a safe distance from the rocket, preferably 50 feet. With that in mind, our transfer hoses will be specific to each propellant, so there is no mixing of propellants while people are on the pad. For the RP-1, we will use a 1" diameter, 65' length Wolflube Equipment kerosene hose [11.7]. For the HTP transfer hose, we are taking extra care to find a hose that will not cause the peroxide to react with any type of coating the hose would have. Currently, we are looking at chemical resistant teflon hoses. For Helium, we plan on using a standard He canister and will regulate down.

On our fueling panel, we will have a removable hatch, that will allow access to the plumbing, where we can regulate the fuel flow with three way ball valves. Since we will be using the same lines that feed the combustion chamber (see

Diagram 11.4.0 at the end of this section), our safest option was to use three way ball valves. The three settings will be no flow, flow up to tank, flow down to combustion chamber. In order to provide leak proof fueling, there will be single point adaptors at every propellant inlet port, as seen in Figure 11.3.1 [11.8] The hoses will have nozzles that lock onto these adaptors.



Figure 11.3.1: These will be pressure regulated: they will stay sealed unless pushed in by fueling pressure.

We will be using the provided compressed nitrogen procedure to fuel the rocket. Our general procedure of fueling is to first statically ground the rocket. We will be using an aviation fueling bonding clamp on a spooled wire that's attached to the transfer tanks. We will fill the He first, then RP-1, then HTP, each at a flow rate of about 1.5 Liters/s. To allow for in-flight fuel dumps, we will use control valves on the fueling ports and we need the He to be able to actuate them, so that is why we are filling the He first. We will be monitoring temperature and pressure across the board from the moment the flight computer gets turned on, to check for any substantial pressure to develop inside the tank during fueling. After all propellants are filled, we will clear the pad, and proceed to the safety bunker, where we will have a Go-No Go for pressurization. If GO for pressurization, we will isolate the He pressure and then pressurize the system remotely.

## 11.4 Contingency De-Fueling

In the event of an on-pad emergency, we have two possibilities. If the rocket has already been pressurized, an abort means closing the pressurization valves and opening the tank vent valves. Without pressurization, an abort requires commanding open just the tank vent valves before approaching the rocket. Our fuel unloading plans follow the plans in the provided safety document.

## **Fueling System**

Jacob Keip | March 19, 2019

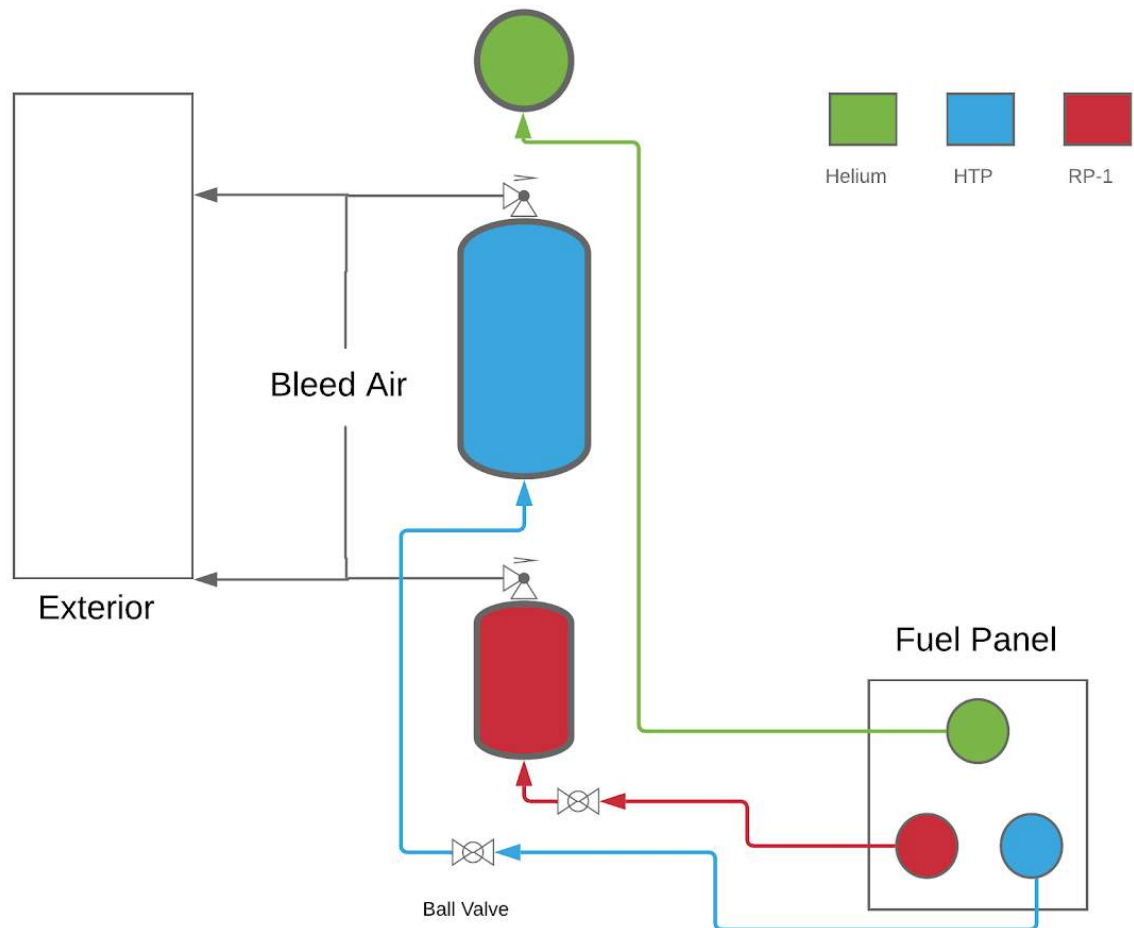


Diagram 11.4.0: P&ID chart of the fueling system

# 12.0 Safety

## 12.1 Hazard Analysis

### 12.1.1 Transport

**Potential Hazard:** Components coming loose in transport either leading to items unexpectedly coming loose during transport or unloading.

**Mitigation Strategy:** Large, heavy, and or fragile items shall be secured by straps to the vehicle or trailer during transport. The primary solution for transport shall be inside a closed vehicle or trailer. Items that have to be transported in a open trailer shall be especially secured. The unloading procedure will prescribe standing clear of doors when opening them incase cargo will fall safely to ground should it have shifted, and unloading crew will wear appropriate work boots.

**Potential Hazard:** Spill of hazardous substances en route.

**Mitigation Strategy:** Every effort will be made to have the fuel, oxidizer and pressurant gas delivered to the launch site by the supplier. Conversations have taken place with other Base 11 Space Race teams also intending to use RP1 and HTP to allow for joint purchase and delivery to Spaceport America. Should this not be possible, arrangements will be made to receive these substances as close as possible to the launch site. Any transport required of Wisconsin Space Race shall take place using two trailers approved by all relevant state DOTs for such use. The trailer transporting Helium bottle(s) and RP1 shall be certified for the transport of flammable liquids and pressurized non-flammable gases. The trailer transporting HTP shall be certified for the transportation of oxidizers. The containers used for transport shall also undergo all necessary certification for use. During transport, drivers of the vehicles towing each of these trailers will be instructed to maintain several minutes of separation to avoid both vehicles being involved in the same crash. Each vehicle shall carry an MDS, internal SOP, spill containment procedure and spill kit for the material being transported. In the case of Helium, procedures will be validated against Safety Guidelines section 4.15.6.3 Transportation.

**Potential Hazard:** Grasping of sharp edges on parts during loading or unloading

**Mitigation Strategy:** Insofar as sharp edges can not be entirely avoided, all items with sharp edges must either be packed in a transport container with a label noting this hazard, or in cases where the part in question is too large to be stored in a container, all sharp edges should be covered in high visibility tape (in order to

insure the tape is removed at the time specified by the assembly procedure). When removing an item from a so labeled container, or handling a part with taped edged, procedures will specify the donning of work gloves.

### 12.1.3 Launch Rail Operations

**Potential Hazard:** Pinching of extremities during loading of rocket onto rail

**Mitigation Strategy:** The OSHA prohibition against one person lifting object of more than 50 lbs will be observed. Any time such an object is being placed, everyone not involved in placing it will step back, and verbal callouts will be used to coordinate placing. These mitigation strategies also apply to mechanically assisted lifting.

### 12.1.4 Fueling

**Potential Hazard:** Contact with propellant

**Mitigation Strategy:** During fueling ops, after the hoses have been connected to the fueling ports, the fueling crew will stand by the transfer tanks which are to be located a safe distance from the pad (see section 11 of this document). To insure against leaks, all fueling hoses, hardware and connectors will have undergone the leak testing regiment as rocket propellant lines. Tanks will be filled one after the other to insure that the event that the fueling hoses leak or come loose, no mixing of propellants can occur. Propellant level inside the tanks will be remotely monitored to avoid spilling any through the vent valves. Once each tank has been indicated as full, the fueling valve in use will be closed and the transfer tank will be vented to drain remaining fuel from the hose so that it can be disconnected without spilling. PPE will be worn as designated by Table 4.15.4.1 "Standard Safety Clothing" of the safety guidelines document.

### 12.1.5 Fueled on Pad

**Potential Hazard:** Oxidizer tank overheat

**Mitigation Strategy:** The high purity hydrogen peroxide used as an oxidizer spontaneously decomposes when exposed to heat. As the decomposition reaction is exothermic, this presents the risk of a runaway reaction in the tank. To mitigate this risk, the oxidizer tank will be cooled by a helium blowdown before propellant loading, propellant loading will be as late in the launch operations order as feasible, and the temperature in the tank will be continuously monitored. Burst disks and relief valves will be sized to be able to vent the pressure spike from such an occurrence, and a redline temperature will be set for a launch abort with oxidizer dumping.

### 12.1.6 Pad Abort

**Potential Hazard:** Approach of an unsafe rocket

**Mitigation Strategy:** Aborts will be divided into two classes. Hazardous and non-hazardous aborts. Non-hazardous are aborts where the rocket does not pose

any danger. This category includes aborts due to high wind-speeds at altitude, a breakdown of the tracking system or other such event. In these cases a simple depressurization of the run tanks is sufficient to bring the rocket back to a safety level equal of that it was in when the fueling crew departed. From there fuel can be unloaded. Hazardous aborts are those where something is going wrong with the rocket itself that could result in danger to the refueling crew were they to approach. This might be a foreign object impacting the rocket and causing structural damage, or sensors indicating that the peroxide has begun uncontrollable decomposition. In these cases an approach of the rocket may be deemed too hazardous, and the propellant will be dumped remotely via gravity drain. Failure modes not foreseen by the procedure will be deemed hazardous or non hazardous by the flight controller and range safety officer.

### 12.1.7 Powered Flight

**Potential Hazard:** Off course rocket

**Mitigation Strategy:** The flight computer will monitor redundant inertial guidance as well as global positioning data to inform the stabilization system. This hazard considers the risk of the rocket going off course for whatever reason. A nominal flight trajectory will be defined by the chief engineer. The guidance officer will monitor the telemetry feeds, contingency APRS feed, and ground tracking. If the determination is made that the rocket has deviated from the nominal trajectory plus a tolerance factor decided on the launch day taking into account prevailing weather conditions, an abort will be commanded.

### 12.1.8 Un-Powered Flight

**Potential Hazard:** Parachute failure

**Mitigation Strategy:** The parachute release system will be tested under as realistic as possible conditions before-hand, and final inspection during assembly, as will the parachute packing. Planned flight trajectory will keep rocket clear of populated areas so that the crash-site will be well clear of people or property in the case of uncontrolled descent. Procedures will be in place to facilitate safe recovery of debris in this event.

### 12.1.9 Recovery

**Potential Hazard:** Contact with fuel or oxidizer

**Mitigation Strategy:** Should the rocket operate nominally, at time of flameout, all but a negligible amount of propellant will have been exhausted. However when approaching a touched-down rocket, procedure will be to treat the tanks and lines as containing fuels. The recovery procedure will provide for draining any remaining fluids from the system before rigging it for transport. The recovery crew will carry spill kits for each propellant. In the case of a crash, each component shall be hosed down with water prior to recovery except in the case of the avionics bay.

**Potential Hazard:** Recovery of damaged battery cells

**Mitigation Strategy:** Batteries shall be contained in protective housing. The recovery crew shall inspect this casing for damage. In case of a crash all avionics components shall then be placed in a fireproof container separate from the rest of the wreckage.

**Potential Hazard:** Hot surfaces

**Mitigation Strategy:** Recovery crew will verify the surface temperature of any grasping points with an infrared thermometer before they are touched.

**Potential Hazard:** Sharp components in the case of a crash

**Mitigation Strategy:** Recovery contingency procedure will specify work gloves.

## 12.2 Risk Assessment

### 12.2.1 Transport

**Potential Risk:** Contamination of tanks or lines leading to unwanted decomposition of HPT.

**Mitigation Strategy:** After pre-assembly cleaning of components and after each assembly step, strategies in line with Safety Guidelines section 4.13.1.3 Packaging shall be included in applicable procedures.

**Potential Risk:** Damage to components in transport

**Mitigation Strategy:** Small and medium sized components will be placed in transport crates with padding appropriate to their sensitivity to shock. For example, the flight computer will require more extensive padding than the parachute. Large components such as tanks will be wrapped in padding material before being strapped in place in a vehicle or closed trailer where possible. The mechatronics will designate all ESD sensitive packages, they will be packed in ESD-safe packaging, and assembly procedures will provide for assembly teams to ground themselves and the rocket before unpacking or installing any so designated package. Procedures will also insure such components are integrated as late as possible, and that they are only unpacked immediately before installation. All batteries will undergo visual inspection for damage prior to installation.

### 12.2.2 Assembly

**Potential Risk:** Foreign object debris entrapment during assembly

**Mitigation Strategy:** All components down to the level of individual fasteners will be checked off the assembly procedure as they are installed. After system assembly or rocket integration, the assembly procedure, spare components and tools will be checked against the packing list. Discrepancy will be cause for disassembly and re-inspection of the system or rocket.

**Potential Risk:** Assembly error

**Mitigation Strategy:** To guard against incorrect assembly, all assembly teams will consist of (an) assembler(s) and a checker. The checker will verbally call out work steps, the assembler(s) will verbally repeat the step before performing it, and finally the checker will visually verify the correct performance of the step.

### 12.2.3 Powered Flight

**Potential Risk:** IMU sensor failure

**Mitigation Strategy:** The flight computer will take input from three independent sensors, and will utilize a voting system to determine the rocket's actual trajectory.

**Potential Risk:** Flight computer crash

**Mitigation Strategy:** The flight computer's microcontroller has a watchdog peripheral: a counter that resets the chip when it reaches a timeout value. During nominal execution, we reload the watchdog timer periodically, preventing chip reset; if the firmware crashes, the timer will reach the timeout and cause a system reset.

This timer is run from a secondary 32 kHz internal RC oscillator, which remains active even if the main clock fails, allowing us to recover from clock instability. We will additionally enable the windowed mode of the watchdog, introducing not only a maximum time between watchdog reloads but a minimum as well, to cause resets if iterations of our control system are taking significantly lower than nominal time to execute.

Flight computer state is journaled to on-chip FLASH memory so that a watchdog reset does not cause a loss of mission state.

In the case of full flight computer loss, a secondary microcontroller (Arduino Due) will register the loss of heartbeat, signal the engine controller to stop over CAN, and handle coasting and recovery by taking control of critical sensors and actuators.

**Potential Risk:** Premature engine flameout

**Mitigation Strategy:** As the decomposition heat of the HTP is sufficient to ignite the RP-1 fuel, engine flameout would indicate either blockage of propellant lines, loss of propellant, or loss of helium pressure. If thrust does not return, an in-flight abort and propellant dump will be commanded.

### 12.2.8 Un-Powered Flight

**Potential Risk:** Flight computer crash

**Mitigation Strategy:** In the case of a flight computer crash during unpowered flight (coasting), the same secondary microcontroller as in powered flight crashes will register the loss of a heartbeat from the main flight computer, and handle recovery system ejection. Critical sensors and actuators will then be controlled by this secondary backup.

**Potential Risk:** Barometer sensor failure

**Mitigation Strategy:** The flight computer will take input from three independent sensors and will utilize a voting system to determine the rocket's altitude.

## 12.3 Safety Training

The Wisconsin Space Race Team recognizes the critical importance of safety training. In preparation for the construction phase of our rocket, our members have gone through a combined total of approximately 320 hours of manufacturing & fabrication training through the UW-Madison College of Engineering Shops. The permit and upgrade training system covers safe use of machinery including: vertical and horizontal bandsaws, drill presses, belt sanders, knee mills, and lathes. Advanced training covers topics such as Computerized Numerical Control, sheet metal fabrication, as well as MIG and TIG welding. Completion of these safety-centered trainings has provided our team with the skills to construct our rocket and the background to hold each other accountable when it comes to safe manufacturing best-practices.

## 12.4 Quality Management System

Mission success depends on work done from the start of the project up to and during the launch. The Quality Management System tailored to the team describes the process required to move from external inputs and competition constraints to actions ensuring safe and successful completion of all tasks.

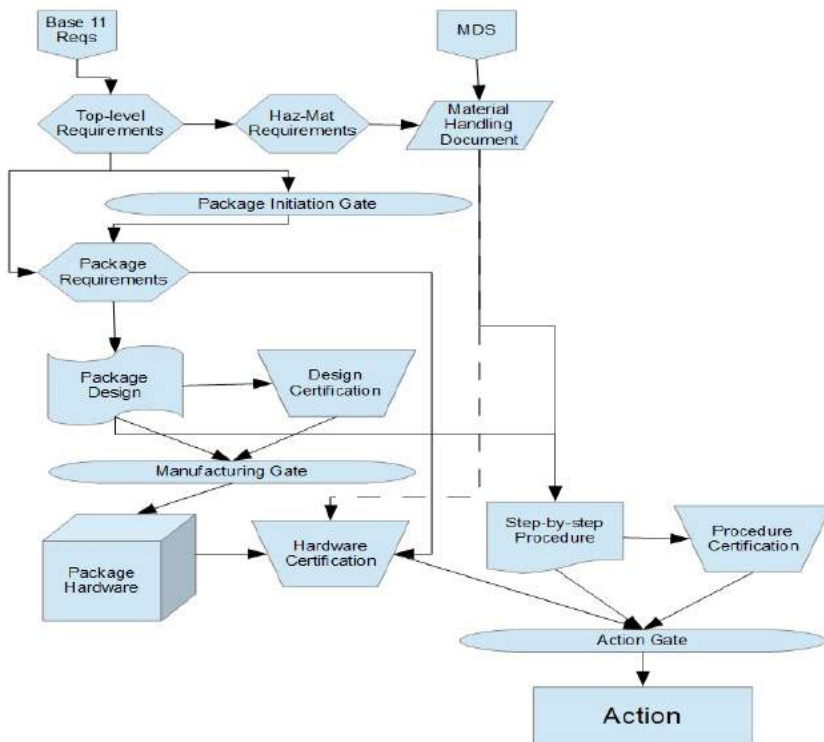


Figure 12.4.1: Quality Management System flow diagram.

### 12.4.1 External Documents

Competition rules, test site policies, material data sheets and other applicable external documents will be relevant to internal policies and procedures. To enable quick and easy access to all pertinent information in a rapidly digestible format, we will create internal documents to repackage external information tailored for this team's use. These documents will cite the external source document to enable updates as necessary.

### 12.4.2 Internal Requirements Documents

As with all large projects, both compartmentalization and effective integration among compartments is key to maintaining workforce agility and project cohesion. To achieve both these ends, we will create a series of internal requirements documents. The top level requirements document will include all competition rules, applicable laws, overall system requirements such as the mass budget defined by the chief engineer, and all other external regulations that apply to the whole team. Other individual requirements documents will contain only requirements relevant to a system or subsystem. For example, the subsystem requirements document for the nose cone should contain requirements such as the maximum design load, allocated fraction of overall mass budget and interface specifications with the rocket shell. This will allow members to track both their own

subteam's and other subteams' design goals and make individual projects easy to assign.

### **12.4.3 Design Documents**

Design documents include all documents such as engineering drawings, wiring schematics, P&IDs and other documents detailing designs.

### **12.4.4 Step by Step Procedures**

Every physical action involving the rocket hardware, its functional prototypes and/or hazardous situations like the presence of RP1 or high voltage should be planned in advance by writing a procedure. These procedures, as laid out by Base 11, will consist of:

- Entry Conditions (checklist)
- Hazards
- Personal Protective Equipment (checklist)
- Required Tools and Equipment (checklist)
- Procedure Functional Diagram
- Step-by-Step Instructions

The one deviation from Base 11's example is that instead of training a member on generic fuel loading and unloading, members will be trained on each specific procedure individually. This eliminates the risk that nuances between procedures with similar goals are lost, or that the intervals between training and execution of a task grow to the point where loss of proficiency becomes a concern.

### **12.4.5 Certification Documents**

Every Material Handling, Procedure, Design and Requirements document as well as physical part will be paired with a certification document. The purpose of this certification document is to track all pertinent information about the document itself (not its contents). This includes but is not limited to:

- Documentation of internal review\* (all Documents)
- Documentation of external review (all Documents)
- Documentation of approval to manufacture/purchase (Design)
- The list of members trained (Procedure)
- Documentation of passivation (Part)
- Documentation of leak tests (Part)
- Documentation of proof pressure test (Design/Part)
- Results of analysis; FEA and manual (Design)

\*Including hazard analysis and FMEA

After a document has been finalized and has gone through all pertinent approval processes, it should be uploaded as a PDF, and a hash of the PDF should be recorded in the certification document to preclude alteration without reapproval.

## 12.4.6 Material Handling Documents

While the current iteration of MDSs consolidate cautions about hazardous chemicals into one place, they can still occasionally be wordy. For example, some MDSs list several pages of different jurisdictional lists of possible carcinogens even if the chemical in question does not appear on any. Before writing procedures involving potentially hazardous chemicals, we will consult MDSs and material compatibility documents and will create an internal summary document. This internal document will describe all necessary PPE, relevant hazards, emergency response and materials compatibility (including cleaning and passivation). The material handling document is not and will not be used as a procedure. We will use it only as a reference guide when creating procedures and certification documents for parts involving relevant chemicals.

## 12.4.7 Gates

This QMS has three gates:

1. **Package Initiation Gate:** This starts the design process. The need for a new part or system is identified, and the relevant requirements are determined.
2. **Manufacturing Gate:** Once the design has been finalized, the manufacturing team will review manufacturability, if applicable, and the design will be checked against its relevant requirements. The certification document will be reviewed to ensure all necessary design reviews have taken place.
3. **Action Gate:** Once all design, manufacturing, and procedures are in place, the procedure certification document is checked to ensure relevant reviews have taken place. The hardware certification document is reviewed to verify that all applicable testing has been performed.

## 12.4.8 Actions

Actions are the outcomes of procedures.

# 13.0 Team Development

## 13.1 Succession Planning

Our team leads combined experiences range from four plus years leading award-winning student engineering teams to eight plus years leading technician units in the military. Given the high turnover rates in both of these types of organizations, we intimately understand the importance of forward planning for job turn over and people moving on from an organization. Therefore, we are hyper-focused on involving our younger team members in the decision making stream that is critical to major roles on the team.

Importantly, a majority of our core leadership will continue on at the University of Wisconsin-Madison with their masters degrees through the duration of the project. Those on our leadership team not continuing with their masters degrees or undergraduate studies are committed to staying on as advisors to help the team access resources and knowledge that they need to complete the project.

In addition to knowledge transfer, another major issue that 'green' student engineering teams often face: knowledge acquisition. That is, acquiring the soft-skills in leadership and project management necessary to see a complex project like building a rocket to finish. Over the past 6 months we've emphasized training in project as well as leadership development.

## 13.2 Knowledge Retention

A core principle for how we delegate work on our team is: "when in doubt [of what work to do], go research and write."

Engineering intensive projects require that a lot of knowledge be aggregated through research in order to solve the given engineering problem. However, the work expended to acquire this knowledge ends up lost, or only used by a specific team for a specific purpose. To overcome this issue, we implemented two simple tactics:

1. We ask our team members to spend 15 minutes writing in free brain dump format into a word document for every 2-3 hours they spend working or researching. We call these brain dump documents 'research memos'. When a team member writes a research memo, we ask that they post the memo into a full-team slack channel called #research\_memos. Posting in this channel lets everyone on the team see what research and work are being done, and also creates a searchable record of what day-to-day work is produced.
2. We ask each of our team members to turn their design work and research into a blog that is easily digestible for a layperson. This tactic has several important benefits for knowledge retention. First, we produce a library of often complex technical topics that new members can read through and learn in an easily understood and fun manner. Second, by asking our team

members to write public-facing content, we force them to think more critical and deeply about the problem, and record their thoughts in the process. We can then adopt the content from these blogs for design reports and other necessary copy.

As we open up bandwidth in the coming months, we plan to appoint one team member to be our internal wiki-manager. They will turn these research memos and blogs into easy to navigate wiki pages. Over time, this internal wiki will grow into a vast, living and breathing knowledge base for how our rocket works, why our rocket works that way, why certain design decisions were made, etc.

Next, thanks to the power of digital technology, we record everything. First, we have an easy-to-search Slack archive, where team members can look back at threads about design decisions to understand the design heritage of a given system. Next, we host the majority of our team meetings via video calls; we record these calls and upload the .MP4 files to our Team Google Drive.

Finally, as mentioned in the last section, as team members move on in their careers, we strongly encourage that they take on advisory roles, to be called on when needed by the remaining team members.

### 13.3 Outreach

First, our team member ages range from seventeen to twenty seven. As part of our emphasis on leadership development, we are focused on empowering the older and more experienced members on the team not only to lead, but to mentor younger team members. Right now, one of our core team members is a high school student. Enrolled part-time at UW-Madison, he is an incoming Freshman to the University.

Tackling two birds with one initiative, we are actively seeking an industry partner to sponsor a competition for high schoolers in Wisconsin to design a science experiment to include in the small payload bay on our rocket. Details of this outreach initiative will be fleshed out as we investigate interest from local high schools and potential partners to sponsor this program.

Further outreach ties in intimately to our fundraising and marketing plans. Namely, we focus heavily on educating the public about the importance and implications of the aerospace industry. As noted already, we write and produce an easy-to-digest, lay-person facing blog about various aspects of the space industry. Similarly, as we elaborate on in the next section, we will host a series of webinars that also help to educate the public about the new-space industry, and WI Space Race's role in that ecosystem. In each of these pieces of content, our first and foremost goal is to provide our audience with an accessible way to learn more about the aerospace industry.

# 14.0 Business and Marketing

## 14.1 Budget Estimate & Management

### 14.1.1 Budget Estimates

Based on initial designs and market research our best budget estimate to accomplish this project is approximately \$250,000. This number is heavily based on preliminary research and will be improved upon as the team moves further into the design and build phases. So far various research projects into exploratory tech and materials have delved into reducing manufacturing costs and could have a major impact on the initial estimate. Following is the subteam breakdown of this budget.

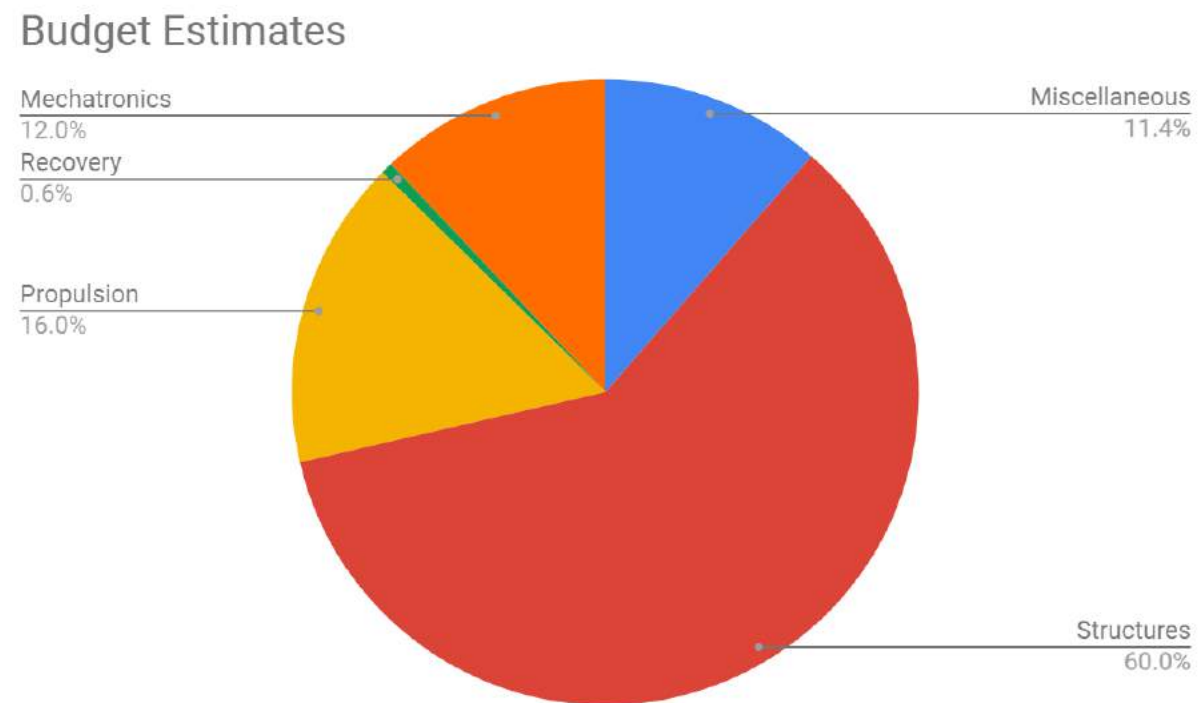


**Figure 14.1.1.1:** Budget Breakdown

### 14.1.2 Budget Management

A project of this magnitude is not cheap and requires diligent handling of funds. We are currently working on implementing a standard Billing of Materials that members will be required to fill out before going forward with any purchases. Microsoft Excel offers some low cost, well-organized templates that should serve all

of our purposes. We have assigned a treasurer whose main role is to oversee all monetary actions and keep an accurate record of all purchases made.

## 14.2 Fundraising

Synthesizing a high level fundraising approach for this type of project is very tricky. Are we a non-profit? Are we a student organization? Are we a business? Are we asking for donations or do we have a product/service to offer? Are we looking for philanthropic sponsors or are we looking for customers?

We decided to focus in on developing a real-business case for our project. Said another way, we know that we have a valuable set of products to offer and a large market of customers who need that product. Rather than seeking donations, our job is to build relationships and sell to our customers. We see this mindset manifest itself in three different ways with three separate classes of customers, each seeking a different type of product at a different price point.

**(1)** \$0 through ~\$1000 | Friends, family, alumni, and proud Wisconsinites. These are low-dollar amount monetary donations that come from supportive friends and family. In the coming weeks, we'll be rolling out a set of crowdfunding perks for under \$1000 donations. We term this group Supporters.

**(2)** \$1500 through \$15,000 | Small businesses, local engineering firms, etc. | Association with innovation, recruiting students, and brand awareness. These are businesses who are looking to increase their recruiting pipeline while giving back to their community. Included here are materials sponsorship purchases, for which we award the retail value monetary equivalent in sponsorship value. We term this group Sponsors.

**(3)** \$15,000+ | Large companies | High-impact innovation marketing campaign. These are companies looking not only for brand association and recruiting, but gain massive value from having a team of ambitious, scrappy engineers actively use their products and generating case-study material. We have several conversations in the works with these types of companies. We term this group Partners.

From these three groups, we aim to raise an average of \$2000 per week from now through the end of the competition. In addition to selling sponsorships, we are pursuing NASA and Air Force Small Business Innovation Research (SBIR) grants for developing various subsystems of the rocket.

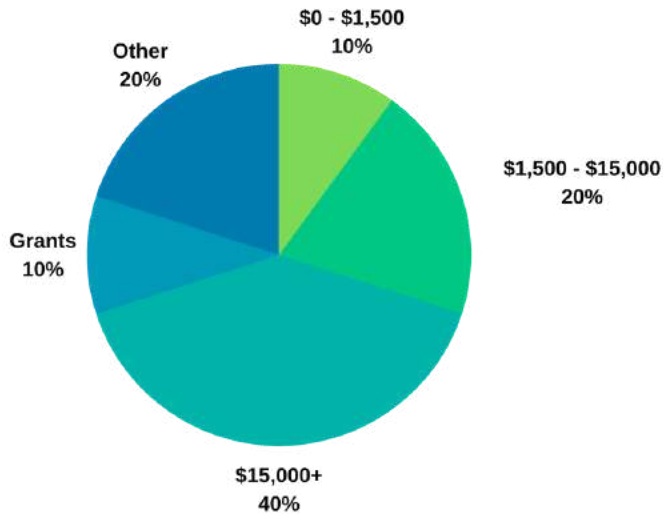


Figure 14.2.1: Projected breakdown of funding sources.

A detailed description of our sponsorship levels can be found in our sponsorship packet, Appendix B.

## 14.3 Marketing

### 14.3.1 Our Brand

We decided to focus our marketing around Wisconsin's rich history of leading American spaceflight. From a practical standpoint, Wisconsin leads in producing aerospace subsystems, coming in as the number one producer of fabricated metal parts, appliances and components, and electrical equipment for aerospace. Beyond materials and parts, Wisconsin also provided some of the greatest leaders and figure-heads in the history of American space-flight. Here are some of the most notable Wisconsinite space-cadets:

- Gemini and Apollo astronaut Jim Lovell (UW-Madison student 1946-1948)
- Apollo-era NASA leadership Deke Slayton (Wisconsin native)
- Space shuttle commander Brewster Shaw (UW-Madison alumnus, 1968)
- Many more shuttle-era and current astronauts, including Mark C. Lee, Daniel Braden Stein, and Jeffrey Williams

University of Wisconsin-Madison engineering students in particular also boast a strong track record of showing up and performing in aerospace engineering competitions. Most recently, the Badgerloop team ranked third in design and won

several awards in SpaceX's international Hyperloop Competition (notably, several of our team leads helped build this award winning hyperloop teams throughout the past four years of the Hyperloop Competition). Before that, a UW-Madison student team won NASA's national X-Hab competition. In parallel, UW-Madison AIAA teams consistently excel in state and national rocketry competitions, placing first in the statewide Wisconsin Rocketry competition last year.

### **14.3.3 Our Marketing**

With the above branding in mind, we are implementing email marketing, social media marketing, and webinar marketing campaigns to drive awareness for our brand and deliver our content. Several of our team members have extensive professional experience with content marketing and fundraising and they are leading these endeavors. Please find our social media pages at:

- **Website:** <https://www.wisc.space>
- **Facebook:** <https://www.facebook.com/wispacerace>
- **LinkedIn:** <https://www.linkedin.com/company/uwspacerace>

# Appendices

## Appendix A - References

- [2.1]
- [2.2] <https://www.springer.com/us/book/9783540692027>
- [2.3] <http://www.spacetethers.com/massfraction.html>
  
- [3.1] Industrial Specialties Manufacturing, Hydrogen Peroxide Material Compatibility Chart. Englewood, CO, 2019: Industrial Specialties Manufacturing.
- [3.2] <https://ntrs.nasa.gov/archive/nasa/casi.ntrs.nasa.gov/19710019929.pdf>
- [3.3] <https://www.sciencedirect.com/science/article/pii/0021951763901052>
- [3.4] (Dierdorff)
- [3.5] <https://www.sciencedirect.com/science/article/pii/0021951763901052>
- [3.6] <https://ntrs.nasa.gov/archive/nasa/casi.ntrs.nasa.gov/19710019929.pdf>
- [3.7] D. K. Huzel and D. H. Huang, Design of Liquid-Propellant Rocket Engines. Washington, DC: National Aeronautics Space Administration, 1967.
- [3.8] Mohammad Naraghi, A Simple Approach For Thermal Analysis of Regenerative Cooling of Rocket Engines, ASME 2008 International Mechanical Engineering Congress and Exposition. Jan 2008.
  
- [6.1]
- [https://en.wikipedia.org/wiki/Specific\\_strength](https://en.wikipedia.org/wiki/Specific_strength)
- [6.2]
- <https://www.mcmaster.com/8459k26>
  
- [6.3]
- [https://www.researchgate.net/figure/Scheme-of-a-engine-with-pressurized-gas-propellant-feed-system\\_fig29\\_272086936](https://www.researchgate.net/figure/Scheme-of-a-engine-with-pressurized-gas-propellant-feed-system_fig29_272086936)
- [6.4]
- [https://www.researchgate.net/figure/Composite-overwrapped-pressure-vessel\\_fig1\\_305623294](https://www.researchgate.net/figure/Composite-overwrapped-pressure-vessel_fig1_305623294)
- [6.5]
- [http://mae-nas.eng.usu.edu/Peroxide\\_Web\\_Page/documents/H2O2%20Material%20Compatibility%20Overview.pdf](http://mae-nas.eng.usu.edu/Peroxide_Web_Page/documents/H2O2%20Material%20Compatibility%20Overview.pdf)
- [6.6]
- [http://mae-nas.eng.usu.edu/Peroxide\\_Web\\_Page/documents/H2O2%20Material%20Compatibility%20Overview.pdf](http://mae-nas.eng.usu.edu/Peroxide_Web_Page/documents/H2O2%20Material%20Compatibility%20Overview.pdf)
- [6.7]
- [http://mae-nas.eng.usu.edu/Peroxide\\_Web\\_Page/documents/H2O2%20Material%20Compatibility%20Overview.pdf](http://mae-nas.eng.usu.edu/Peroxide_Web_Page/documents/H2O2%20Material%20Compatibility%20Overview.pdf)
- [6.8]
- [http://mae-nas.eng.usu.edu/Peroxide\\_Web\\_Page/documents/H2O2%20Material%20Compatibility%20Overview.pdf](http://mae-nas.eng.usu.edu/Peroxide_Web_Page/documents/H2O2%20Material%20Compatibility%20Overview.pdf)
- [6.9]
- [http://mae-nas.eng.usu.edu/Peroxide\\_Web\\_Page/documents/H2O2%20Material%20Compatibility%20Overview.pdf](http://mae-nas.eng.usu.edu/Peroxide_Web_Page/documents/H2O2%20Material%20Compatibility%20Overview.pdf)
- [6.10]
- <http://multimedia.3m.com/mws/media/714747O/pultrusion-flyer.pdf?fn=Pultrusion%20Flyer.pdf>
- [6.11]
- <https://ntrs.nasa.gov/archive/nasa/casi.ntrs.nasa.gov/20080009730.pdf>
- [6.12]

[https://www.toraycma.com/file\\_viewer.php?id=4465](https://www.toraycma.com/file_viewer.php?id=4465)  
[6.13] <http://multimedia.3m.com/mws/media/7556800/matrix-resin-5832-technical-data-page.pdf?fn=MatrixResin5832TechDataPage.pdf>  
[6.14] <http://www.ardeinc.com/sketches/copy/4929.pdf>  
[6.15] <http://www.ardeinc.com/sketches/copy/5066.pdf>  
[6.16] <http://www.ardeinc.com/sketches/copy/4816.pdf>  
[6.17] <https://www.qd-ots.com/wp-content/uploads/2017/11/Composite-Pressure-Vessels.pdf>  
[6.18] <https://www.titaniumjoe.com/index.cfm/products/sheet-plate/>  
[6.19] <http://www.kobelco.co.jp/english/titan/files/details.pdf>  
[6.20] <http://www.kobelco.co.jp/english/titan/files/details.pdf>  
[6.21] <https://www.neaelectronics.com/assets/product-sheets-nea/NEA Model 9103 Data Sheet.pdf>  
[6.22] <http://airfoiltools.com/airfoil/details?airfoil=naca0006-il>  
[6.23] <https://catalog.orientalmotor.com/item/2-phase-bipolar-stepper-motors/60mm-pkp-series-2-phase-bipolar-stepper-motors/pkp264d28a2-sq18>  
[6.24] <https://www.cfinotebook.net/notebook/aerodynamics-and-performance/aircraft-components-and-structure>  
[6.25] [https://drive.google.com/file/d/1k2AHtoUMk-IpFql\\_IT7bOq6Ijxcx-Iih/view](https://drive.google.com/file/d/1k2AHtoUMk-IpFql_IT7bOq6Ijxcx-Iih/view)  
....

[7.1] [https://github.com/openrocket/openrocket/releases/download/OpenRocket\\_technical\\_documentation-v13.05/Open\\_Rocket\\_technical\\_documentation-v13.05.pdf](https://github.com/openrocket/openrocket/releases/download/OpenRocket_technical_documentation-v13.05/Open_Rocket_technical_documentation-v13.05.pdf)  
[7.2] [https://en.wikipedia.org/wiki/Nose\\_cone\\_design](https://en.wikipedia.org/wiki/Nose_cone_design)  
[7.3] [https://en.wikipedia.org/wiki/Nose\\_cone\\_design](https://en.wikipedia.org/wiki/Nose_cone_design)  
[7.4] [https://en.wikipedia.org/wiki/Nose\\_cone\\_design](https://en.wikipedia.org/wiki/Nose_cone_design)  
[7.5] <http://airfoiltools.com/airfoil/details?airfoil=naca0006-il>  
[7.6] <http://airfoiltools.com/airfoil/details?airfoil=naca0006-il>  
....

[8.1] <https://sensing.honeywell.com/MLH02KPSB06A-heavy-duty-pressure-transducers>  
[8.2] <http://www.thermometricscorp.com/thertypk.html>  
[8.3] <https://www.maximintegrated.com/en/products/sensors/MAX31855.html>  
[8.4] <https://www.batteryspace.com/high-power-polymer-li-ion-cell-3-7v-4000-mah-6050140-10c-14-8wh-40a-rate---ul-listed-un38-3-passed-ndgr.aspx>  
[8.5] <https://www.batteryspace.com/PCM-with-Equilibrium-and-Temperature-protection-function-for-14.8V-Li-Ion.aspx>  
[8.6] <https://www.cui.com/product/resource/v78xx-2000.pdf>  
[8.7] <https://www.tracopower.com/products/tsr2.pdf>  
[8.8] <https://www.cui.com/product/resource/pqde6w-t.pdf>  
[8.9] <https://www.pjrc.com/store/mp3115a2.pdf>

- [8.10] <https://sensing.honeywell.com/honeywell-sensing-asdx-series-analog-pressure-sensors-product-sheet-008090-12-en.pdf>
- [8.11] <https://www.digi.com/products/models/a09-hasm-7>
- [8.12] <https://www.mouser.com/datasheet/2/3/AEACAC053010-S433-1314095.pdf>
- [8.13] <https://www.tracksoar.com/product/tracksoar-v2/>
- [8.14] <http://www.l-com.com/wireless-antenna-900-mhz-8-dbi-circular-polarized-rh-flat-patch-antennas>
- [8.15] <https://www.hamradio.com/detail.cfm?pid=H0-007343>
- [8.16] <https://www.amazon.com/428-438MHz-Antenna-Aluminum-N-Female-connector/dp/B06XDJQV42>
- [8.17] <https://www.digi.com/products/embedded-systems/rf-modules/sub-1-ghz-modules/xbee-sx#partnumbers>
- [8.18] <https://www.digi.com/pdf/ds-xbee-xbeepro-sx-modules.pdf>
- [8.19] <http://www.rfcafe.com/references/electrical/ew-radar-handbook/polarization.htm>
- [8.20] [https://cdn-learn.adafruit.com/assets/assets/000/031/659/original/RFM95\\_96\\_97\\_98W.pdf?1460518717](https://cdn-learn.adafruit.com/assets/assets/000/031/659/original/RFM95_96_97_98W.pdf?1460518717)
- [8.21] <http://srecord.sourceforge.net/crc16-ccitt.html>
- [8.22] [https://www.matec-conferences.org/articles/matecconf/pdf/2018/17/matecconf\\_se2018\\_01008.pdf](https://www.matec-conferences.org/articles/matecconf/pdf/2018/17/matecconf_se2018_01008.pdf)

- [10.1] <https://store.arduino.cc/usa/arduino-uno-rev3>
- [10.2] <https://www.adafruit.com/product/2088>
- [10.3] <https://www.adafruit.com/product/964>
- [10.4] <https://www.amazon.com/Phonetone-Outdoor-Directional-1710-2700Mhz-Connector/dp/B00EC804SO/>
- [11.1] [http://www.cooperindustries.com/content/public/en/wiring\\_devices/interconnect/products/custom\\_mil\\_aero\\_connectors/umbilical\\_connectors.html](http://www.cooperindustries.com/content/public/en/wiring_devices/interconnect/products/custom_mil_aero_connectors/umbilical_connectors.html)
- [11.2] <https://www.movable-type.co.uk/scripts/latlong.html>
- [11.7] <http://www.wolftube.com/product/hose-wolf-wire-reinforced-smooth-hose-for-fuel-260-psi-w-p-1-65-m1-x-f1/>
- [11.8] <https://www.qammontechstore.com/ProductDetails.asp?ProductCode=SC-8167>
- ....

[#] Industrial Specialties Manufacturing, Hydrogen Peroxide Material Compatibility Chart. Englewood, CO, 2019:  
Industrial Specialties Manufacturing.

[#] D. K. Huzel and D. H. Huang, Design of Liquid-Propellant Rocket Engines. Washington, DC: National Aeronautics Space Administration, 1967.

[#] F. M. White, Fluid Mechanics. New York, NY: McGraw-Hill Education, 2018.

[#] Mohammad Naraghi, A Simple Approach For Thermal Analysis of Regenerative Cooling of Rocket Engines, ASME 2008 International Mechanical Engineering Congress and Exposition. Jan 2008.

[#] Benjamin Waxman et. al. Mass Flow Rate and Isolation Characteristics of Injectors For Use With Self-Pressurizing Oxidizers in Hybrid Rockets, American Institute of Aeronautics and Astronautics. 2013.

[#] R.W. Miller, Discharge Coefficient For Nozzles and Orifices. Neutrium, 2015.

[#] H.J. Baumgartner, "Decomposition of Concentrated Hydrogen Peroxide on Silver I. Low Temperature Reaction and Kinetics." Journal of Catalysis. Vol 2 Iss 5, Oct 1963 p405-414.

## Appendix B - Sponsorship Packet



**OUR MISSION & MASSIVELY TRANSFORMATIVE PURPOSE**

Be the first to space.

There is extraordinary momentum in the commercial space world right now. Base II, a STEM education non-profit, is holding a \$1 Million competition for the first undergraduate student team to build and launch a liquid rocket to the edge of space (known as the Karman Line).

Ignite new-space in WI.

Wisconsin has a rich history of making massive contributions to American spaceflight. We plan to propel Wisconsin onto the mainstream of today's new-space industry by winning the competition and deploying the winnings to strategically invigorate a space-startup ecosystem in Madison, WI.

Empower UW aerospace engineers.

Aerospace is hard, and classroom theory needs complimentary, hands-on engineering design and fabrication experience. High-stakes, hard engineering problems have proven time and time again to be the best way to ensure engineers have the skills they need to make meaningful contributions after graduation. These projects provide an essential forum to guide and inspire a passion for building innovative hardware.

WISCONSIN  
SPACE RACE

sponsor@wisc.space

**SOME OF WISCONSIN'S RICH SPACEFLIGHT HISTORY...**

**ASTRONAUTS**

- Jim Lovell (UW '46-'48)  
Gemini 7 & 12, Apollo 8 & 13
- Brewster Shaw (UW Alum. '68)  
STS 9, STS 61-B, STS-28
- Daniel Brandenstein (UW Alum. '65)  
STS 8, STS 51-G, STS-32, STS-49
- Jeffrey Williams (Wi Native)  
Record 534 days in space on ISS
- Deke Slayton  
Mark C. Lee  
Many more ...

**MANUFACTURING COMPETITIONS**

#1 Fabricated Metal Products	SpaceX Hyperloop Award Winning
#1 Appliances & components	NASA X-HAB National Winners
#1 Electrical Equipment	Many more ...

sponsor@wisc.space

**OUR ADVISORS**

**Prof. Matt Allen**  
UW Faculty

- Associate Professor, Department of Engineering Physics, University of Wisconsin-Madison

**Riccardo Bonazza**  
UW Faculty

- Professor, Department of Engineering Physics, University of Wisconsin-Madison

TBA

sponsor@wisc.space

**ABOUT OUR ROCKET**

KEROSENE FUEL	660 LBS PROPELLANT
90% H <sub>2</sub> O <sub>2</sub> OXIDIZER	90% H <sub>2</sub> O <sub>2</sub> OXIDIZER
5000 LBS THRUST	330 LBS DRY MASS
290 ISP	1000 LBS WET MASS
40 SECOND BURN	PRESSURE-FED ENGINE

sponsor@wisc.space

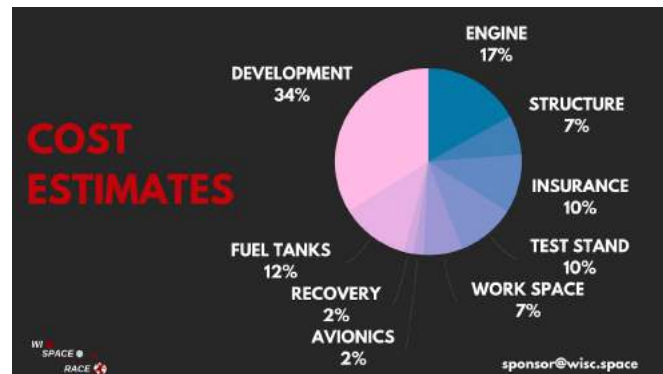
**HOW WE'LL USE THE Winnings (\$1,000,000)**

**Kickstart & Fund Future Student Teams & Projects**  
 Part of the winnings will be designated to support rocketry and other STEM-related educational efforts by establishing a fund to support various future student competitions and projects including, but not limited to, space-themed projects. Expected recipients include student organizations, competition teams, and individual students. Previous projects that would have qualified for such funding include the Badgerloop hyperloop team, the WI Space Race team, and the WI Flying team.

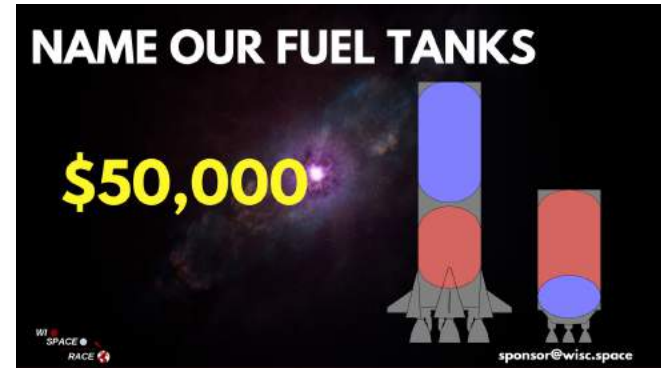
**Invigorate Student Aerospace Startup Innovation**  
 Further use of the awarded funds will include activities that inspire individual students to pursue aerospace ventures, that may include: (1) an aerospace hackathon (2) an aerospace-focused business plan/pitch competition (3) special awards for "Best Aerospace Pitch" at the University's innovation competition(s), etc.

**Madison-based Student Run Seed Fund**  
 (Tentative) In addition to the above initiatives, the team is working with the University and Competition sponsors (see 1) to allow a portion of the winnings to a student-run seed fund, with a focus on investing in hard-tech startups. This fund will operate similarly to those found at the University of Michigan, University of Colorado-Boulder, University of Southern California, New York University, and others.

WI SPACE RACE









**HOW CAN YOU PARTNER WITH US?**

**NAME OUR ROCKET \$150,000**

**NAME OUR ENGINE \$75,000**

**NAME OUR FUEL TANKS \$50,000**

**NAME OUR TEST STAND \$35,000**

(SpaceX Raptor Engine)

(SpaceX Fuel Tanks)

(SpaceX Test Stand)

sponsor@wisc.space

WISC SPACE RACE

This advertisement lists four naming opportunities with their respective prices: a rocket for \$150,000, an engine for \$75,000, fuel tanks for \$50,000, and a test stand for \$35,000. It includes small images of each component and the SpaceX Raptor Engine.

LET'S SAY YOU YOU'D LIKE  
TO GO ANOTHER ROUTE...

<b>SATURN</b>	<b>FALCON</b>	<b>ATLAS</b>
<b>\$21,600</b>	<b>\$16,200</b>	<b>\$10,800</b>
All FALCON benefits	All ATLAS benefits	All APOLLO benefits
Logo on Rocket (100%)	Logo on Rocket (75%)	Logo on Rocket (50% size)
Invitation to static fire test	2x EXCLUSIVE technical "HOW OUR ROCKET WORKS" webinars	Social Media thank you selfie-video
MOONSHOT Supporter Plaque	3D Printed Scale Model of Rocket	1X high-level "DESIGN OVERVIEW" webinar
Produced Social Media thank you video		
WISC SPACE RACE		sponsor@wisc.space

LET'S SAY YOU YOU'D LIKE  
TO GO ANOTHER ROUTE...

<b>APOLLO</b>	<b>GEMINI</b>	<b>MERCURY</b>
<b>\$7,200</b>	<b>\$5400</b>	<b>\$1800</b>
All GEMINI benefits	All MERCURY benefits	Logo on Rocket (20% Size)
Logo on Rocket (40% size)	Logo on Rocket (30% size)	Logo on website
10 x UW Space Race t-shirts	5 x UW Space Race t-shirts	Social media thank you post
Team resume handbook		
WISC SPACE RACE		sponsor@wisc.space

**QUESTIONS?**

"FROM NOW ON, WE LIVE IN A WORLD WHERE MAN HAS WALKED ON THE MOON. IT WASN'T A MIRACLE, WE JUST DECIDED TO GO."  
-JIM LOVELL

WISC SPACE RACE

sponsor@wisc.space

## Appendix C - Propulsion Calculations

### Nozzle sizing calculation

$$\frac{A_e}{A^*} \equiv \varepsilon = 8 = \frac{1}{M_e} \left[ \frac{2}{\gamma + 1} \left( 1 + \frac{\gamma - 1}{2} M_e^2 \right) \right]^{\frac{\gamma+1}{2(\gamma-1)}} \Rightarrow \text{Solve for exit Mach \# (root finder)}$$

$$P_e = P_0 \left( 1 + \frac{\gamma - 1}{2} M_e^2 \right)^{\frac{\gamma}{1-\gamma}} \Rightarrow \text{Solve for exit pressure}$$

$$T_e = T_0 \left( 1 + \frac{\gamma - 1}{2} M_e^2 \right)^{-1} \Rightarrow \text{Solve for exit Temperature}$$

$$\rho_0 = \frac{P_0}{RT_0} \Rightarrow \text{Solve for stagnation density}$$

$$\rho_t = \rho_0 \left( 1 + \frac{\gamma - 1}{2} \right)^{\frac{1}{\gamma-1}} \Rightarrow \text{Solve for density at throat}$$

$$T_t = T_0 \left( 1 + \frac{\gamma - 1}{2} \right)^{-1} \Rightarrow \text{Solve for temperature at throat}$$

Force flow to be choked at throat, yields 2 equations and 3 unknowns ( $A_t$ ,  $\dot{m}$ , and  $A_e$ ):

$$\Rightarrow \dot{m} = \rho_t A_t \sqrt{\gamma R T_t} = [F_T - (P_e - P_{atm}) A_e] \frac{1}{M_e \sqrt{\gamma R T_t}}$$

Rearrange and introduce known expansion ratio  $\varepsilon$  (3 equations, 3 unknown):

$$\Rightarrow \frac{F_T}{M_e \sqrt{\gamma R T_t}} - \frac{(P_e - P_{atm}) \varepsilon A_t}{M_e \sqrt{\gamma R T_t}} - \rho_t A_t \sqrt{\gamma R T_t} = 0$$

Solve for throat area |

$$\Rightarrow A_t = \frac{F_T}{(P_e - P_{atm}) \varepsilon + M_e \rho_t \gamma R \sqrt{T_e T_t}}$$

Solve for exit area:

$$\Rightarrow A_e = \varepsilon A_t$$

*Solve for mass flow rate:*

$$\Rightarrow \dot{m} = \rho_t A_t \sqrt{\gamma R T_t}$$

## Injector Sizing Calculations

The diagram to the below represents a cross section of the injector hole. The upper region contains fluid at pressure  $P_1$  and has a cross sectional area of  $A_1$ . The hole is a cylinder of diameter  $D$  and length  $\Delta h$  that connects the upper region to the combustion chamber. Fluid exits the injector hole at pressure  $P_2$ . The following calculations were done to find the ideal diameter size for the holes of the injector plate for HTP and RP-1

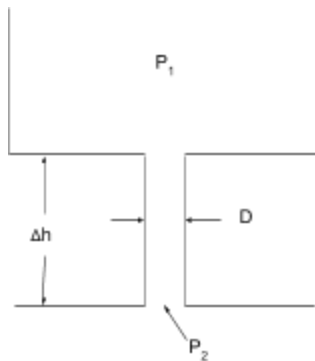


Figure C.1: Injector plate cross section

Symbol	Definition	Units
A	Cross-sectional area	$m^2$
$c_d$	Discharge coefficient	-
g	Acceleration due to gravity	$m/s^2$
h	Height	m
$\dot{M}$	Mass flow rate	$kg/s$
N	Number of holes	-
P	Pressure	Pa
$\rho$	Density	$kg/m^3$

		$m^3$
v	Flow velocity	m/s

Definition of  $\dot{M}$ :

$$\dot{M} = \rho A v$$

$$v = \frac{\dot{M}}{\rho A}$$

From Bernoulli's Equation:

$$P_1 + \rho gh_1 + \frac{1}{2}\rho v_1^2 = P_2 + \rho gh_2 + \frac{1}{2}\rho v_2^2$$

$$\Delta P + \rho g \Delta h = \frac{1}{2}\rho(v_2^2 - v_1^2)$$

Assume  $\rho g \Delta h$  term is negligible due to small  $\Delta h$ . Substitute  $v = \frac{\dot{M}}{\rho A}$ .

$$\Delta P = \frac{1}{2}\rho\left[\left(\frac{\dot{M}}{\rho A_2}\right)^2 - \left(\frac{\dot{M}}{\rho A_1}\right)^2\right]$$

$$\Delta P = \frac{1}{2}\rho \frac{\dot{M}^2}{A_2^2} \left[\left(\frac{1}{A_2}\right)^2 - \left(\frac{1}{A_1}\right)^2\right]$$

$$\Delta P = \frac{\dot{M}^2}{2\rho A_2^2} \left[1 - \left(\frac{A_2}{A_1}\right)^2\right]$$

Assume  $\frac{A_2}{A_1}$  is negligible due to tiny size of  $A_2$ . Solving for  $\dot{M}$

gives:

$$\dot{M} = A_2 \sqrt{2\rho \Delta P}$$

This assumes one dimensional flow. To account for uneven flow resulting from turbulence, a discharge coefficient  $c_d$  is added.

$$\dot{M} = c_d A_2 \sqrt{2\rho \Delta P}$$

Note that the injector plate will have N holes and that  $A_2$  is simply the surface area of a circle with diameter D.  $A_2 = \pi(\frac{D}{2})^2$

$$\dot{M} = N c_d \frac{\pi}{4} D^2 \sqrt{2\rho \Delta P}$$

Solve for D.

$$D = \left( \frac{M}{c_d \pi N} \right)^{1/2} \left( \frac{8}{\rho \Delta P} \right)^{1/4}$$

The discharge coefficient  $c_d$  can be approximated from the resistance coefficient for pipe flow with a sudden contraction and sudden expansion.

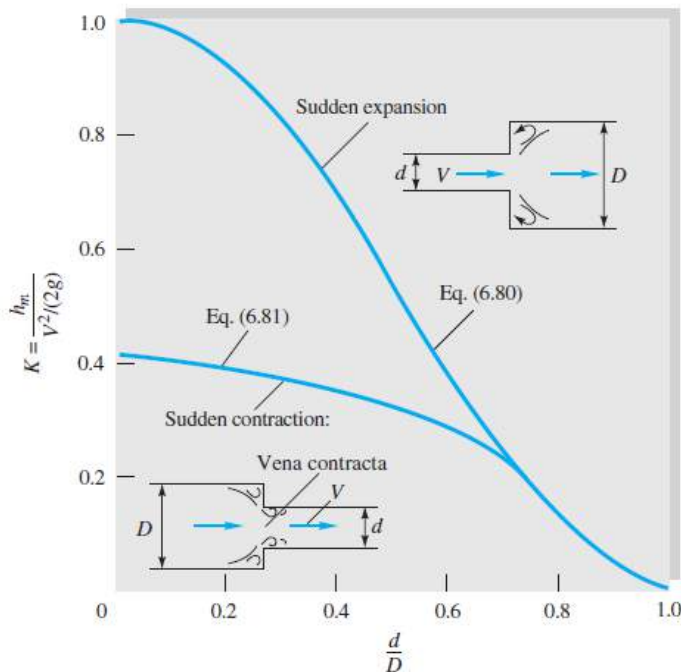


Figure C.2 Resistance coefficients for pipe flow

For a sudden contraction followed by a sudden expansion, assuming that  $d/D$  is approximately zero for both cases, the overall resistance coefficient is  $0.4 + 1.0 = 1.4$ . Lastly, the relationship between the discharge coefficient and resistance coefficient is used.

$$c_d = \frac{1}{\sqrt{K}} = \frac{1}{\sqrt{1.4}} = 0.845$$

With an equation for  $D$  derived, we can substitute in data for HTP and RP-1.

Calculations supported by the following references: [Waxman] [Miller].

# Procedure for Silver Plating Monel Mesh for Catalyst Bed

## Materials

- 1 Glass Beaker (1000mL)
- 15g AgCN
- 22.5g KCN
- 15g  $K_2CO_3$
- 500mL Deionized Water
- 99.9% Silver Electrode
- Variable power supply
- Multimeter
- Monel Mesh
- Electrical Wiring
- Steel wool
- 6M or greater HCl
- Deionized water
- Agitator / magnetic stir bar

## Procedure

- 1) Clean and prepare the mesh
  - a) Lightly clean mesh with steel wool
  - b) Dunk in concentrated HCl for 10 seconds
  - c) Rinse in deionized water
- 2) Construct the following electrolytic cell: Concentrations of aqueous solutions are dictated by the mass of chemicals and the volume of water stated in the materials list.
- 3) Plate for 30 minutes at the following conditions:
  - a) Cathode current density: 25 A/ft<sup>2</sup>
  - b) Temperature: 25°C (Room Temp)
  - c) Cathode agitation: cathode rod movements 6-15 ft/min (2-6 m/min)
    - i) Use a small agitator or magnetic stir bar operating very slowly. Ensure enough agitation that an even coating is applied.
  - d) Silver consumption: 0.13 oz/A-hr (4 g/A-hr)
  - e) Time for deposition 1  $\mu$ m (0.04  $\mu$ inch) at 1.5 A/dm<sup>2</sup>: 1 min.
- 4) Silver deposition will be evident due to a color change. If the current density is too high, "burning" and a blackening of the monel mesh will occur. This can be fixed by lowering the current density or increasing agitation.

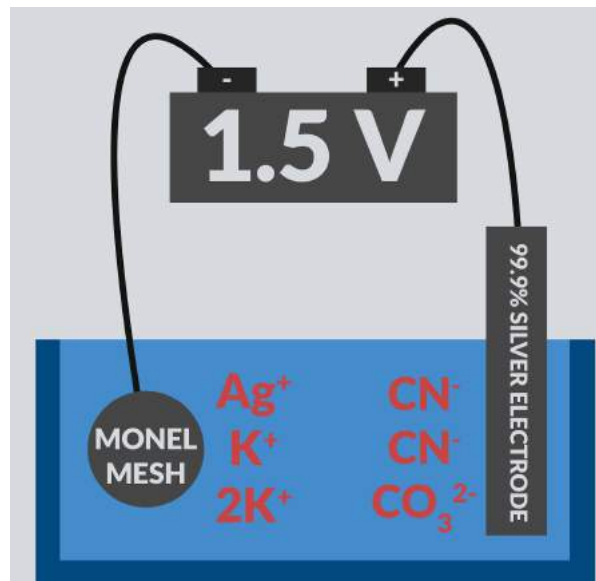


Figure C.4: Electrolytic Cell used to silver-plate monel mesh

# Appendix D - MATLAB code for altitude prediction and rocket parameterization

## Table of Contents

WI Space Race Rocket Parameterization Code .....	1
Rocket Parameters .....	1
Rocket Altitude Predictions .....	2
Universal Constants .....	3
Defining variable from input .....	3
Initial Calculations .....	3
Solving EOM .....	4
Nozzle geometry .....	5
Plotting .....	5
Results output .....	6
Engine Paramaters .....	7
GetMassFlowAndNozzleDimensions Function .....	8
eom_rocket Function .....	9
Get_rho_T_P Function .....	10
Get_flow Function .....	11
GetPropTankVol Function .....	12
Volume Calcs .....	12
propTankWt_Size function .....	12
Tank thickness calcs .....	13
Tank sizing calcs .....	13
Weight Calcs .....	13
GetFeedPress Function .....	13
Rao Function .....	14
newtzero Function .....	15

## WI Space Race Rocket Parameterization Code

Author: Brandon Wilson ([bwilson8@wisc.edu](mailto:bwilson8@wisc.edu)) This script solves the equation of motion of a sounding rocket during the vertical ascent phase of flight. The eom\_rocket function is called to solve the EOM using several linear and non-linear equations to provide relatively accurate predictions with minimal paramters

```
clear; clc; close all;

global ft2m psi2Pa

% Simulation time
simTime = 230;
```

## Rocket Parameters

```
%----- feel free to change these parameters
-----

m_veh_structure = 120;      % dry mass of rocket [kg]
m_prop = 300;                % Initial propellant mass, kg
r_veh = 7/12*ft2m;          % radius of vehicle [m]
epsilon = 8;                  % expansion ratio of nozzle
```

```

F_T_max = 15e3;           % Thrust when exit pressure = atm pressure
r_tank = 6/12;            % tank radius [ft]

% feed pressure parameters
inj_percentDrop = 25;    % pressure drop across injector [% of chamber
                         % press]
catBed_pressDrop = 100*psi2Pa; % pressure drop across catalyst bed
                               [Pa]
ox_lineDiameter = 1.5-2*0.083; % ox feed line diameter [in]
f_lineDiameter = 3/8-2*0.035; % fuel feed line diameter [in]

% from CEARUN
P0_eng = 2.76e6;
T0_eng = 2734;
M_bar_prop = 21.9;
gamma_prop = 1.14;

% call altitude prediction model
for i = 1:length(epsilon)
[xx, R_x, Pe(i)] =
altitude_prediction(simTime,r_veh,r_tank,m_veh_structure, ...
m_prop,F_T_max,epsilon(i),P0_eng,T0_eng,M_bar_prop,gamma_prop, ...
inj_percentDrop,catBed_pressDrop,ox_lineDiameter,f_lineDiameter);
end
% for i = 1:9
% figure(i)
% legend(['Expansion Ratio: ',num2str(epsilon(1))],['Expansion Ratio: ...
% ',num2str(epsilon(2))],...
% ['Expansion Ratio: ',num2str(epsilon(3))],['Expansion Ratio: ...
% ',num2str(epsilon(4))],...
% ['Expansion Ratio: ',num2str(epsilon(5))],['Expansion Ratio: ...
% ',num2str(epsilon(6))],...
% ['Expansion Ratio: ',num2str(epsilon(7))],['Expansion Ratio: ...
% ',num2str(epsilon(8))])
% end
%
% figure(10)
% plot(epsilon,Pe/psi2Pa,'d')
% xlabel('Expansion Ratio')
% ylabel('Exit Pressure [psia]')

```

## Rocket Altitude Predictions

main function that calls sub functions and does plotting

```

function [xx, R_x, Pe] =
altitude_prediction(sim_t,R,r_tank,m_struct,m_propellant, ...
F_T,epsilon,P0,T0,M_bar,gamma,inj_percentDrop,catBed_pressDrop, ...
ox_lineDiameter,f_lineDiameter)

global A_veh g m_veh_empty eng_time m_dot r_veh R_bar M_bar_prop Ae...
At gamma_prop P0_eng Pe_eng T0_eng n_rao expansionRatio ue Isp...
m_veh_wet ft2m psi2Pa in2m Pa2psi

```

---

## Universal Constants

```

g = 9.807;                                % gravitational constant [m/s^2]
R_bar = 8314.3;                            % universal gas constant [J/kmol-K]
kg2lbf = 2.20462;                          % kg to lbf conversion
lbf2kg = 0.453592;                          % lbf to kg conversion
Pa2psi = 0.000145038;                      % Pascal to psi conversion
psi2Pa = 6894.76;                           % psi to Pascal conversion
m2ft = 3.28084;                            % meter to foot conversion
ft2m = 0.3048;                             % foot to meter conversion
in2m = 0.0254;                             % inch to meter conversion
kN2lbf = 224.81;                           % kN to lbf conversion

```

## Defining variable from input

```

m_veh_structure = m_struct;
simTime = sim_t;
m_prop = m_propellant;
P0_eng = P0;
T0_eng = T0;
M_bar_prop = M_bar;
F_T_max = F_T;
gamma_prop = gamma;
expansionRatio = epsilon;
r_veh = R;

```

## Initial Calculations

```

% mass flow, throat area, and exit area for engine
[Pe_eng, ue, m_dot] = GetMassFlowAndNozzleDimensions(F_T_max);
eng_time = m_prop/m_dot; % burn time
Pe = Pe_eng

% Propellant tank calculations
rho_ox = 1400; % oxidizer density [kg/m^3]
rho_f = 810;   % fuel density [kg/m^3]
OF = 7; % ox:fuel ratio

m_dot_ox = (OF * m_dot) / (1 + OF); % mass flow of oxidizer [kg/s]
m_dot_f = m_dot - m_dot_ox; % mass flow of fuel [kg/s]

inj_PressDrop = inj_percentDrop/100*P0_eng; % pressure drop across
injector

ox_lineLength = 24; % guess for ox run line length [in]
% oxidizer tank pressure
ox_tankPressure = 2*GetFeedPress(ox_lineDiameter*in2m,P0_eng, ...
catBed_pressDrop,inj_PressDrop,m_dot_ox,rho_ox,ox_lineLength);

f_lineLength = 144; % guess for fuel run line length [in]
% fuel tank pressure
f_tankPressure = 2*GetFeedPress(f_lineDiameter*in2m,P0_eng, ...

```

---

```

catBed_pressDrop*0,inj_PressDrop,m_dot_f,rho_f,f_lineLength);

% get tank volumes
[vol_ox,vol_f,m_ox,m_f] = GetPropTankVol(OF,m_prop,rho_ox,rho_f);

% get ox tank size and weight estimates
[ox_tankWt,ox_tank_length,ox_t_cyl,ox_t_hemi,ox_l_tank_cyl]...
    = propTankWt_Size(vol_ox*m2ft^3,r_tank,ox_tankPressure*Pa2psi);

% get fuel tank size and weight estimates
[f_tankWt,f_tank_length,f_t_cyl,f_t_hemi,f_l_tank_cyl]...
    = propTankWt_Size(vol_f*m2ft^3,r_tank,f_tankPressure*Pa2psi);
tankWt = ox_tankWt + f_tankWt;

m_tanks = tankWt*lbm2kg; % propellant tank total

m_veh_empty = m_veh_structure+m_tanks; %empty mass of vehicle [kg]
m_veh_wet = m_veh_empty+m_prop;        % wet mass of vehicle [kg]
A_veh = pi*r_veh^2;                  % Cross sectional area of vehicle
[m^2]

```

## Solving EOM

Initial Conditions

```

x0 = 0;
v0 = 0;
IC = [x0;v0];
t_span = [0,simTime];

% Call ode45 to solve EOM
options = odeset('RelTol',1e-13,'AbsTol',1e-13);
[tout, yout] = ode45('eom_rocket',t_span,IC);

% only want data up to max altitude
for i = 1:length(tout)
    if(yout(i,2) >= 0)
        alt(i) = yout(i,1);
        vel(i) = yout(i,2);
        time(i) = tout(i);
    else
        break;
    end
end

% Back Solving for acceleration, Force of Drag, Cd, Ma, Re
acc_num = zeros(length(time),1);
F_d = zeros(length(time),1);
F_T = zeros(length(time),1);
Ma = zeros(length(time),1);
Re = zeros(length(time),1);
rho = zeros(length(time),1);
Cd = zeros(length(time),1);

```

---

```
% back out acceleration, drag, Mach and Reynolds
for i = 1:length(time)
    [acc_num(i),F_T(i),F_d(i),Ma(i),Re(i),rho(i), Cd(i)] =
    BackoutPerformance...
        (time(i),alt(i), vel(i));
end
```

## Nozzle geometry

```
n.rao = 200; % number of mesh points
R_t = sqrt(At*4/pi)/2; % throat radius [m]
epsilon = Ae/At; % expansion ratio
Lf_ratio = 0.9; % conical nozzle fraction
theta_E = 8*pi/180; % exit angle
theta_N = 23*pi/180; % diverging angle
theta_C = 30*pi/180; % converging angle

% Rao parabolic approximation
[xx, coeffs, R_x] = Rao(R_t, epsilon,
    Lf_ratio, theta_E, theta_N, theta_C);

% converting to inches
R_x_in = R_x*39.3701;
xx_in = xx*39.3701;
```

## Plotting

```
figure(1)
hold on;
plot(time,alt/1000,'LineWidth',1.7)
title('Altitude Vs Time','FontSize',13)
xlabel('Time [s]', 'FontSize',12)
ylabel('Altitude [km]', 'FontSize',12)
grid on;

figure(2)
hold on;
plot(time,vel,'LineWidth',1.7)
grid on;
title('Vertical Velocity Vs Time', 'FontSize',13)
xlabel('Time [s]', 'FontSize',12)
ylabel('Velocity [m/s]', 'FontSize',12)

figure(3)
hold on;
plot(time,acc_num/g,'LineWidth',1.7)
grid on;
title('Acceleration Vs Time', 'FontSize',13)
xlabel('Time [s]', 'FontSize',12)
ylabel('Acceleration [g]', 'FontSize',12)

figure(4)
```

---

---

```

hold on;
plot(time,F_d,'LineWidth',1.7)
grid on;
title('Force of Drag Vs time', 'FontSize',13)
xlabel('time [s]', 'FontSize',12)
ylabel('Force of Drag [N]', 'FontSize',12)

figure(5)
hold on;
plot(time,Ma,'LineWidth',1.7)
grid on;
title('Mach # Vs Time', 'FontSize',13)
xlabel('Time [s]', 'FontSize',12)
ylabel('Mach #', 'FontSize',12)

figure(6)
hold on;
plot(alt,F_T/1000,'LineWidth',1.7)
grid on;
title('Thurst Vs Altitude', 'FontSize',13)
xlabel('Altitude [km]', 'FontSize',12)
ylabel('Thrust [kN]', 'FontSize',12)

figure(7)
hold on;
plot(xx_in,R_x_in,'b-','LineWidth',1.7)
plot(xx_in,-R_x_in,'b-','LineWidth',1.7)
grid on;
title('Nozzle Dimensions', 'FontSize',13)
xlabel('x [in]', 'FontSize',12)
ylabel('Radius [in]', 'FontSize',12)
axis equal

figure(8)
hold on;
plot(Ma,Cd,'d','LineWidth',1.2)
grid on;
title('Drag Coefficient vs Mach #', 'FontSize',13)
xlabel('Mach #', 'FontSize',12)
ylabel('Cd [-]', 'FontSize',12)

figure(9)
hold on;
plot(alt/1000,F_d/1000,'d','LineWidth',1.2)
grid on;
title('Drag vs Altitude', 'FontSize',13)
xlabel('altitude [km]', 'FontSize',12)
ylabel('Drag [kN]', 'FontSize',12)

```

## Results output

```
% max drag force
max_Fd = max(F_d);
```

---

```
% max dynamic pressure
q = zeros(length(time),1);
for i = 1:length(vel)
    q(i) = 1/2*rho(i)*vel(i)^2;
end
maxQ = max(q);

% max velocity
maxVelocity = max(yout(:,2));

% max Mach #
maxMach = max(Ma);

% specific impulse
Isp = ue/g;

clc;
disp('----- Rocket Parameters
-----')
fprintf('Vehicle dry weight: %3.2f [lb]', (m_veh_empty)*kg2lbf)
fprintf('\nVehicle wet weight: %3.2f [lb]', (m_veh_wet)*kg2lbf)
fprintf('\nVehicle diameter: %3.2f [ft]', 2*r_veh*m2ft)
fprintf('\nPropellant mass (total): %3.2f [kg], %3.2f [lb]', ...
    m_prop,m_prop*kg2lbf)
fprintf('\nPeroxide mass: %3.2f [kg], %3.2f [lb]', ...
    m_ox,m_ox*kg2lbf)
fprintf('\nKerosene mass: %3.2f [kg], %3.2f [lb]', ...
    m_f,m_f*kg2lbf)
fprintf('\nPropellant mass fraction: %3.2f [-]', m_prop/m_veh_wet)
fprintf('\nPropellant tank Weight : %3.2f [lb]', tankWt)
fprintf('\nPeroxide tank Wall thickness : %3.2f [in]', ox_t_cyl)
fprintf('\nKerosene tank Wall thickness : %3.2f [in]', f_t_cyl)
fprintf('\nPeroxide tank length (inner dim): %3.2f [ft]', ...
    ox_tank_length)
fprintf('\nKerosene tank length (inner dim): %3.2f [ft]', ...
    f_tank_length)
fprintf('\nPeroxide tank volume: %3.2f [m^3]', vol_ox)
fprintf('\nKerosene tank volume: %3.2f [m^3]', vol_f)
fprintf('\nPeroxide tank max operating pressure: %3.2f [psi]', ...
    ox_tankPressure*Pa2psi)
fprintf('\nKerosene tank max operating pressure: %3.2f [psi]', ...
    f_tankPressure*Pa2psi)
fprintf('\nPeroxide tank mean operating pressure: %3.2f [psi]', ...
    ox_tankPressure*Pa2psi/2)
fprintf('\nKerosene tank mean operating pressure: %3.2f [psi]', ...
    f_tankPressure*Pa2psi/2)
fprintf('\n')
```

## Engine Parameters

```
disp('----- Propulsion Parameters
-----')
```

```

fprintf('Sea level thrust: %3.2f [kN], %3.2f [lbf]', F_T(1)/1000, ...
        F_T(1)/1000*kN2lbf)
fprintf('\nExpansion ratio: %3.2f [-]', expansionRatio)
fprintf('\nChamber Pressure: %3.2f [MPa], %3.2f [psia]', ...
        P0_eng*1e-6, ...
        P0_eng*Pa2psi)
fprintf('\nExit Pressure: %3.2f [MPa], %3.2f [psia]', Pe_eng*1e-6, ...
        Pe_eng*Pa2psi)
fprintf('\nChamber temperature %3.2f [K]', T0_eng)
fprintf('\nMolar mass of propellant: %3.2f [kg/kmol]', M_bar_prop)
fprintf('\nSpecific heat ratio of propellant (frozen-flow) %3.2f
        [-]', ...
        gamma_prop)
fprintf('\nPressure at catalyst bed: %3.2f [psia]', ...
        (P0_eng+catBed_pressDrop+inj_PressDrop)*Pa2psi)
fprintf('\nPressure at injector: %3.2f [psia]', ...
        (P0_eng+catBed_pressDrop)*Pa2psi)
fprintf('\nMass flow rate (total): %3.2f [kg/s]', m_dot)
fprintf('\nMass flow rate (oxidizer): %3.2f [kg/s], %3.2f [lb/s]', ...
        m_dot_ox,m_dot_ox*kg2lbf)
fprintf('\nMass flow rate (fuel): %3.2f [kg/s], %3.2f [lb/s]', ...
        m_dot_f, ...
        m_dot_f*kg2lbf)
fprintf('\nNozzle exit diameter: %3.2f [in]', 2*R_x(length(R_x))/in2m)
fprintf('\nThroat Diameter: %3.2f [in]', 2*R_t/in2m)
fprintf('\nPeroxide feed line diameter %3.2f [in]', ox_lineDiameter)
fprintf('\nKerosene feed line diameter %3.2f [in]', f_lineDiameter)
fprintf('\nBurn time %3.2f [s]', eng_time)
fprintf('\n\n')

disp('----- Results
-----')
fprintf('Max Altitude: %3.2f [m], %3.2f [ft]', ...
        max(yout(:,1)), 3.28*max(yout(:,1)))
fprintf('\nMax Velocity: %3.2f [m/s]', maxVelocity)
fprintf('\nMax Mach #: %3.2f [-]', maxMach)
fprintf('\nMax Thrust: %3.2f [kN], %3.2f [lbf]', max(F_T)/1000, ...
        max(F_T)/1000*kN2lbf)
fprintf('\nSpecific Impulse: %3.2f [s]', Isp)
fprintf('\nMax Drag Force: %3.2f [kN], %3.2f [lbf]', max_Fd/1000, ...
        max_Fd/1000*kN2lbf)
fprintf('\nMax dynamic pressure: %3.2f [kPa]', maxQ/1000)
fprintf('\nActual expansion ratio %3.2f [-]', pi*R_x(length(R_x))^2/At)
fprintf('\n\n')
total_impulse = max(cumtrapz(F_T)/4.448/1000)
R_t/in2m*sqrt(3)

end

```

## GetMassFlowAndNozzleDimensions Function

returns mass flow based on initial thrust

```
function [Pe,ue,m_dot] = GetMassFlowAndNozzleDimensions(F_T_0)
```

---

```

global P0_eng Pe_eng T0_eng expansionRatio gamma_prop R_bar M_bar_prop
At...
Ae Isp

epsilon = expansionRatio;
P0 = P0_eng;
gamma = gamma_prop;
T0 = T0_eng;
R = R_bar/M_bar_prop;
P_atm = 101.3e3;

% calculate Me from expansion ratio
Ae_Astar_expr = @(Me) 1./Me.*(2/(gamma+1)*(1+(gamma-1)/2*Me.^2))...
.^((gamma+1)/(2*(gamma-1))) - epsilon;
Me = newtzero(Ae_Astar_expr, 1);

% 2 solutions, only want supersonic
if(length(Me) == 2)
    Me = Me(2);
end
% get exit pressure and temp
Pe = P0*(1+(gamma-1)/2*Me^2)^(gamma/(1-gamma));
Pe_eng = Pe;
Te = T0*(1+(gamma-1)/2*Me^2)^(-1);

% solving for throat area and m_dot
rho0 = P0/(R*T0);
rho_t = rho0*(1+(gamma-1)/2)^(-1/(gamma-1));
Tt = T0*(1+(gamma-1)/2)^(-1);
At = F_T_0/((Pe-P_atm)*epsilon+Me*rho_t*gamma*R*sqrt(Tt*Te));
m_dot = rho_t*At*sqrt(gamma*R*Tt);

% exit area, velocity and ISP
Ae = epsilon*At;
ue = Me*sqrt(gamma*R*Te);
Isp = ue/9.807;
end

```

## eom\_rocket Function

2nd order non-linear differential equation for vertical ascent and constant thrust

```

function [ydot] = eom_rocket(t,y)

global A_veh g m_veh_empty eng_time m_dot Ae Pe_eng ue m_veh_wet

massFlow = m_dot;
Pe = Pe_eng;
% altitude, temp and pressure as a function of altitude
[rho, T, P] = Get_rho_T_P(y(1));

```

---

---

```

% Get Cd, Ma and Re
[Cd, Ma, Re] = GetFlow(T,rho,y(2));

% Force due to drag [N]
F_d = 0.5* Cd * A_veh * rho * y(2)^2;

% Thrust is constant piecewise
if t < max(eng_time)

    % thrust
    F_T = massFlow*ue+(Pe-P)*Ae;
%    F_T = 20e3;

    % rocket mass decreases linearly with m_dot (assumed ~constant
m_dot)
    m_veh = m_veh_wet-massFlow*t;

else
    F_T = 0;                      % Thrust = 0 after motor burnout
    m_veh = m_veh_empty;          % Mass is constant after burnout
    massFlow = 0;
end

% returned ydot values
ydot(1,1) = y(2);
ydot(2,1) = F_T/m_veh-F_d/m_veh-massFlow*y(2)/m_veh-g;

end

```

## Get\_rho\_T\_P Function

returns temperature, pressure and density from an altitude input

```

function [rho,T,P] = Get_rho_T_P(alt)
% Model based on NASA.gov:
% https://www.grc.nasa.gov/www/k-12/airplane/atmosmet.html

%atmospheric definitions
Tropopause = 11000;      % Altitude of initial Tropopause reg [m]
lowerStrat = 25000;       % Altitude of lower stratosphere [m]

% Temp linearly decreases then becomes constant at tropopause
if(alt > lowerStrat)
    T = -131.21 + 0.00299*alt; %C
    P = 2.488*((T+273.15)/216.6)^(-11.388); % kPa
elseif(alt > Tropopause && alt < lowerStrat)
    T = -56.46; % C
    P = 22.65*exp(1.73-0.000157*alt); %kPa
else
    T = 15.04 - 0.00649*alt;      % C
    P = 101.29*((T+273.15)/288.08)^5.256; % kPa

```

---

---

```

end

% Air density as a function of pressure and temp [kg /m^3]
rho = P/(0.2869*(T+273.15));

% convert back to SI
P = P*1000; %Pa
T = T + 273.15; % K

end

```

## Get\_flow Function

returns drag coefficient, Mach and Reynolds #

```

function [Cd, Ma, Re] = GetFlow(T,rho,V)

global r_veh R_bar

gamma = 1.4; % Ratio of specific heat for air
M_bar_air = 28.97; % kg/kmol
R = R_bar/M_bar_air; % Ideal gas constant [j/(Kg-K)]
c = sqrt(gamma*R*T); % Speed of sound
Ma = norm(V/c); % Mach Number
mu0 = 18.27e-6; % Dynamic viscosity at 291.15 K [Pa-s]
T0 = 291.15;
C = 120; % Sutherland constant
mu = mu0*((T0+C)/(T+C))*(T/T0)^(3/2); % Dynamic viscosity
    % (Sutherland's eq)
Re = rho*V*r_veh^2/mu; % Reynold's number

% approximationg drag coefficient from "rocket ans spacecraft
% propulsion"
% from Marting Turner (page 150). Esssentiall Cd is roughly constant
in
% subsonic regime, then exponentially increases to mach 1, then
% exponentiall decreases.
a = 0.15;
b = 0.35;
if (Ma < 1)
    Cd = a + b*Ma^6;
else
    Cd = a + b/Ma^2;
end

end

```

## GetPropTankVol Function

Returns tank volumes

```
function [vol_ox_total,vol_f_total,m_ox,m_f] = GetPropTankVol[OF,
propellantMass, ...
rho_ox, rho_f)

% Inputs: OF: ox:fuel ratio, propellantMass: kg, rho_ox: kg/m^3,
rho_f:
% kg/m^3
```

## Volume Calcs

```
m_ox = (OF * propellantMass) / (1 + OF); % mass oxidizer [kg]
m_f = propellantMass - m_ox; % mass fuel [kg]
vol_ox = m_ox / rho_ox; % Volume of oxidizer [m^3]
vol_f = m_f / rho_f; % Volume of fuel [m^3]
vol_ox_boilOff = vol_ox * 0.01; % boil off volume (rough
approx)
vol_f_boilOff = vol_f * 0; % non cryo, wont boil off
vol_ox ullage = (vol_ox_boilOff + vol_ox) * 0.05;
vol_f ullage = (vol_f_boilOff + vol_f) * 0.05;

vol_ox_total = vol_ox + vol_ox_boilOff + vol_ox ullage;
vol_f_total = vol_f + vol_f_boilOff + vol_f ullage;

end
```

## propTankWt\_Size function

returns overall tank weight, overall length, thickness of cylinder, thickness of hemispherical ends, thickness of junction, and length of tank

```
function [tankWt,tank_length,t_cyl,t_hemi,l_tank_cyl]...
= propTankWt_Size(vol_total, r_tank, operatingPressure)

% Parameters are: outer radius of tank [ft], and operating pressure
[psi]

%%%%%%%%%%%%% Tank size and weight %%%%%%%%%%%%%%
%%%%%%

rho_Al = 170; % Density of 6066 t-6 aluminum,
lbm/ft^3
al_yield = 39000; % Yield strength of 6066 t-6 al
al_ultimate = 45000; % Ultimate strength of 6066 t-6 al
K = 1/0.67; % Knuckle factor for stress
concentrations

% Max allowable stress per MIL-STD1522A (USAF)
maxAllowStress = min(al_yield/1.25, al_ultimate/1.5);
```

---

## Tank thickness calcs

Required wall thickness at the weld [in]

```
t_k = K * operatingPressure * r_tank * 12 / maxAllowStress;

% Required wall thickness of the hemispherical ends [in]
t_cr = operatingPressure * r_tank * 12 / (2 * maxAllowStress);

% Hemispherical end thickness [in]
t_hemi = (t_k + t_cr) / 2;

% Required thickness of cylindrical section [in]
t_cyl = operatingPressure * r_tank * 12 / maxAllowStress;
```

## Tank sizing calcs

Inner radii of hemi and cyl [ft]

```
r_inner = r_tank - t_hemi/12;

% volume of end cap
vol_hemi = 2/3 * pi * r_inner^3;

% Volume required for cylinders
vol_cyl = vol_total - 2 * vol_hemi;

% oxidizer tank length cylinder only
l_tank_cyl = vol_cyl / (pi * r_inner^2);

% tank overall Length (inner dimensions)
tank_length = l_tank_cyl + 2 * r_inner;
```

## Weight Calcs

Weight of components

```
weight_tank_cyl = rho_Al * pi * l_tank_cyl * (r_tank^2 - r_inner^2);
weight_Tank_Hemis = 2/3 * pi * rho_Al * (r_tank^3 - r_inner^3);

% Overall weight
tankWt = weight_tank_cyl + 2 * weight_Tank_Hemis;

end
```

## GetFeedPress Function

returns tank pressure based on pressure drops, losses, and line diam and mass flow, density, and line length [m]

```
function [tank_press] =
GetFeedPress(lineDiam,P0_eng,catBed_pressDrop,...
```

---

```

inj_PressDrop, m_dot, rho, L_in)

global in2m

A = pi/4*lineDiam^2; % area [m^2]
v = m_dot/(rho*A); % velocity [m/s]
mu = 1.003e-3; % viscosity (using water)
Re = rho*v*lineDiam/mu; % reynolds #
epsilon = 0.005/1000; % guess for pipe roughness [m]
L= L_in*in2m; % line length [m]

if(Re > 2200)
    f_expr = @(f) -2*log(epsilon/lineDiam/3.7+2.51./(Re*sqrt(f)))-1./
sqrt(f);
    f = fsolve(f_expr, 0.05);
else
    disp('laminar') % shouldnt ever be laminar, if it is I want to
    know
end

deltaP = rho*f*L/lineDiam*v^2/2; % TODO: calculate friction losses and
% pressure drops from relief valves, etc

backPress = P0_eng+catBed_pressDrop+inj_PressDrop; % pressure at inlet
tank_press = rho*v^2 + backPress + deltaP;

end

```

## Rao Function

Rao Parabolic Approximation Method for sizing nozzles

```

function [xx, coeffs, R_x] = Rao(R_t, epsilon,
Lf_ratio,theta_E,theta_N,theta_C)

% returns coefficients for parabola, and the radius vector
% note: using fixed exit and entrance angles, need to get numeric
% data for plots so these can be chosen automatically

global n_rao

n = n_rao;
% **** Don't change anything in this section
*****
R_dt = 0.382*R_t;
R_ut = 1.5*R_t;
R_cu = R_ut + R_t;
R_cd = R_dt + R_t;

% geometry (see notes for figure)
L_n = Lf_ratio*(R_t*(sqrt(epsilon)-1)+...

```

---

```

R_dt*(sec(15*pi/180)-1))/tan(15*pi/180);

% solving for parabola coeffs
x_N = tan(theta_N)*R_dt/(sqrt(1+tan(theta_N))^2);
R_N = R_cd - sqrt(R_dt^2-x_N^2);
c = (tan(theta_N)-tan(theta_E))/(2*(x_N-L_n));
b = tan(theta_N)-2*c*x_N;
a = R_N-x_N*(b+c*x_N);

coeffs = [a;b;c];

x_co = tan(theta_C)*R_ut/sqrt(1+tan(theta_C)^2);

xx = linspace(-1.5*x_co,L_n,n);
for i = 1:n
    if(xx(i) >= x_N)
        R_x(i) = a + b*xx(i) + c*xx(i)^2;
    elseif (xx(i) < x_N && xx(i) >= 0)
        R_x(i) = R_cd-sqrt(R_dt^2-xx(i)^2);
    else
        R_x(i) = R_cu-sqrt(R_ut^2-xx(i)^2);
    end
end

```

## newtzero Function

```

function root = newtzero(f,xr,mx,tol)
%NEWTZERO finds roots of function using unique approach to Newton's
Method.
% May find more than one root, even if guess is way off. The function
f
% should be an inline object or function handle AND capable of taking
% vector arguments. The user can also pass in a string function.
% NEWTZERO takes four arguments. The first argument is the function to
be
% evaluated, the second is an optional initial guess, the third is an
% optional number of iterations, and the fourth is an absolute
tolerance.
% If the optional arguments are not supplied, the initial guess will
be set
% to 1, the number of iterations will be set to 30, and the tolerance
will
% be set to 1e-13. If the initial guess is a root, no iterations will
take
% place.
%
% EXAMPLES:
%
%           % Use any one of these three equivalent function
definitions.
%           f = inline('cos(x+3).^3+(x-1).^2'); % Inline object.
%           f = 'cos(x+3).^3+(x-1).^2'; % String function.
%           f = @(x) cos(x+3).^3+(x-1).^2; % Anonymous function.

```

---

```

%
    newtzero(f,900) % A very bad initial guess!
%
    fb = @(x) besselj(2,x)
    rt = newtzero(fb); % Finds roots about the origin.
    rt = rt(rt>=-100 & rt<=100); % Plot about origin.
    x = -100:.1:100;
    plot(x,real(fb(x)),rt,abs(fb(rt)),'*r')
%
    f = @(x) x.^3 +1;
    newtzero(f,1) % Finds the real root;
    newtzero(f,i) % Finds the real root and two imaginary roots.
%
    f = @(x) x.^3 + 2*x.^2 + 3*x -exp(x)
    newtzero(f) % Finds two roots.
%
    % Try it with Wilkinson's famous polynomial.
    g = @(x)prod(bsxfun(@(x,y)(x-y),[1:20]',x.'));
    % For brevity
    newtzero(g,0)
%
%
% May work when the initial guess is outside the range of fzero,
% for example compare:
%
%           fzero(f,900) % for f as in the above example.
%
% This function may also find complex roots when fzero fails. For
example,
% try to find the roots of the following using NEWTZERO and FZERO:
%
%           f1 = @(x) x.^(2*cos(x)) -x.^3 - sin(x)+1;
%           ntz1 = newtzero(f1,[],[],1e-15) % NEWTZERO finds 5 roots
%           fzrt1 = fzero(f1,0) % FZERO aborts.
%
%           f2 = @(x) x.^2 + (2 + .1*i); % could use 'roots' here.
%           ntz2 = newtzero(f2,1) % NEWTZERO finds 2 roots
%           fzrt2 = fzero(f2,1) % FZERO fails.
%
% See also fzero, roots
%
% Author: Matt Fig
% Contact: popkenai@yahoo.com

defaults = {1,30,1e-13};% Initial guess, max iterations, tolerance.

switch nargin % Error checking and default assignments.
    case 1
        [xr,mx,tol] = defaults{::};
    case 2
        [mx,tol] = defaults{2:3};
    case 3
        tol = defaults{3};
end

```

---

---

```
if isempty(xr)    % User called newtzero(f,[],50,1e-3) for example.
    xr = defaults{1};
end

if isempty(mx)
    mx = 30;
end

if ~isa(xr,'double')
    error('Only double values allowed. See help examples.')
end

if tol < 0 || ~isreal(tol)
    error('Tolerance must be greater than zero.')
end

if mx < 1 || ~isreal(mx)
    error('Maximum number of iterations must be real and >0.')
end

[f,err] = fcchk(f,'vectorized'); % If user passed in a string.

if ~isempty(err)
    error(['Error using NEWTZERO:',err.message])
end

if abs(f(xr))< tol
    root = xr; % The user supplied a root as the initial guess.
    return % Initial guess correct.
end

LGS = logspace(0,3,220); % Can be altered for wider range or denser
% search.
LNS = 0:1/19:18/19; % Search very close to initial guess too.
xr = [xr-LGS xr+LGS xr-LNS(2:end) xr+LNS].'; % Make vector of
% guesses.
iter = 1; % Initialize the counter for the while loop.
mn1 = .1; % These will store the norms of the converging roots.
mn2 = 1; % See last comment.
sqrteps = sqrt(eps); % Used to make h. See loop.
warning off MATLAB:divideByZero % WILL BE RESET AT THE END OF WHILE
LOOP.

while iter <= mx && abs(mn2-mn1) > 5*eps
    h = sqrteps*xr; % From numerical recipes, make h = h(xr)
    xr = xr-f(xr)./((f(xr+h)-f(xr-h))./(2*h)); % Newton's method.
    xr(isnan(xr) | isinf(xr)) = []; % No need for these anymore.
    mn1 = mn2; % Store the old value first.
    mn2 = norm(xr,'fro'); % This could make the loop terminate early!
    iter = iter+1; % Increment the counter.
end

if abs(f(0)) < tol % The above method will tend to send zero root to
Inf.
```

---

```
    xr = [xr;0]; % So explicitly check.
end

warning on MATLAB:divideByZero % Reset this guy, as promised.

% Filtering. We want to filter out certain common results.
idxi = abs(imag(xr)) < 5e-15; % A very small imag term is zero.
xr(idxi) = real(xr(idxi)); % Discard small imaginary terms.
idxr = abs(real(xr)) < 5e-15; % A very small real term is zero.
xr(idxr) = complex(0,imag(xr(idxr))); % Discard small real terms.
root = xr(abs(f(xr)) < tol); % Apply the tolerance.

% Next we are going to delete repeat roots. unique does not work in
% this case because many repeats are very close to each other but not
% equal. For loops are fast enough here, most root vectors are
% short(ish).

if ~isempty(root)
    cnt = 1; % Counter for while loop.

    while ~isempty(root)
        vct = abs(root - root(1))<5e-6; % Minimum spacing between
        roots.
        C = root(vct); %C has roots grouped close together.
        [idx, idx] = min(abs(f(C))); % Pick the best root per group.
        rt(cnt) = C(idx); %#ok<AGROW> Most root vectors are small.
        root(vct) = []; % Deplete the pool of roots.
        cnt = cnt + 1; % Increment the counter.
    end

    root = sort(rt).'; % return a nice, sorted column vector
end
```

Published with MATLAB® R2016a